Exploring Performance of Metamaterial Emitters for Applications of Energy Harvesting and Gas Sensing: Modeling and Simulation Approach

Gemechis Mathewos Fite

A PhD Dissertation Submitted to the Department of Applied Physics

College of Applied Natural Science

For the Partial Fulfillment of the Requirements for the Degree of Doctor of Philosophy in Applied Physics (Condensed Matter Physics)

School of Graduate Studies
Adama Science and Technology University

January, 2026

Adama, Ethiopia

Exploring Performance of Metamaterial Emitters for Applications of Energy Harvesting and Gas Sensing: Modeling and Simulation Approach

Ph.D Candidate: Gemechis Mathewos Fite

Main Supervisor: Fekadu Tolessa Marami (PhD)

Co-supervisor: Prof. Abebe Belay (PhD)

Co-supervisor: Gashaw Beyene (PhD)

A Dissertation Submitted to the Department of Applied Physics Program

College of Applied Natural Science

For the Partial Fulfillment of the Requirements for the Degree of Doctor of Philosophy in Applied Physics (Condensed Matter Physics)

School of Graduate Studies

Adama Science and Technology University

January, 2026

Adama, Ethiopia

Declaration

I declare that this dissertation entitled "**Exploring Performance of Metamaterial Emitters for Applications of Energy Harvesting and Gas Sensing: Modeling and Simulation Approach**" is my own work and has not been submitted to any university for a similar purpose. The references used in this dissertation are duly recognized by proper citations.

Name of candidate	Signature	Date

Recommendation of Supervisors

I/we, the supervisor (s) of this dissertation, hereby certify that we have closely advised/supervised the student while developing this dissertation and read the final dissertation entitled "**Exploring Performance of Metamaterial Emitters for Applications of Energy Harvesting and Gas Sensing: Modeling and Simulation Approach**" prepared under our guidance by **Gemechis Mathewos Fite**. Therefore, we recommend the submission of the dissertation to the department for further approval.

______________________	_______________	_______________
Name of Major Supervisor:	Signature	Date
______________________	_______________	_______________
Name of Co-supervisor 1	Signature	Date
______________________	_______________	_______________
Name of Co-supervisor 2	Signature	Date

Approval Sheet

I/we hereby certify that the recommendation and suggestion given by the dissertation review committee are appropriately incorporated into the final dissertation entitled "**Exploring Performance of Metamaterial Emitters for Applications of Energy Harvesting and Gas Sensing: Modeling and Simulation Approach**" prepared under my/our guidance by **Gemechis Mathewos Fite** submitted in the partial fulfillment of the requirements of the degree of Doctor of Philosophy in Applied Physics (Condensed Matter Physics).

______________________________	________________	_______________
Major Supervisor	Signature	Date
Co-Supervisor 1	Signature	Date
Co-Supervisor 2	Signature	Date

We, the undersigned, members of the Board of Examiners of the dissertation open defense by **Gemechis Mathewos Fite** have read and evaluated the dissertation entitled "**Exploring Performance of Metamaterial Emitters for Applications of Energy Harvesting and Gas Sensing: Modeling and Simulation Approach**" and examined the candidate during open defense. This is therefore to certify that the dissertation is accepted for the partial fulfillment of the requirement of the degree of Doctor of Philosophy in Applied Physics (Condensed Matter Physics).

______________________________	________________	_______________
Chairperson	Signature	Date
External Examiner 1	Signature	Date
External Examiner 2	Signature	Date
Internal Examiner 1	Signature	Date
Internal Examiner 2	Signature	Date

Finally, approval and acceptance of the dissertation is contingent upon submission of its final copy to the School of graduate Studies (SGS) through the candidate's Department Graduate Council (DGC) and College Graduate Committee (CGC).

______________________________	________________	_______________
Department Head	Signature	Date
College Dean	Signature	Date
School of graduate Studies, Dean	Signature	Date

DEDICATION

I dedicate this dissertation to the cherished memory of my beloved mother, Yeshimabet Bekele, who departed this world before she could witness the completion of this work. Her boundless love, selfless sacrifices, and steadfast prayers have been the bedrock of my journey. Though she is no longer physically present, her wisdom and values continue to guide and strengthen me every day.

To my dear mother, Yehimabet Bekele whose unwavering love and care shaped me into the person I am, I owe you everything. Your patience, resilience, and sacrifices laid the foundation for my achievements. I wish you were here to celebrate this milestone with me, but I find comfort in knowing that your blessings have always surrounded me.

Though she is no longer with me in body, her love, prayers, and sacrifices live on in my heart. This work stands as a tribute to her a testament to the lasting impact she has had on my life. May her soul rest in eternal peace.

BIOGRAPHICAL SKETCH

The candidate was born from his family **Yeshimabet Bekele** and **Mathewos Fite** in May 1989 in Gimbi town, located in the West wallaga Zone, approximately 573 km from Adama, Ethiopia. His educational journey commenced at **Mendi Primary School**, where he completed his primary education from 1992 to 1999. He pursued his secondary education at **Mendi Secondary School** from 2000 to 2004 and subsequently where he laid the groundwork for his future academic endeavors.

Upon completing his high school education, he joined **Jimma University** in 2005. His dedication and hard work culminated in earning a **Bachelor of Science (BSc)** degree in Applied Physics in 2009. After graduation, he was employed as a teacher at **Gimbi Preparatory school**, where he began his academic career. Following six years of service in this role, the researcher furthered his education by enrolling in the postgraduate program in 2014/15 to pursue a **Master of Science** (MSc) degree in Physics. Upon the successful completion of his MSc studies, he served as a lecture in Wallaga University, for two and a half years. This work allowed him to contribute to the academic community and gain valuable leadership experience.

In 2022/23, he joined **Adama Science and Technology University** to pursue his PhD studies. Over the last three years, he dedicated himself to rigorous research, honing his expertise in his field. Now, he is prepared to present his PhD dissertation work, marking a significant milestone in his academic journey and his commitment to advancing knowledge in the discipline of physics.

ACKNOWLEDGMENTS

First and foremost, I am profoundly grateful to Almighty **God** for granting me health, strength, wisdom and perseverance to complete this dissertation. His endless blessings have guided me through every challenge and triumph in this academic journey.

I extend my deepest gratitude to my supervisor, **Dr.Fekadu Tolessa**, for his invaluable guidance, patience and continuous support throughout this research. His insightful advice and encouragement have been instrumental in shaping this work. I would also like to sincerely thank my co-supervisors, **Pro. Abebe Belay** and **Dr.Gashawu Beyene**, for their constructive feed- back, encouragement and invaluable contributions to this study. Their expertise and dedication have greatly enriched my research experience. Additionally, I want to thank **Dr. Mesfin Asfaw** for his early supervision and advice during the beginning of my research. Despite having to move before to the defense of my proposal, his backing provided a solid basis for this endeavor. My appreciation also goes to all Wallaga University Shambu Compus staff members for their unwavering support and encouragement during this journey. I am equally grateful to all my PhD candidate colleagues, whose collaboration and discussions have been a source of motivation and learning. Additionally, I acknowledge **Mr. Leulseged Bekele**, for his support during my computational work.

I extend my sincere appreciation to Adama Science and Technology University, Wallaga University for their support, resources and contributions that have facilitated the successful completion of this dissertation. Their assistance has been invaluable in providing the necessary environment for my research.

I am deeply thankful to my beloved wife (**Urge Aga**) and my Son (**Kena Gemechis**) for their patience, love and sacrifices throughout this endeavor. Their unwavering support and understanding have been my greatest source of motivation. With-out their encouragement, this achievement would not have been possible

Finally, I am grateful to everyone who has contributed, directly or indirectly, to the successful completion of this work. Your encouragement and support will always be cherished.

Table of Contents

LIST OF FIGURES

LIST OF TABLES

List of Acronyms

TPV	Thermophotovoltaic
MM	Metamaterials
MDM	Metal-dielectric-metal
SAR	Absorption Rate
EM	Electromagnetic
SPP	Surface Plasmon Polariton
Mp	Magnetic Polariton
μ	Permeability
ε	Permittivities
FEM	Finite Element Method
ENG	Epsilon Negative
SRR	Split ring resonance
GHz	Gigahertz
HfO_2	Hafnium dioxide
SiO_2	Silicon dioxide
TM	Transverse Magnetic
TE	Transverse Electric
IR	Infra-red
NRHE	Non-radiative heat exchange

Abstract

This dissertation presents a theoretical investigation into the spectral performance of a multilayer and grating metamaterial composed of tungsten (W) and Aluminumnitride (AlN), hafnium dioxide (HfO_2) designed to enhance thermophotovoltaic (TPV) energy conversion efficiency. Utilizing advanced electromagnetic simulations based on Maxwell's equations, the study explores the optical properties of a W/HfO_2/W metamaterial structure, focusing on its ability to produce high emissivity within the wavelength range of 1.5 to 2.0 μm optimal for interfacing with InGaAsSb TPV cells. The results demonstrate that the metamaterial achieves an average emissivity exceeding 96%, with a peak of 99.9%, primarily driven by resonant mechanisms such as surface plasmon polaritons and magnetic polaritons. The design exhibits polarization independence and maintains high performance across incident angles of 0° to 60°, indicating robustness for practical applications. Furthermore, the study assesses the impact of material selection and structural parameters on emissivity characteristics, emphasizing the potential of engineered metamaterials to significantly improve thermal radiation control. The findings suggest that the proposed W/HfO_2/W metamaterial has promising implications for advancing high-efficiency TPV systems, contributing to sustainable energy solutions through optimized thermal emission engineering. Additionally, it presents the design and simulation of a terahertz metamaterial-based gas sensor aimed at detecting toxic atmospheric gases such as ozone (O_3) and nitric oxide (NO). Utilizing a metal-dielectric-metal (MDM) structure composed of tungsten and hafnium dioxide, the sensor exhibits dual resonance frequencies with absorption rates approaching 99%. Finite Element Method (FEM) simulations demonstrate high sensitivity to variations in refractive index, with sensitivities up to 4.58 THz/RIU and a figure of merit exceeding 11.82/RIU. Distinct resonance shifts corresponding to different gases affirm the sensor's potential for real-time, selective gas detection. The findings underscore the effectiveness of metamaterials in environmental monitoring applications and lay the groundwork for developing practical, high-performance gas sensors for air quality assessment.

Key words: Metamaterials, Selective emitter, TPV, Sensitivity, Q-factor, Harmful gas sensor.

1. INTRODUCTION

1.1 Background of the Study

In contemporary research, the pursuit of innovative and efficient methods for generating re newable energy is paramount (Ghanekar et al., 2016a). A notable advancement in this domain is the emergence of Thermophotovoltaic (TPV) systems. As the name suggests, thermophotovoltaic refers to the conversion of heat (thermo-) into light (-photo), which is then transformed into electricity (-voltaic) (Hosani & Emziane, 2013). These systems are attracting significant interest due to their novel approach to harnessing thermal energy, enabling direct conversion into electrical power (Liu et al., 2023) (W. Chan, 2010). Fundamentally, TPV technology represents a paradigm shift, as it facilitates the conversion of radiant heat emitted by high-temperature sources into electricity via photovoltaic (PV) cells (Rinnerbauer, Lenert, Bierman, Yeng, Chan, Geil, Senkevich, Joannopoulos, & Wang, 2014) (Ghanekar et al., 2017). Specifically, thermal energy from a high-temperature heat source is utilized to raise the temperature of an emitter, which subsequently emits radiation that is captured and converted into electrical power by a PV cell (Pfiester & Vandervelde, 2017a). TPV technology has the potential to revolutionize power generation across various sectors, providing an environmentally sustainable, durable, and efficient solution for electricity production.

This introduction intends to provide a comprehensive overview of the functioning of TPV systems and their potential to represent a significant advancement in renewable energy research (Saloom & Al-Dergazly, 2024). My goal is to engage your interest as this dissertation explores the intriguing aspects of TPV systems in the subsequent sections. The rapid expansion of human activities has resulted in an elevated emission of greenhouse gases (GHGs) into the atmosphere, contributing to global warming. The consequences of this phenomenon are extensive, encompassing rising sea levels and an increase in the frequency and intensity of natural disasters (C. Hao et al., 2023). Worldwide energy generation has undergone significant transformation in recent years, driven by the urgent need for sustainable practices and the reduction of greenhouse gas emissions. The energy mix has increasingly diversified, with renewable sources such as solar, wind, and hydropower playing a pivotal role in meeting global energy demands (Datas & Vaillon, 2020) (Gilroy, 2021). In many regions, advancements in technology have made renewables not only more accessible but also cost-competitive with traditional fossil fuels (Bitnar et al., 2013). This shift is bolstered by investments in infrastructure and policy frameworks that promote clean energy initiatives, enabling countries to reduce their carbon footprints while enhancing energy security. Despite the growth of renewable energy, conventional sources like coal, natural gas, and nuclear power still account for a substantial portion of global energy generation (Saidov et al., 2008). Emerging economies, in particular, continue to rely heavily on fossil fuels to support their rapid industrialization and energy needs. This reliance poses challenges for achieving climate goals, as fluctuations in energy prices and geopolitical tensions can disrupt supply chains (Landy et al., 2008). To address these issues, a concerted effort is required to integrate more renewable technologies, improve energy storage solutions, and enhance grid infrastructure , ensuring a reliable and resilient energy generation system for the future.

In response to environmental crises, there has been a shift towards renewable energy resources. Solar, wind, and hydroelectric power have emerged as primary contributors to this transition, facilitating a sustainable and cleaner energy future (Saidov et al., 2008). However, each of these energy sources presents distinct challenges; hydroelectric power is geographically limited, while solar and wind energy generation is contingent upon specific meteorological conditions and temporal variations (Al-Hamdani et al., 2024). To enhance energy reliability, it is pragmatic to integrate renewable energy systems with backup solutions that utilize fossil fuels or biomass (Burger et al., 2020). Additionally, innovative strategies such as thermal energy storage enable the capture of surplus energy as heat for later use during periods of low resource availability. Recently, the critical role of thermophotovoltaics (TPV) in the transition to clean energy has gained recognition, prompting increased research efforts aimed at optimizing TPV systems for improved efficiency and effectivenes.nA critical barrier to the early development of TPV was the scarcity of high-quality, low-bandgap photovoltaic cells capable of functioning at elevated temperatures. The advent of these cells in the 1990s to mid-2000s facilitated research in the 2000s and 2010s, focusing on components for spectral control, including selective emitters, front-side filters, and back surface reflectors. Notably, if a TPV system is optimized with a selective emitter tailored to the photovoltaic cell, efficiencies could potentially exceed 50% (Zhong et al., 2021). Essentially, thermophotovoltaic technology is a specific type of photovoltaic process that converts light into electricity, with the key difference being that the light source originates from a different part of the electromagnetic spectrum. Both systems convert electromagnetic waves into electricity (Ghanekar et al., 2016a). However, traditional photovoltaic (PV) cells primarily convert visible and ultraviolet light wavelengths, which have a larger bandgap. Photons with energy levels exceeding this bandgap are inefficiently converted into electrical energy, largely due to heat loss from the charge carriers (Verma et al., 2025). Photons with energy levels lower than the bandgap energy are not absorbed (Tao et al., 2021). When exposed to one solar illumination, this results in an optimal bandgap of approximately 1.4 eV. Conver sely, a TPV (Thermophotovoltaic) system converts infrared photons emitted from a heated surface into electrical energy. A typical TPV system consists of three main components: a heat source, an emitter, and a photovoltaic cell. The heat source such as joule heating, fuel combustion, or solar energy provides heat to the emitter (Qin et al., 2022). The emitter filters the incoming thermal energy, emitting only the desired wavelengths through radiation. Finally, the photovoltaic cell transforms this radiated energy into electricity using the photovoltaic effect (Bendelala & Cheknane, 2022).

TPV systems provide the benefit of high efficiency by converting a broader range of low-frequency photons into electricity (Horak et al., 2014). However, their development can be complex because it requires the coordination of multiple components and various design factors. Key challenges include ensuring the emitter's stability at high temperatures and creating a low bandgap photovoltaic cell (Gilroy, 2021). Additionally, increasing the view factor between the PV cell and emitter can be achieved by reducing the distance between them.TPV (Thermophotovoltaic) technology can harness various heat sources to elevate emitter temperatures between 1,300 K and 2,000 K (Kuznicki & Meyrueis, 2010). At these temperatures, the emitted radiation generates a theoretical hemispherical total radiation flux of approximately 16-91 W/cm², as dictated by the Stefan-Boltzmann law, assuming an emissivity of 1 (σTs^4) (Mihai et al., 2022). Due to the lower temperature range, the majority of this radiation falls within the infrared spectrum, in accordance with Planck’s radiation law and Wien's displacement law (Potyrailo et al., 1998). When the TPV cell is optimally positioned near the emitter, energy loss is minimized, facilitating high energy conversion efficiency. Coupling this system with a cutting-edge MMM emitter from UCSD could potentially elevate the energy conversion efficiency beyond 50%, resulting in a cost of less than $0.50 per watt (Esmail et al., 2022). Furthermore, since the TPV system primarily relies on thermal energy, it can maintain consistent operation throughout the day when integrated with a waste heat recovery storage system. This approach presents a cost-effective, reliable, and scalable solution for power generation, with significant potential to mitigate CO_2 emissions (Kudyshev et al., 2019). Spectral shaping can be accomplished by either developing a selective emitter or by pairing a broadband emitter with a selective filter. Consequently, optical metamaterial emitters are structured differently for various applications, incorporating cells with cutoff wavelengths that align with selective emitters and cell band gaps. With periodic boundary conditions applied along the x and y axes; the designed emitter is subjected to a plane wave incident along the z-axis. The finite element method (FEM) was utilized to quantitatively analyze the differential form of Maxwell's equations. The COMSOL Multiphysics software was used for structural design, simulations, and parameter analysis.

In the ongoing pursuit of advanced environmental monitoring and industrial safety protocols, the demand for gas sensors that transcend the limitations of conventional technologies particularly in terms of sensitivity, selectivity, and miniaturization has catalyzed the exploration of novel material platforms, chief among them being metamaterials. As artificially engineered structures whose electromagnetic properties are dictated by their subwavelength architecture rather than their constituent materials' inherent chemistry, metamaterials offer an unprecedented capacity to manipulate light-matter interactions. This dissertation is founded upon the premise that these exotic properties, such as the generation of strongly localized electromagnetic fields in plasmonic metamaterial or the sharp resonance shifts in terahertz meta-atom, can be harnessed to create a new generation of gas sensors. When functionalized with gas-selective receptors, these metamaterial transducers can detect the adsorption of target analyte molecules through pronounced resonance shifts or signal amplification, enabling the parts-per-billion level identification of harmful gases like ammonia, carbon monoxide, or volatile organic compounds with a specificity and speed unattainable by current methods. Additionally, this research therefore seeks to systematically design, and optimize a novel metamaterial-based sensor, addressing a critical gap in real-time, high-fidelity gas detection technology.
This study employs a numerical simulation and modeling for exploring the optical properties of the materials specifcally tungusten-hafiniumdioxide MDM which analyzed using the finite element method and kirchhof's rule and resonant wavelength, refractive index sensitivity, Q-factor, material properties, geometry, gas concentration, absorption bands, boundary conditions, mesh size, incident wave, and performance metrics like sensitivity and figure of merit.The emissivity for transverse magnetic (TM) and transverse

electric (TE) modes was evaluated using Kirchhoff's law, revealing high absorptivity/emis sivity within the cutoff wavelength range. Numerical calculations were performed with various software tools, including OriginPro 2022 and Microsoft Excel.

1.2 Statement of the Problems

The global imperative for sustainable energy and advanced environmental monitoring demands technologies that surpass the limitations of current systems. In energy harvesting, traditional photovoltaics exhibit constrained efficiency, while in gas sensing, existing devices often lack the sensitivity and selectivity for detecting trace-level hazardous gases. Nanophotonic metamaterials, with their unparalleled ability to manipulate light, present a transformative solution for fields, enabling enhanced solar energy capture and highly sensitive gas detection (Andreev et al., 2009). However, the practical application of these materials is hindered by significant challenges, including the absence of robust modeling frameworks to predict their complex light-matter interactions and the difficulties in their fabrication and integration. Current research often lacks a cohesive synergy between theoretical design and experimental validation, and advanced manufacturing techniques remain expensive and intricate. Furthermore, issues of durability, thermal stability, and cost-effectiveness persist. This research directly addresses these gaps by systematically investigating the limitations of current optical metamaterial systems for gas sensing and energy harvesting. It aims to propose innovative designs and practical strategies to enhance performance, focusing on achieving high spectral efficiency, superior sensing capability, cost-effectiveness, and long-term durability, thereby contributing to the development of more efficient and sustainable technological solutions.

1.3 Objectives of the Study

1.3.1 General objective

The general objective of this research is to design and simulate metamaterial emitter structures for application in energy harvesting and gas sensing**.**

1.3.2 Specific objectives of the research

- To design and optimize the performance of metamaterial emitters through numerical simulations to enhance their absorption and emission for InGaAS TPV Cell.
- To analysis the spectral efficiency of metamaterials, focusing on their emissive properties across a broad wavelength range and under varying shapes of Metamaterials fot cut off wavelength λ=2.2μm.

- To fine-tune unit cell geometry, periodicity, and substrate parameters in order to maximize sensor sensitivity at low gas concentrations.

1.4 The Scope of the Study

The scope of this study encompasses the exploration of nanophotonic metamaterials and their applications in two critical areas: energy harvesting and gas sensing. Specifically, the research will focus on the modeling and simulation of metamaterial structures designed to optimize light absorption for enhanced heat energy capture. By employing advanced computational techniques, the study aims to identify key design parameters that influence the performance of these materials under various environmental conditions. This aspect of the research will provide insights into how nanophotonic metamaterials can be effectively integrated into existing photovoltaic technologies, ultimately contributing to more efficient energy solutions.

In addition to energy harvesting, the study will investigate the utilization of nanophotonic metamaterials in gas sensing applications. This will involve the development of models that accurately predict the interaction between gas molecules and metamaterial structures, enhancing sensitivity and selectivity in detection processes. The research will also address the challenges of scalability and reproducibility in the fabrication of these materials, exploring innovative manufacturing techniques that can facilitate their practical implementation. By bridging the gap between theoretical modeling and experimental validation, this study aims to provide a comprehensive understanding of how nanophotonic metamaterials can revolutionize both energy harvesting and environmental monitoring technologies.

1.5 Significance of the Study

The significance of this study lies in its potential to advance the fields of energy harvesting and gas sensing through the innovative application of nanophotonic metamaterials. By enhancing TPV energy capture and improving the sensitivity of gas sensors, this research addresses critical global challenges related to sustainable energy production and environmental safety. The findings could lead to the development of more efficient photovoltaic systems and reliable gas detection technologies, ultimately contributing to reduced carbon emissions and improved public health. Additionally, the integration of modeling and simulation with experimental validation offers a comprehensive framework that can accelerate the practical implementation of nanophotonic metamaterials, fostering further advancements in these high-impact areas.

1.6 Structure of Dissertation

This dissertation is structured into five Sections, each focusing on a distinict aspect of the research regarding the principles and applications of metamaterials on energy harvesting and harmfulgas sensing. Section 1 focuses on an introduction, providing essential background on thermophotovoltaic, their relevance in energy harvesting, resaerch gaps, and the motivations for the study, while outlining the research objectives. In Section 2 a comprehensive literature review will be conducted, highlighting prior research efforts and the challenges encountered in developing TPV systems.

This review will provide a holistic understanding of the current state of the field and identify potential avenues for further research and development. Additionally, the chapter will address existing challenges and opportunities within TPV research, proposing directions for future investigation. Section 3: Building on the principles discussed in section 2, I will outline our group's methodology and design considerations for constructing a thermophotovoltaic (TPV) system. This chapter will elaborate on the strategies employed to tackle the challenges associated with creating a high-temperature emitter and detail how the principles of TPV energy conversion informed our design choices. A thorough account of the approaches taken to develop the TPV system will be provided, along with an explanation of the various challenges and considerations encountered throughout the process. By sharing our methodology and design insights, this chapter aims to serve as a valuable resource for future researchers pursuing the development of TPV systems. Section 4: A comprehensive analysis of the results obtained from our thermophotovoltaic (TPV) system will be conducted, with comparisons made to existing work in the field. This chapter will discuss the performance metrics and efficiency of the system, as well as explore potential areas for improvement and refinement.Finally; section 5 summarizes the key findings, highlights their significance, and proposes recommendations for future research directions. The references section provides a comprehensive list of all scholarly articles cited throughout the dissertation, ensuring adherence to the required citation style.

2. LITERATURE REVIEW

This chapter is structured into two distinct sections. The first section explores the background of theory of electromagnetic, optical metamaterials, their classification, and the electromagnetic interactions they exhibit. We also cover topics such as perfect absorption, the mechanisms of absorbance and emittance, the unique properties these materials possess, and the approaches used for electromagnetic studies. Additionally, we discuss harmful gases, thermophotovoltaics and along with a detailed analysis of radiation heat transfer, the mechanisms of energy conversion, and the photovoltaic effect. The second section will present a comprehensive literature review of prior investigations in TPV. This will encompass methodologies and findings from various research groups, thereby offering an extensive overview of the current advancements in the field. This structured approach aims to clarify the essential concepts and research trajectories in thermophotovoltaics, facilitating the identification of potential avenues for future inquiry and technological development.

2.1 Theory of electromagnetic

The theoretical foundations of light propagation in metamaterials involve understanding how electromagnetic waves interact with structured materials that have sub-wavelength features. The arrangement of these micro- or nanoscale components alters the effective values of permeability and permittivity at different scales. Thus, by applying Maxwell's equations, researchers examine the relationship between electromagnetic waves and the metamaterial structure to gain insights into the optical properties of these materials.

2.1.1 Maxwell's Equations

Maxwell's equations form the foundation for describing all classical electromagnetic phenomena, including the behavior of MDM structures. These four equations, consolidated by James Clerk Maxwell in 1865 (Decem, 1927), relate electric fields, magnetic fields, electric displacement fields, and magnetic field intensity. The differential form leads to differential equations that can be solved using the finite element method. When considering monochromatic electromagnetic fields in linear, isotropic, and homogeneous materials, the equations can be expressed as follows:

$$\nabla \cdot B = 0 \quad \textbf{(Gauss's law, for magnetic field)} \tag{2.1}$$

$$\nabla \cdot E = \rho_{ext} \quad \textbf{(Gauss's law, for electric field)} \tag{2.2}$$

$$\nabla \times E = \frac{-\partial B}{\partial t} \quad \textbf{(Faraday's law)} \tag{2.3}$$

$$\nabla \times H = J_{ext} + \frac{\partial D}{\partial t} \quad \textbf{(Ampere's law)} \tag{2.4}$$

In this context, H, B, E, D, and ρ denote the intensity of the magnetic field, magnetic flux density, electric field intensity, electric displacement (or electric flux density), and external electric charge density, respectively. Additionally, the constitutive equations link D, E, B, and H. Consequently, magnetic and electric flux describes the behavior of magnetic and electric fields across surfaces, and as shown by electromagnetic waves and circuits, changing one can influence the other.

$$D = \varepsilon_o E + P \tag{2.5}$$

$$B = \mu_o(H + M) \tag{2.6}$$

The vacuum's permittivity and permeability are represented by ε_0 and μ_0, respectively. Polarization (P) and magnetization (M) in a medium result from the influence of individual electric or magnetic dipoles within the material. As shown in Eq. (2.7), in a linearly isotropic medium, magnetization is directly related to the magnetic field, while the induced polarization P aligns with the electric field.

$$P = \varepsilon_o \chi_e E, \quad M = \chi_m H \tag{2.7}$$

Here, χ_e and χ_m represent the electric and magnetic susceptibility, respectively. The alignment of electric dipoles leads to P aligning with E, while the alignment of magnetic dipoles makes M proportional to B. Consequently, the constitutive laws for linearly isotropic metamaterials can be expressed as Eq. (2.8) for magnetic flux density and Eq. (2.9) for electric flux density.

$$D=\varepsilon_o (1+\chi_e) E = \varepsilon_o \varepsilon_r E = \varepsilon E \tag{2.8}$$

$$B=\mu_o(1+\chi_m)H=\mu_o\mu_r H=\mu H \tag{2.9}$$

In this context, ε_r and μ_r denote the relative permittivity and relative permeability of the materials, respectively. The electric flux density in an electric field refers to the quantity of electric flux that passes through a unit area, accounting for both the permittivity of the metamaterial and the free charge. Meanwhile, magnetic flux density measures the direction and strength of the magnetic field per unit area, illustrating the influence of a magnetic field on moving charges and magnetic materials.

2.1.2 Wave Equations

By applying Maxwell's equations and constitutive relations, we can connect the microscopic interactions of charges with dynamic fields to the macroscopic optical properties, such as ε and μ that we attribute to materials. Furthermore, by integrating the general form of an oscillating electromagnetic wave, as shown in Eq. (2.7), into Maxwell's equations (Eqs. (2.1) – (2.4)), we can derive further characteristics of the electromagnetic wave as it travels through the medium.

Maxwell's equations can be utilized to derive the wave equations for magnetic flux density (B) and electric field (E). By assuming that the magnetization M = 0, we start with Faraday's law (Eq. (2.2)) and incorporate the constitutive equation (Eq. (2.6)); this leads us to the wave equation for E, as presented in Eq. (2.10).

$$\nabla\times E = -\mu \frac{\partial B}{\partial t} \quad (2.10)$$

By taking the curl of both sides of the previous equation (Eq. (2.10)) and multiplying them, we obtain:

$$\nabla\times(\nabla\times E) = -\mu \frac{\partial(\nabla\times H)}{\partial t} \quad (2.11)$$

The right side of Equation (2.11) clearly represents Ampere's law, and the resulting time-dependent wave equation is provided in Eq. (2.12).

$$\nabla\times(\nabla\times E) + \mu\varepsilon \frac{\partial 2(E)}{\partial t} = -\mu \frac{\partial Jext}{\partial t} \quad (2.12)$$

Including the source term in the wave equation solution illustrates how the source influences light propagation. In the case of conducting (neutral isotropic) media, the current density term plays a significant role. Thus, the general electric field wave equation is:

$$\nabla^2 E - \mu\varepsilon \frac{\partial 2(E)}{\partial t} = -\mu \frac{\partial Jext}{\partial t} \quad (2.13)$$

Here $\nabla\times(\nabla\times E) = \nabla(\nabla\cdot E) - \nabla 2E = -\nabla^2 E$. Because, $\nabla(\nabla\cdot E) = 0$

Where, ω represents the angular frequency, $j = \sqrt{-1}$ is the imaginary unit, and t denotes time. Therefore, we utilize Eq. (2.13) to manipulate the electric field E in metamaterials. In non-magnetic and non-conducting media, the volume densities of electric charge (ρ_{ext}), electric current density (Jext), and magnetization (H) are all zero, as Maxwell's equations indicate that there are no free charges, currents, or magnetic dipoles. Consequently, the wave equation is given by:

$$\nabla^2 E = \mu\varepsilon \frac{\partial^2(E)}{\partial t^2} \quad (2.14)$$

Assuming that the electric and magnetic fields display harmonic time dependence in a monochromatic context, we apply this time-harmonic behavior to solve the differential equation (2.14).

$$E(r, t) = E_0\, e^{j(k\cdot r - \omega t)} \quad (2.15)$$

The magnetic and electric fields are represented by the complex amplitude vectors B_0 and E_0, respectively. The wave vectors k, r, ω, and t signify the wave propagation direction, position vector, angular frequency, and time variable, respectively. The expression $e^{j(k\cdot r-\omega t)}$ illustrates a plane wave moving in the direction of k.

Therefore, by substituting Equation (2.14) into Equation (2.15), we obtain the wave vector and refractive index as follows:

$$k = \frac{\omega}{c}\sqrt{\mu_r \mathcal{E}_r} = \frac{\omega}{c}.n \tag{2.16}$$

The symbols μ_r and ϵ_r represent the relative permeability and permittivity, respectively.

$$n = \mu_0\epsilon_0\frac{\mu\epsilon}{\mu_o \mathcal{E}_0} = \sqrt{\mu_r \mathcal{E}_r} = \frac{C}{V} \tag{2.17}$$

Here, n represents the refractive index and c is the speed of light in a vacuum (approximately 2.99792458×10^8 m/s). The solution to the wave equation, including the source term, demonstrates how the source influences light propagation. The phase velocity (v_p) indicates how quickly a wave's phase of a particular frequency component moves through space. It can be calculated using the following equation:

$$v_p = \frac{C}{\sqrt{\mu_r \mathcal{E}_r}} \tag{2.18}$$

Likewise, applying a similar approach, the B field can also be derived from the wave equation based on harmonic time dependence in the monochromatic case, expressed as follows:

$$B(r, t) = B_0\, e^{\,j\,(k\cdot r-\omega t)} \tag{2.19}$$

For conducting media (which are neutral and isotropic), the wave equation for current density is expressed as follows:

$$\nabla^2 B - \mu\varepsilon\omega^2 B = -\mu j\omega J_{ext} \tag{2.20}$$

For non-conducting media (which are neutral and isotropic), the wave equation for non-current density is expressed as follows:

$$\nabla^2 B = \mu\varepsilon\partial^2 B/\, \partial t^2 \tag{2.21}$$

Thus, the wave equations for both the electric field (E) and the magnetic field (B) describe the propagation of electromagnetic waves in metamaterials. In a medium or in free space (vacuum), these fields interact such that they both satisfy wave equations. Additionally, many electromagnetic issues are grounded in the wave equations for E and B, demonstrating how electromagnetic waves move through a metamaterial medium. The Finite Element Method (FEM) is employed to numerically solve these wave equations, which includes discretizing the problem domain, transforming the equations into a weak form, and resolving the resulting system of equations.

2.2 Metamateials

Metamaterials are engineered materials designed to have properties not found in naturally occurring substances. They achieve this by arranging their structural components at a scale smaller than the wavelength of the phenomena they influence, such as electromagnetic waves (Jung et al., 2024). This unique configuration enables metamaterials to manipulate waves in novel ways, leading to applications in optics, acoustics, and electromagnetism. The concept of metamaterials emerged in the early 2000s, with significant advancements in the understanding of their properties and potential uses (Z. Wang et al., 2022). Researchers have explored various designs and structures, such as artificial atoms and resonators, to create materials that can bend, absorb, or even cloak electromagnetic waves (Z. Wang et al., 2024). Metamaterials hold the promise of revolutionizing technology in fields ranging from telecommunications to medical imaging, making them a focal point of ongoing scientific research and development.

The term "metamaterial" is derived from the Greek word "meta," signifying "beyond," "altered," or "changed" (Hou et al., 2021). Initially, various scholars offered definitions of metamaterials. The European Union Metamorphose Network describes a metamaterial as a configuration of artificial structural elements designed to exhibit beneficial and unusual electromagnetic properties (Kuznicki & Meyrueis, 2010). In their book, Cai and Shalaev define metamaterials as intentionally engineered materials that rely on the unit structure, rather than the base materials, to determine their characteristics (Lei et al., 2022). Many researchers concur that metamaterials represent a new category of ordered composites with exceptional properties not commonly found in nature. These properties emerge from the introduction of extrinsic, low-dimensional, artificially created inhomogeneities, which lead to unique response functions absent in the constituent materials (Jin et al., 2016).

Metamaterials consist of multiple distinct elements crafted from small, straight materials such as plastics, dielectrics, or metals. These materials are usually arranged in periodic patterns, as illustrated in Fig. 2.1.

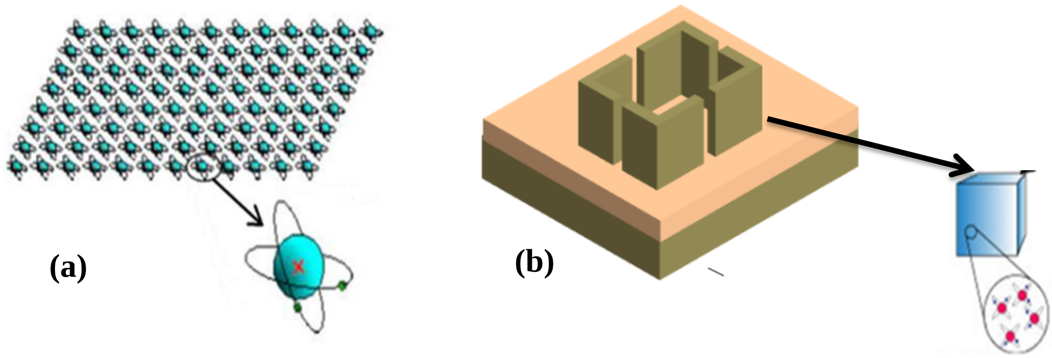

Figure 2.1 (a) A natural material with its atoms (Valipour et al., 2022) (b) A metamaterials with artificially structured atoms

By carefully manipulating shape, geometry, size, orientation, and arrangement, metamaterials can achieve material properties unattainable with conventional materials, enabling new interactions with light and sound waves (Anggraini et al., 2022). These materials can be designed in various symmetrical structures, including squares (Tao et al., 2021), cross-based designs (Patel et al., 2022), pyramids (Progress In Electromagnetics Research M, Vol. 8, 27–37, 2009, 2009), discs (Esmail et al., 2022), nanowires (Ross Macdonald, 1974), and cones(Anwar & Khan, 2024). Unlike traditional materials, the effective optical properties of metamaterials are mainly influenced by the geometry of their unit cells (internal structure) rather than their chemical compositions (Anwar & Khan, 2023). Their design flexibility allows for integration into a variety of applications, such as spatial light modulators (Cheng et al., 2021), perfect absorbers (Anwar & Khan, 2024), invisibility cloaks (Curreli et al., 2023), sensors (Mahmud et al., 2021), superlenses (Zhang et al., 2022),and antennas (Zhang et al., 2022).

2.2.1 Classifications of metamaterials

Metamaterials come in various structures, each with unique properties tailored to the types of waves they interact with and their intended applications. The three primary subcategories are acoustic, mechanical, and electromagnetic metamaterials (Garín et al., 2015). Acoustic metamaterials are specifically designed to control, direct, and manipulate sound waves, providing advantages over natural materials; "acoustic" refers to sound. A prime example is the negative Doppler effect (Pfiester & Vandervelde, 2017a).

Mechanical metamaterials are engineered to exhibit exceptional mechanical properties not found in conventional materials (Rinnerbauer, Lenert, Bierman, Yeng, Chan, Geil, Senkevich, Joannopoulos, Wang, et al., 2014a). They are designed to manage mechanical waves, such as stress, vibration, and strain. These metamaterials often display unusual characteristics, like a negative Poisson's ratio (auxetic behavior) or unique methods for distributing mechanical stress (Fadel et al., 1998). Their mechanical properties can be applied in areas like vibration damping, noise reduction, and the development of strong yet lightweight structures. The final category is electromagnetic metamaterials, designed to exhibit specific material properties by manipulating traveling electromagnetic fields such as light, radio, or microwaves through random or periodic sub-wavelength structures (Bitnar et al., 2002). These metamaterials can be artificially engineered to produce remarkable electromagnetic effects and are classified in various ways based on their fundamental characteristics, including permeability and permittivity.

Common types of electromagnetic metamaterials include left-handed materials (which have negative permittivity and permeability simultaneously) (Y. Li, 2009), photonic crystals (Raghu et al., 2008), and plasmonic materials (with permittivity less than one) (Zhang et al., 2022). Left-handed materials, first theoretically explored by Veselago in 1968, possess negative phase velocity and refractive index (Oh et al., 2020). These materials can be created using photonic structures like open photonic rings and arrays of thin metallic wires, also known as split ring resonators. Photonic crystals are typically made of dielectric materials and exhibit periodic structures that allow electromagnetic wave transmission in certain frequency bands while blocking it in others.

Plasmonic metamaterials, characterized by a permittivity of less than one or negative electric polarizability, are observed in metals, semiconductors, and ionized gases (Valipour et al., 2022). This plasmonic behavior arises because electrons or charged particles respond to changing electric fields over time. The structural features of metamaterials are smaller than the wavelengths of the electromagnetic radiation they interact with, allowing them to function as uniform substances with useful properties.In this dissertation, we concentrate on plasmonic metal-dielectric-metal metamaterials (MDMs), which effectively manipulate electromagnetic radiation. These structures consist of a thin dielectric layer sandwiched between two metallic layers, enabling the formation of surface plasmon polaritons (SPPs) and magnetic polaritons (MPs) at the MDM interface due to interactions between material geometry and electromagnetic fields(Valipour et al., 2022). Consequently, the electromagnetic waves in MDMs, often utilized in perfect absorbers, behave according to Maxwell's equations.

2.2.2 Propagation of Electromagnetic Waves in Metamaterials

The analysis of light propagation in metamaterials can be performed using the Finite Element Method (FEM). This method allows for the simulation of light as it passes through metamaterials by solving the wave equation for the electromagnetic fields. Due to the complex geometries of optical metamaterials, certain properties are challenging to address analytically. FEM, which is an effective approach for solving partial differential equations (PDEs), is particularly useful for tackling such complex problems. By discretizing Maxwell's equations over a meshed geometry, FEM computes optical properties and facilitates accurate modeling of intricate materials and boundary conditions. It reformulates Maxwell's equations into matrix form using basis functions, enabling the determination of key optical characteristics such as reflectance, transmittance, and absorption by solving for the distribution of the electromagnetic field. The FEM approach for solving PDEs is outlined in Eq. (2.22).

$$L[f] = S \qquad (2.22)$$

In this context, S represents the source term, which could be a heat source, charge density, external force, or similar factors. L denotes the differential operator, while f is the unknown function we aim to determine within a domain (region) Ω, such as temperature or electric potential. Elements are small subdomains that are discretized within Ω. Basis functions, also referred to as shape functions, are employed to approximate the solution within each element. These functions utilize the values at the mesh's nodes to define the solution for the element. To approximate the solution f, the solution domain is divided into cells, and a finite number of basis functions $[\phi k]_{k=1}^{N}$ are introduced, defined as follows:

$$f(r) \approx \sum_{k=1}^{N} f_k \, \phi_k(r) \qquad (2.23)$$

Here, f_k represents the unknown coefficients that need to be determined. The basis functions are piecewise low-order polynomials, which are nonzero only in a limited number of neighboring elements. The requirement for the residual to be close to zero can be reformulated as Eq. 2.24.

$$r = L[f] - S \qquad (2.24)$$

In formal terms, we require the weighted average to be zero to achieve this in a weak sense. By selecting a set of test functions $\{\omega_k(r)\}$ as k is from 1 to N, known as Galerkin's method(Horak et al., 2014), where the basis functions and test functions are identical, we can proceed. By multiplying the equation by a test function and integrating over the domain Ω, the strong form of the equation is converted into its weak form, as shown below:

$$\langle \omega_k, r \rangle = \int_\Omega \omega_k(r)\, r(r)\, d\Omega(r) \qquad (2.25)$$

Here, $\langle \omega_k, r \rangle$ represents the inner product, with k ranging from 1 to N. This approach can be applied to the wave equation using edge elements, where the normal components are allowed to be discontinuous, while the tangential components remain continuous across the boundaries of the elements. Consequently, by rearranging the wave equation (2.13), we can express the residual as follows:

$$R = \nabla \times (\nabla \times E) - \mu_0 \varepsilon \omega^2 E + \mu_0 j \omega J = 0 \qquad (2.26)$$

The scalar product of the final equation with Wn can be computed and integrated over the simulation domain Ω when the set of test functions is defined as {Wn} as *m* is from 1 to N. This involves projecting Wn onto R, necessitating orthogonality as illustrated in Eq. 2.25, resulting in the inner product expressed as follows:

$$\langle W, R \rangle = \int_\Omega ds\, Wn \cdot (\nabla \times (\nabla \times E) - \mu_0 \varepsilon \omega^2 E + \mu_0 j \omega J) = 0 \qquad (2.27)$$

When the electric field E is expressed in terms of nodal basis functions $\{N_m(r)\}$ as *m* is from 1 to N, it can be represented as Eq. (2.28).

$$E(r) = \sum_{m=1}^{N} EmNm(r) \qquad (2.28)$$

To isolate and, which is one of N equations that collectively create a system of equations, substitute Eq. (2.28) into Eq. (2.27), resulting in the following expression:

$$-\mu_0 j \omega \int_\Omega dsW_n.J + \sum_{m=1}^{N} \int \Omega\, \mathrm{Wn}.\,(\nabla \times (\nabla \times \mathrm{Nm}(r)) - \varepsilon\omega 2\mathrm{Nm}(r))\mathrm{dsEm} = 0 \qquad (2.29)$$

Rewriting Equation (2.29) in matrix and vector form allows us to express it as:

$$S_{nm} = \int_\Omega d\Omega W_n.(\nabla \times (\nabla \times N_m(r)) - \varepsilon \omega^2 N_m(r)) \qquad (2.30)$$

$$c_n = -\mu_0 j \omega \int_\Omega dsW_n.J \qquad (2.31)$$

Therefore, the matrix is introduced as follows.

$$\mathbf{S} = \begin{bmatrix} S_{11} & S_{12} & \cdots & S_{1N} \\ S_{21} & S_{22} & \cdots & S_{2N} \\ \vdots & \vdots & \ddots & \vdots \\ S_{N1} & S_{N2} & \cdots & S_{NN} \end{bmatrix} \qquad (2.32)$$

Ultimately, the vectors of the matrix can be represented as:

$$C = [c_1 \ c_2 \ c_3 \ldots c_n]^T, \quad e = [E_1 \ E_2 \ E_3 \ldots E_n]^T \qquad (2.33)$$

Where "e" is the unknown we are attempting to solve for, and "c" represents external influences such as sources, boundary conditions, or applied loads included in the force (or load) vector. Given that "S" is a square matrix, we can assume that "det S" = 0;

$$Se - c = 0 \Rightarrow \quad Se = c \Rightarrow \quad e = S^{-1}c \qquad (2.34)$$

A set of equations derived from discretizing the partial differential equations governing a physical problem is numerically represented by Equation (2.34). In this instance, B is the global system matrix, which incorporates geometric data, material properties, and finite element interactions. The discretization involved in FEM typically results in sparse and large datasets. For example, the computational values of the electromagnetic field are unknown quantities included in the solution vector **e**. This formula underpins FEM simulations, enabling the analysis of complex physical processes across various scientific and engineering domains (Sreenivasulu & Narendar, 2022). One key advantage of FEM compared to other methods is the ability to tailor the shape of the mesh cells. COMSOL, utilizing the finite element method, forms the basis for simulations that determine electric and magnetic fields based on Maxwell's equations (Cakiroglu et al., 2019). Generally, COMSOL defaults to using Lagrange elements and second-order shape functions as nodal basis functions (Saidov et al., 2008). To prevent numerical inaccuracies, a discretization step of $\lambda = 1/10$ is chosen.

2.2.3 Floquet and Scattering Boundary Condition

In problems involving periodic structures, the Floquet condition is applied when the solution exhibits periodicity in space. This condition serves as the boundary requirement for addressing wave propagation challenges in periodic structures like metamaterials, hybrids, and photonic crystals. It is often utilized in wave propagation scenarios or electromagnetic simulations where the domain features periodic boundaries (Durisch & Bitnar, 2010). In COMSOL, the Floquet condition is frequently employed to analyze electromagnetic waves in various periodic structures such as pyramids, cones, cylinders, diffraction gratings, and honeycombs. It determines the wave behavior within a single unit cell of the periodic structure by setting periodic boundaries, allowing the results to be extended to the entire domain. The boundaries are defined based on a field simulated using the Floquet condition, which is given by:

$$E(r,t) = E_0 \, e^{-j(kr-\omega t)} \qquad (2.35)$$

The Floquet condition mandates that the solution at one boundary must correspond to the solution at the opposite boundary, possibly with a phase shift (Datas & Martí, 2017). This ensures that the solution remains consistent throughout a periodic domain. Therefore, by assuming $r \rightarrow r+T$;

$$E(r+T,t) = E_0 e^{-jkr} e^{j\omega t} e^{-jk.T}$$

$$E(r+T, t) = E(r+T, t)\, e^{-jk.T} \quad (2.36)$$

Here, T denotes an arbitrary translation vector. Equation (2.36) is based on Floquet's theorem, which states that the solution to the wave equation in a spatially periodic medium must exhibit a periodic phase shift across the boundaries of unit cells. Additionally, the electric field difference between the points r and r+T is expressed as $e^{-jk.T}$. This implies that the electric field within the simulation domain can represent the electric field throughout the entire space. To minimize reflections, a scattering boundary condition (SBC) was implemented alongside a perfectly matched layer (PML). The PML serves as an artificial absorbing boundary condition that helps prevent spurious reflections by mimicking the absorption of outgoing waves at the domain edges. However, since discretizations can lead to reflections, the PML is not entirely effective (Veselago, 1968). Thus, the SBC is designed to allow outgoing waves to exit the computational domain with minimal reflection (Nam et al., 2014). By employing complex coordinates to modify Maxwell's equations, the PML absorbs outgoing waves, while the SBC directly applies boundary conditions to ensure that outgoing waves radiate outward without reflection, as given by:

$$n.\nabla E_z + jk_o E_z = 0 \quad (2.37)$$

2.2.4 Fresnel’s Equations

Fresnel’s equations describe the behavior of light as it crosses the boundary between two different media. These equations utilize the angle of incidence and the refractive indices of the materials to determine the proportion of light that is reflected and transmitted at the interface. In the context of metamaterials, they explain how light interacts with a layered structure composed of metal and dielectric materials, accounting for reflection and transmission at each boundary (Ni et al., 2016). Additionally, Fresnel’s equations are employed to establish boundary conditions based on the polarization of the incoming wave, such as transverse electric (TE) and transverse magnetic (TM) modes. The reflection and transmission coefficients help assess how the electric and magnetic fields vary across the boundary. The electric field is then calculated using the boundary conditions at the interface (Bitnar et al., 2002). The reflection coefficients for TE polarization, where the electric field is perpendicular to the plane of incidence, are represented in Eq. (2.38) (Garín et al., 2015).

$$R_{TE} = \frac{n_1\ cos\theta_i - n_2\ cos\theta_t}{n_1\ cos\theta_i + n_2\ cos\theta_t} = \left(\frac{cos\theta_i - n_{2/n1}\ cos\theta_t}{cos\theta_i + n_2/n1\ cos\theta_t}\right)^2 \qquad (2.38)$$

Likewise, the reflection coefficients for TM polarization, where the magnetic field is perpendicular to the plane of incidence, are presented in Eq. (2.39) (H. Wang, Prasad Sivan, et al., 2015).

$$R_{TE} = \frac{n_2\ cos\theta_i - n_1\ cos\theta_t}{n_2\ cos\theta_i + n_1\ cos\theta_t} = \left(\frac{n_{2/n1}cos\theta_i - cos\theta_t}{n_2/n1\ \ cos\theta_i + cos\theta_t}\right)^2 \qquad (2.39)$$

Here, θi represents the angle of incidence in free space, while n_1 and n_2 are the refractive indices of the two different media. The angle of transmission in the medium, θt, is determined by Snell's law, which states that $n_1 sin\theta_i = n_2 sin\theta_t$.

2.2.5 Optical Properties of Metamaterials

Electromagnetic radiation interacts with matter to create various phenomena, including transmission, absorption, reflection, emission, and scattering. Consequently, optical absorption (or emission) in metamaterials is highly sensitive to the energy of incoming photons and significantly influenced by the material properties, shape, and dimensional features of its unit cell. A unit cell consists of various parameters, including height, width, and periodicity, orientations, and aspect ratio. To enhance absorption and emission performance, improve light-matter interaction, and allow for tunability in metamaterial structures, impedance matching is essential. This matching is affected by the relative permittivity, relative permeability, and a material's polarization capability, as detailed in Eq. (2.40) and Eq. (2.41) (Banerjee et al., 2023).

$$\varepsilon_r = \varepsilon_r' + i\varepsilon_r^n \qquad (2.40)$$

$$\mu_r = \mu_r' + i\mu_r^n \qquad (2.41)$$

Here, ε_r and μ_r represent relative permittivity and relative permeability, respectively. ε′ and ε″ denote the real and imaginary parts of permittivity, while μ′ and μ″ refer to the real and imaginary parts of permeability, respectively. Therefore, the optical impedance (Z) of an interface, as shown in Eq. 2.42, can be utilized to derive the permittivity and permeability related to the optical response (Shemelya et al., 2014).

$$z = \sqrt{\frac{\mu_r}{\varepsilon_r}} = \sqrt{\frac{\mu_r' + i\mu_r''}{\varepsilon_r' + i\varepsilon_r''}} \qquad (2.42)$$

As mentioned earlier, by manipulating or organizing the structure of a metamaterial, it is possible to align the impedance in free space (Z_0) with the effective impedance (Z) such that $Z=Z_0$. This adjustment minimizes the reflection and transmission coefficients to zero, as illustrated in Eq. (2.43).

$$Z=\sqrt{\frac{\mu_{eff}}{\varepsilon_{eff}}} = Z_o \qquad (2.43)$$

Where, ε_{eff} = n/Z, μ_{eff} = nZ, n represents the materials' refractive index.

Additionally, achieving nearly perfect optical absorption and emission across the examined wavelength range from ultraviolet to far-infrared is highly dependent on the effective coupling between different resonant modes, such as the interband transitions in metals like tungsten.

2.2.6 Metamaterials near perfect absorber

A new area of research has emerged within the broader metamaterials field due to the advent of frequency-dependent perfect absorbers (PAs). A perfect absorber refers to a material or structure that absorbs all incident electromagnetic radiation such as heat, light, or sound within a specific range of wavelengths or frequencies, without reflecting, transmitting, or scattering any of it (Banerjee et al., 2023). This concept is often linked to a black body and has attracted significant interest. The electric and magnetic responses of these materials can be adjusted by modifying the size and shape of the metamaterial structure, allowing for precise control over the absorptive response in terms of frequency or wavelength (Fourniea T. Rashwana T.L. Switzer C. J.I. Gerharda, 2018). Initially developed by Landy et al. in 2008, the PA featured a three-layer design that operated within the microwave range of the electromagnetic spectrum(H. Wang, Prasad Sivan, et al., 2015). Subsequent studies expanded its functionality to include THz frequencies (Dmitriev, 2008), infrared (Ni et al., 2016), and optical ranges(Bitnar et al., 2002). This study provides a comprehensive analysis of PAs operating in the optical region, examining a series of samples with resonances between 0.2 µm and 30 µm. Today, perfect absorbers with diverse propertiesincluding broadband, narrowband, multiband, and polarization-sensitive or insensitive designs are available, functioning across both microwave and optical regions (Nam et al., 2014).

Narrow-band Perfect Absorbers

The narrow-band perfect absorbers are specialized materials or structures designed to achieve almost total absorption of incident electromagnetic waves at a particular, small range of frequencies (Veselago, 1968) (Pfiester & Vandervelde, 2017a). These absorbers use resonance processes to control and modify how electromagnetic waves interact with the material. The principles of resonance tuning and impedance matching underpin the operation of narrow-band perfect absorbers. Certain resonances where electromagnetic energy is effectively trapped and dissipated are supported by the structure.

Broad and Multi-band Perfect Absorber

Broadband or multi band perfect absorbers are designed to nearly entirely absorb electrom agnetic waves across several distinct frequency bands or over a broad spectrum of frequencies. Unlike narrow-band absorbers, these devices are engineered for wide-ranging performance and adaptability, making them ideal for applications requiring effective absorption across various frequency ranges(Raghu et al., 2008). They play a crucial role in applications such as radiative cooling, solar energy harvesting, thermal emitters, and sensing, which necessitate efficient energy capture or wave manipulation across multiple spectral areas. By employing innovative structural and material designs such as gradient impedance matching, overlapping resonances, lossy materials, multiple resonators, hybrid structures, and control over polarization and angles broadband and multiband perfect absorbers operate effectively across a wide frequency range(Han et al., 2023).

2.2.7 Mechanism of Metamaterials Perfect Absorbers

Most perfect metamaterial absorbers consist of multiple layers, including periodic metallic patterns, dielectric spacers, and continuous metallic plates (Lin et al., 2000). The arrangement of these metallic layers is meticulously designed to create a specific resonance at the desired frequency. By altering the size of the resonators shaped as gratings, rectangular cuboids, rings, crosses, patches, pyramids, and more the impedance matching with free space is achieved. In metal-dielectric-metal (MDM) structures, perfect absorption can be attained using various combinations of dielectric layers, patterned metals, porous coatings, composite materials, plasmonic elements, microsphere coatings, and nanoparticles(J. Hao et al., 2011). In this study, we designed a three-layer metamaterial structure and focused on three key parameters to achieve perfect absorption: impedance-matching losses, resonance-based losses, and material-based losses. The first theory suggests that by adjusting the permeability and permittivity of the metamaterial, its impedance can be matched to the surrounding environment (Nicol & Carbotte, 2005). Proper structural design can generate magnetic and electric resonances in MDM, allowing for customization of these material properties. When electromagnetic radiation interacts with the metamaterial's structure, it penetrates the dielectric layer and attenuates as it moves toward the metal layer(Nicol & Carbotte, 2005), which reflects the remaining energy, causing further attenuation.

Another type of absorption arises from resonances like surface plasmon polaritons (SSP) and magnetic polaritons (MP)(Nicol & Carbotte, 2005). SSP represents an electromagnetic wave that travels along the interface between a metal and a dielectric, accompanied by the collective oscillations of the metal's free electrons. A magnetic polariton resonance occurs when an electromagnetic wave couples with a magnetic dipole moment in a structured material through MDM layers, leading to opposing oscillation directions of electrons in the top and bottom metal layers(Nicol & Carbotte, 2005), which induces a current that generates a magnetic field.

Material-based losses refer to the dissipation of electromagnetic (EM) energy within a material due to its inherent properties(W. R. Chan et al., 2013). Some energy from the electromagnetic waves is lost as heat, scattering, or other non-recoverable forms. The dielectric layer primarily traps the incident electromagnetic wave, causing it to oscillate at the absorber's resonance frequency to dissipate energy efficiently. The structure's design creates a resonant cavity, with the quality factor linking the cavity's lifespan to the resonance's frequency selectivity. Various material properties, including dielectric losses, ohmic (conductive) losses, and magnetic losses, are involved. When electromagnetic radiation interacts with the material's structure, the atomic lattice begins to oscillate, resulting in the formation of phonon polaritons. Consequently, the effective impedance (Z) of the micro/nanostructure is determined by the "S" parameters (Omair et al., 2019).

$$S=\sqrt{\frac{(1+s_{11})^2-(s_{21})^2}{(1-s_{11})^2-(s_{21})^2}} = \sqrt{\frac{(1+ref)^2-(tran)^2}{(1-ref)^2-(tran)^2}} \qquad (2.45)$$

In the metal-dielectric-metal interference theory, the top resonating element array is positioned above a bottom ground plane, separated by dielectric layers. For effective absorption in this decoupled setup, both near-field interactions and magnetic resonance are considered(Valipour et al., 2022). The top metallic layer, which features a resonator pattern, acts as a partially reflecting surface that alters the complex transmission and reflection coefficients. The dielectric middle layer plays a crucial role in regulating energy dissipation, field confinement, and resonance phenomena, such as surface plasmon polaritons (SPP). When incoming electromagnetic waves reach the bottom metallic layer, they experience a 180° phase shift due to its reflective properties. As the top metallic layer encounters the air-dielectric interface, it reflects part of the electromagnetic signal while allowing some to pass into the substrate (Bendelala & Cheknane, 2022). The primary role of the third metallic layer is to prevent any transmission of the incoming waves. Thus, the term "Perfect Absorber" is applicable when an electromagnetic wave interacts with this tri-layered medium, as all electromagnetic energy is absorbed, resulting in zero transmission and negligible reflection at resonance.

To function as an emitter, absorbers need to be heated by absorbing thermal energy from the source(Shruti et al., 2023). When sufficient thermal energy is applied, photons will be emitted within the desired emission spectrum. Several physical mechanisms can enhance the amount of spectrum absorbed or emitted. In this section, we will discuss some of the methods employed in spectral absorbtion by proposed emitter.

2.2.7.1 Impedance Matching

The metamaterial is designed so that its effective impedance matches that of free space (≈377 Ω).This minimizes reflection at the interface, allowing incident waves to enter the structure without bouncing back.

2.2.7.2 Surface plasmon polariton

When an incoming photon interacts with a surface plasmon (SP), it creates a surface plasmon polariton (SPP). The surface plasmon is a collective excitation of electrons at the interface between dielectric and metal(Argyropoulos, 2014), resulting from the positive permittivity of the dielectric and the negative permittivity of the metal at optical frequencies. Metals are typically regarded as effective reflectors due to the excitation of surface plasmon polaritons (SPPs) on textured metal surfaces or the stimulation of resonant modes confined within sub-wavelength metallic cavities. However, when structured at a wavelength scale, reflection diminishes, leading to enhanced absorption with a spectrum that is much narrower than that of a blackbody (Bergström et al., 2008).

Once stimulated, the surface plasmon polaritons (SPPs) travel along the metal-dielectric interface in parallel as indicated in figure 2.2. Their wavelengths are significantly shorter than those of incoming photons. SPPs have a short lifespan and quickly dissipate in a direction perpendicular to the metal-dielectric interface.

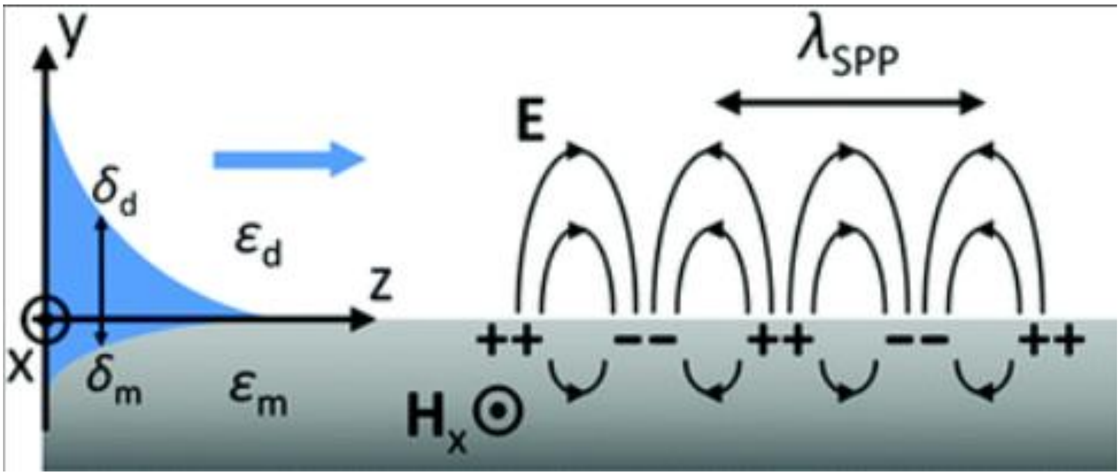

Figure 2.2: Schematic representation of an electron density wave propagating along a metal–dielectric interface. (Fadel et al., 1998)

This study indicates that the surface plasmon is generated by the collective excitation of electrons between tungsten and aluminum nitride. When the combined excitation of photons and the incoming electromagnetic wave enters through the port, SPPs are activated.

2.2.7.3 Magnetic Polariton

Magnetic polariton refers to the resonance of magnetic oscillation at a material's surface in conjunction with incoming photons, primarily influenced by the material's plasmonic properties and geometric parameters as revieled in figure 2.3 below(Zhou et al., 2022). When significant diamagnetism is present, the material's response enhances the overall magnetic field, leading to a negative real component of magnetic permeability.

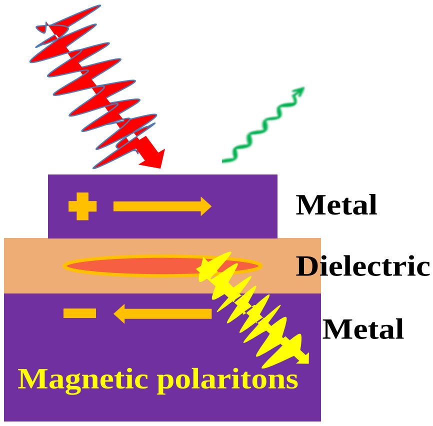

Figure 2.3: Schematic representation of an magnetic polariton wave propagating along a metal–dielectric interface.

As photons collide, they generate an oscillating magnetic field, causing a current to flow in one direction within the metamaterial (MM) and in the opposite direction near the surface of the metal substrate. The presence of free charges on the metal substrate results in a net flow of oscillating electric currents, which induces magnetic fields and produces a diamagnetic response (Bergström et al., 2008). This study indicates that magnetic polaritons are excited due to the free charges on the top and bottom tungsten, leading to a net current flow in the dielectric that induces a magnetic field.

2.3 Application of Metamaterial Thermal Emitters

Metamaterial thermal emitters are engineered surfaces designed to manipulate infrared radiation with exceptional precision, opening new frontiers in energy conversion and sensing technologies (Oh et al., 2020). By tailoring their electromagnetic response through sub-wavelength structural design, these emitters can achieve highly selective spectral emission, polarization control, and directional radiation all capabilities that surpass traditional blackbody emitters. In thermophotovoltaic systems, for instance, metamaterial emitters enhance efficiency by matching their emission spectrum to the bandgap of photovoltaic cells, minimizing energy loss and maximizing power output. Beyond energy harvesting, these emitters find critical roles in infrared spectroscopy, gas sensing, and thermal camouflage. Their ability to produce narrowband, tunable emission makes them ideal for detecting specific molecular signatures in environmental monitoring or industrial diagnostics (Wynn et al., 2024). In aerospace and defense applications, metamaterial thermal emitters can be designed to suppress or shift thermal signatures, contributing to stealth technology. Their compact, planar structure also enables integration into MEMS devices, paving the way for miniaturized and high-performance infrared sources in wearable sensors and smart electronics(Burger et al., n.d.).

2.3.1 Energy harvesting

Thermophotovoltaic (TPV) energy conversion is an innovative technology that presents several distinct advantages. TPV cells cleverly harness solar energy and recycle waste heat from various industrial processes, including nuclear generation (Collector et al., 2021), concentrated solar power (CSP) waste heat (Chen & Shan, 2022), and other high-temperature industrial applications. These cells are static energy conversion devices, meaning they have no moving parts, and consist of a thermal emitter linked to a photovoltaic (PV) cell. The PV cell converts the thermal radiation emitted into electricity. A significant improvement in this method involves using an emitter with a spectrum specifically designed to align with the PV cell's response, rather than relying on blackbody radiation. Additionally, according to Carnot's efficiency, it is theoretically possible to achieve efficiencies up to 80%, depending on the operating temperature. These features position TPV cells as a promising option for energy harvesting, and this work is driven by the pursuit of new design improvements. Periodic electromagnetic structures have been extensively researched in recent decades due to their exceptional properties. Photonic crystals, which can be one, two, or three-dimensional and have a characteristic wavelength comparable to their periodicity, have been modeled and applied in various innovative technologies. Similarly, metamaterials, where the characteristic wavelength is much larger than the periodic structure's dimensions, have been studied both numerically and experimentally, achieving successful implementation since their introduction by Veselago (H. Wang, Chen, et al., 2015). Among these periodic structures, gratings are particularly valuable for a wide range of applications. These include waveguide grating couplers(W. Li et al., 2014), optical spectrometers (Maqsood, 2011), X-ray spectroscopy for space missions(Lee et al., 2017) , and thin-film tandem solar cells (Gamel et al., 2021) . A key aspect of their utility is that gratings exhibit Wood’s anomalies (Bendelala & Cheknane, 2022), which facilitate the management of optical properties such as transmittance, reflectance, and absorptance. Consequently, they have been employed in TPV cells to enhance thermal-electric energy conversion efficiency.

A key component of a TPV cell is the selective emitter, designed to produce thermal radiation that aligns with the PV cell's response to enhance conversion efficiency as seen in (fig.2.3). Periodic structures have shown significant promise in adjusting the emittance of these emitters. Although there is a substantial amount of literature focused on their theoretical and experimental analysis, as well as simulations, there remains room for improvement, particularly by exploring various materials and geometries that could streamline the manufacturing of TPV devices. The second motivation of this thesis is to optimize the thermal emittance of gratings to better match the spectrum between the emitter and the PV cell.

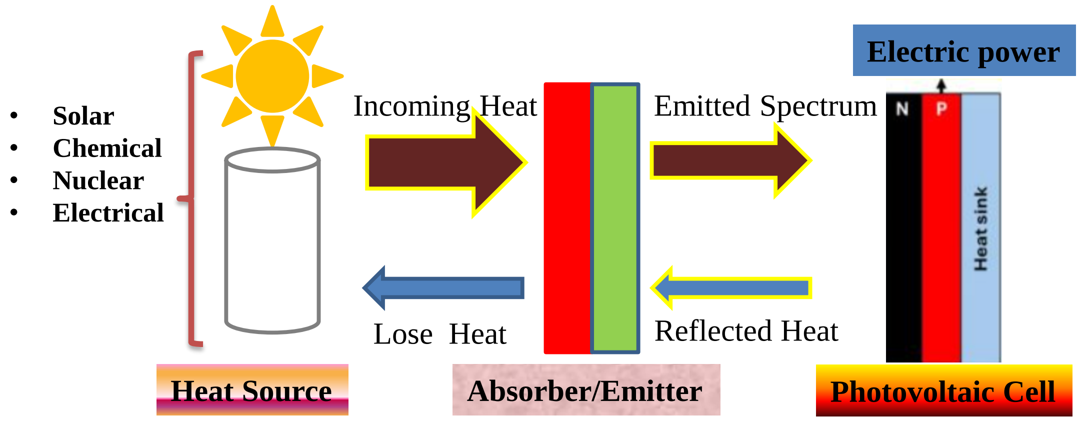

Figure 2.4: Components of a TPV cell: Heat source , absorber and emitter (light blue), PV cell (black and red), and the heat sink (blue light).

2.3.2 Gas sensing

There is significant interest in creating sensors that are highly selective, sensitive, compact, and affordable for detecting and monitoring harmful gases, particularly in the fields of health, safety, security, and environmental protection. The detection of harmful gases is a significant concern for health, safety, security, and environmental sectors. Rapid modernization and industrialization, along with increased time spent indoors (in homes, offices, and laboratories), are major contributors to hazardous gas emissions in the air ("Green Energy Technol.," 2006). Globally, around 7 million premature deaths occur annually due to air pollutants, both indoors and outdoors. Key pollutants include carbon monoxide (CO), nitrogen dioxide (NO_2), and carbon dioxide (CO_2) from indoor air ventilation, as well as ground-level ozone (O_3) from outdoor sources. Greenhouse gases like carbon dioxide (CO_2), methane (CH_4), and nitrous oxide (N_2O) also significantly impact environmental and human health(Zhu et al., 2020).

One of the most commonly used methods for detecting and monitoring various gas molecules in mixtures is mid-infrared (Mid-IR) spectroscopy (Tabassum et al., 2022). This technique is effective because the gases of interest have specific absorption features within this part of the electromagnetic spectrum. Mid-IR gas sensors vary in cost and efficiency based on their design. Some of the most sensitive systems, capable of detecting concentrations down to parts-per-trillion, include mid-infrared sensor systems that utilize continuous-wave interband cascade lasers (ICLs) and those based on Tunable Diode Laser Absorption Spectroscopy (TDLAS) and Quartz-Enhanced Photoacoustic Spectroscopy (QEPAS), which employ lasers as their light sources (Schossmann & Bergmann, 2024).

Their drawbacks include high costs, such as the expensive price of QCL lasers, and their size, as they are typically benchtop setups. Additionally, a significant challenge for these types of sensors, as well as gas sensors in general, is their selectivity. This is crucial when identifying multiple gases that have overlapping absorption spectra (e.g., around 7.5 m; see Figure 2.2).

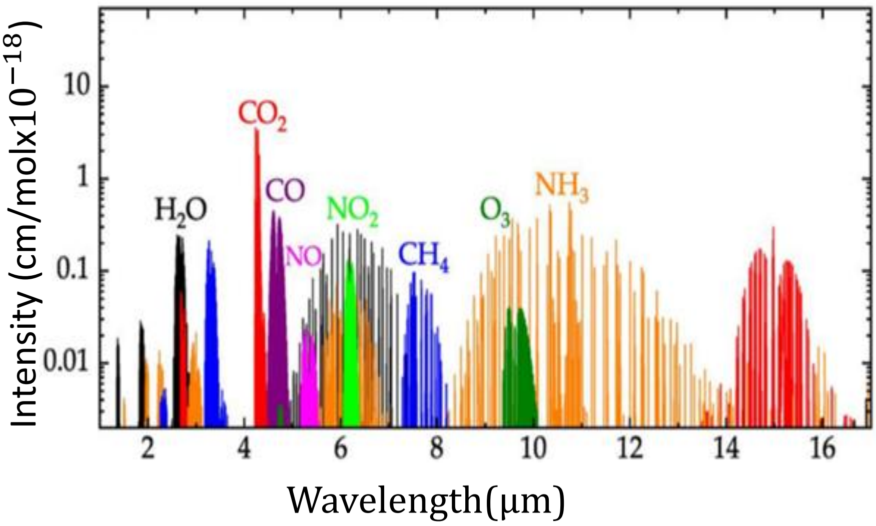

Figure 2.5: The spectral features for the main indoor and outdoor harmful gases(Y. Wang et al., 2023) .

Recent studies have highlighted IR quasi-monochromatic sources using "perfect" absorbers based on metamaterials as an alternative to laser-based gas sensors (Banerjee et al., 2023). The main advantage of these IR sources is their wavelength selectivity, which can be adjusted from the UV to the THz range simply by altering the material type and geometric configuration. Additionally, recent evidence has shown that metamaterials are compatible with traditional fabrication methods, such as photolithography and lift-off, which helps reduce production costs (Pfiester & Vandervelde, 2017b). These IR emitters are constructed using a metal-dielectric-metal (MDM) metamaterial that functions as a perfect absorber and narrow-band emitter, complemented by an external thermal source that acts as a broadband IR source. The MDM structure includes periodic or random micro- and nanostructures, a dielectric layer, and a back reflector. Spectral emissivity and absorptivity are controlled through geometrically tuned electromagnetic resonances of these nanostructures.

2.3.2.1 Technology Process

Metamaterials can also function as absorbers of electromagnetic radiation, referred to as metamaterial absorbers (MAs) (H. Wang, Chang, et al., 2016). These MAs have a broad range of potential applications in various fields, including terahertz (THz) sensing, wireless power transfer, and filtering, among others. MAs are composed of sub-wavelength periodic array components, with each component referred to as a unit cell. Each unit cell of the MA has three layers: the bottom layer is metallic to prevent the transmission of electromagnetic (EM) waves (Banerjee et al., 2023), the middle layer is a dielectric substrate that facilitates the resonance effect, and the top layer is also metallic to ensure impedance matching. The concept of resonant MAs involves achieving zero transmission and reflection at a specific frequency, which enhances the absorption rate. Reflection can be reduced by matching the impedance of the MAs to that of free space, approximately 377 ohms (H. Wang & Wang, 2013). The absorption rate can be further improved by properly designing the resonance structure, such as creating a co-planar arrangement and vertically stacking multiple layers. Furthermore, narrowband MAs with a reconfigurable absorption spectrum are more suitable for sensing applications than broadband sensors (Vora et al., 2014). They display sharp resonant peaks, resulting in greater sensitivity and a larger Figure of Merit (FoM).

The high absorption rate reflects high sensitivity, attributed to the strong electric and magnetic field confinement between the metallic layers. MAs that function in the THz spectrum are referred to as THz MAs (TMAs). A flexible THz MA was reported in (Anwar et al., 2024), achieving an absorption rate of 97% at 1.6 THz for measuring refractive indices. Additionally, a nearly perfect metamaterial plasmonic absorber was theoretically demonstrated in (Nitas et al., 2024), showing 96% absorption across the visible wavelength range. These TMAs can be employed to sense various parameters. One crucial parameter that can be detected using reconfigurable TMAs is the refractive index (RI), which plays a significant role in chemical identification and biosensing applications. A dual-band TMA that is reconfigurable for refractive index measurement, consisting of two identical square metallic patches, was designed in (Da & Xuan, 2015). This TMA demonstrates a sensitivity of 1.90 THz/RIU and a Figure of Merit (FoM) of 229.04 for biochemical sensing.

A multiband reconfigurable TMA featuring multiple splits has been proposed in (Shruti et al., 2023) for sensing and detection applications, achieving maximum sensitivities of 0.119 THz/RIU, 0.248 THz/RIU, and 0.662 THz/RIU. An ultra-sensitive TMA with a high Q-factor of 60.09 and a maximum refractive index sensitivity of 34.40% RIU^{-1} has been simulated in(Tabassum et al., 2022), utilizing the Mach–Zehnder interferometer. A sickle-shaped TMA designed for biosensing applications has been simulated in (Kumari et al., 2024), exhibiting a sensitivity of 471 GHz/RIU and a Figure of Merit (FoM) of 94 RIU^{-1}. An ultra-narrowband TMA for refractive index sensing has been designed in(Shruti et al., 2023), featuring a sensitivity of 1.94 THz/RIU, an absorptivity of 99.49%, and a Q-factor of 637 at 2.44 THz. Additionally, a THz MA designed for both refractive index and temperature sensing in (Zhong et al., 2021) achieves a sensitivity of 2.04 THz/RIU and 7144 nm/K, respectively. Cancer detection was explored in(Elhelw et al., 2023) using metamaterial absorbers. Various configurations, such as elliptical nanoparticles and two triangular-shaped nanoparticles, were also implemented in(Anwar & Khan, 2023) and (Rahimi et al., 2024), respectively. Recent research focusing on anisotropic plasmonic metasurfaces is presented in (Tabassum et al., 2022). While much of the literature cited shows high absorption rates, none of these studies have demonstrated the detection of harmful and toxic gases using refractive index sensors with high sensitivity.

In response to this issue, this dissertation proposes a novel design of a reconfigurable TMA for refractive index sensing, specifically intended for gas detection applications. This work detects harmful and toxic gases by achieving an ultra-narrow band with an exceptional absorptivity of 99.85% at 2.85 THz, along with a Q-factor and Figure of Merit (FoM) of 167.25 and 87, respectively. The innovation of this paper lies in its design, which attains an ultra-narrow peak with high sensitivity and is polarization insensitive, a crucial requirement for sensing applications. Additionally, the equivalent circuit model of the proposed structure is derived, demonstrating that the simulation results align well with the analytical findings. This proposed absorber can function as a refractive index sensor with a high sensitivity of 3.01 THz/RIU, covering a refractive index range from 1.000 to 1.030 at 273 K. The selected range of refractive indices is based on the fact that most harmful gases fall within this spectrum, as outlined in Table 1.

Table 2.1**:** refractive index of some harmful gases(Tabassum et al., 2022)

Toxic and harmful gases	Refractive index
Nitric oxide (NO)	1.000297
Methane (CH_4)	1.000444
Carbon Monoxide (CO)	1.000482
Hydrogen Sulfide (H_2S)	1.000630
Ozone(O_3)	1.00052
Nitrogen Dioxide (NO2)	1.000297
Sulfur Dioxide (SO2)	1.000686
Carbon Dioxide (CO2)	1.000452

In the pursuit of efficient detection of harmful gases, metamaterial-based sensors have emerged as promising candidates due to their tunable electromagnetic properties and enhanced field confinement. A key parameter in assessing the sensor's performance is the resonant frequency shift, which occurs as gas molecules interact with the sensor surface, altering its dielectric environment. The sharpness of this resonance is quantified by the quality factor (Q-factor) as given by Eq(2.48), defined as the ratio of the resonance frequency to its bandwidth, with higher values indicating greater selectivity and precision

$$Q = \frac{f_r}{FWHM} \quad (2.48)$$

Where fr is the resonance frequency, and FWHM is full width at maxima.

Sensitivity Equ (2.49), measured as the frequency change per unit concentration of analyte, is crucial for detecting trace gases and is often coupled with the figure of merit (FOM) to benchmark sensor efficacy.

$$S = \frac{\Delta f}{\Delta n} \quad (2.49)$$

$$FoM = \frac{S}{FWHM} \quad (2.50)$$

Where Δf is the frequency shift and Δn is the change in refractive index, Refractive index sensitivity further enhances gas discrimination by tracking variations induced by molecular adsorption. Selectivity plays a vital role in ensuring specificity to target gases, typically achieved through tailored surface functionalization or geometry optimization(Shruti et al., 2023). Operational parameters such as response and recovery times define the dynamic behavior of the sensor, critical for real-time monitoring. Additionally, the limit of detection (LOD) determines the smallest detectable concentration, and thermal stability ensures consistent performance under fluctuating environmental conditions. Finally, linearity between sensor response and analyte concentration underpins accurate quantification across a broad measurement range. Together, these parameters form a comprehensive framework for evaluating the effectiveness of metamaterial-based gas sensors in environmental and industrial applications.

Kirchhoff's Rule and Thermal Emitter

Thermal emission refers to the spontaneous release of photons resulting from the thermal movement of charges, such as electrons, within a material(Rinnerbauer, Lenert, Bierman, Yeng, Chan, Geil, Senkevich, Joannopoulos, Wang, et al., 2014b). A material that emits electromagnetic radiation because its temperature is above absolute zero is termed a thermal emitter(Woolf et al., 2014). This concept is grounded in Planck's equation of blackbody radiation, which indicates that an object's temperature influences the wavelengths of the emitted radiation. A blackbody serves as the ideal thermal emitter, absorbing all incident radiation and efficiently releasing energy at a specific temperature. Examples of thermal emission can be observed in everyday life, such as sunlight, hot plates, and heated light bulbs. At the nano or micro scale, thermal emission originates from fluctuating currents within a system, caused by various particle interactions that continuously alter particle velocities (Lin et al., 2003).

The emissivity of a material is defined as the ratio of its emitted flux to that of a blackbody of the same shape (Fadel et al., 1998). Similarly, absorptivity is the ratio of the flux absorbed by a material to that of a blackbody with the same geometry. Under thermal equilibrium, the absorptivity and emissivity of a substance are closely related. The second law of thermodynamics asserts that there should be no net energy exchange between a system and its surroundings when they reach thermal equilibrium. Consequently, a material in thermal equilibrium must re-emit the optical flux it has absorbed. This principle, established by Kirchhoff in 1860(Fadel et al., 1998) , was recognized forty years before the spectral distribution of thermal emission could be explained. Depending on the structure of the material system, the emitted electromagnetic waves can be transmitted, reflected, or absorbed (Esmail et al., 2022). Kirchhoff's law states that at thermodynamic equilibrium, a material's emissivity equals its absorptivity. Therefore, during simulation processes, Kirchhoff's law can be used to indirectly deduce absorbance from the scattering parameters (S-parameters) Thus, Kirchhoff's rule, defined by Eq. (2.46), can be employed to evaluate the waves that are absorbed, reflected, or transmitted.

$$\alpha(\omega) = |1 - s_{11}^2| - |s_{21}^2| \quad (2.46)$$

Here, absorptivity, reflectivity, and transmissivity are represented by α(ω), S_{11}, and S_{12}, respectively. Given that our design incorporates metals for the ground layer and the oblique materials prevent sunlight from passing through(Sang et al., 2016), Kirchhoff's rule is refined as shown in Eq. (2.47).

$$\alpha(\omega) = 1 - |S_{11}|^2 \quad (2.47)$$

The design and optimization of metamaterial structures for various applications, including harmful gas sensing, thermophotovoltaics, and solar thermophotovoltaics, are assessed based on Kirchhoff's rule.

2.4 Spectra Efficiency of TPV System

Spectral efficiency describes how effectively thermophotovoltaic (TPV) systems can convert thermal radiation especially in the infrared range into usable electrical energy. In a TPV cell, the photovoltaic material has a defined band gap: radiation with energy exceeding this threshold is deemed useful and can be transformed into electricity, while radiation below the band gap is considered non-convertible and wasted. Consequently, the spectral efficiency of TPV systems is influenced by various factors, including the emitter's temperature, the spectral distribution of the thermal radiation source, and the bandgap energy of the semiconductor materials(Rinnerbauer, Lenert, Bierman, Yeng, Chan, Geil, Senkevich, Joannopoulos, Wang, et al., 2014b). It reaches its maximum when the system minimizes thermal and re-absorption losses, and the semiconductor's band gap aligns closely with the peak emission spectrum of the thermal source.

The relationship between temperature, wavelength, and photon energy which relate to the energy band gap was taken into consideration to point to specific emitter materials that release particular photon wavelengths. The Wien's Displacement Law establishes the distribution of radiation wavelengths and shows that as the temperature rises, the emission's peak wavelength shifts to shorter wavelengths. Thus, the photon energy that considered with the band gap of the TPV cell can be determined using Eq. 2.51 (Mahmud et al., 2021), and Wien's displacement rule, which is provided in Eq.(2.52), can be used to estimate the wavelength change with temperature and the target peak wavelength.

$$E = \frac{1.24}{\lambda_{max}} \quad (2.51)$$

$$\lambda_{max} = \frac{b}{T} \quad (2.52)$$

In this context, **T** represents the temperature of blackbody radiation in Kelvin, **b** denotes Wien's displacement constant (set at 2898 μm·K), $\boldsymbol{\lambda_{max}}$ refers to the peak wavelength in micrometers (μm), and **E** indicates the energy or band gap in electron volts (eV).

Additionally, the impact of the TPV system on both radiative power and output power can be utilized to evaluate the efficiency of an emitter when combined with a TPV cell functioning at room temperature. The effectiveness of a TPV system in converting radiation-induced heat into electrical power is quantified by Eq. 2.53(Science, 2015).

$$\eta_{TPV} = \frac{P_{abs}P_{out}}{P_{rad}P_{abs}} = \frac{P_{out}}{P_{rad}} \qquad (2.53)$$

Here, η_{PV}denotes the efficiency of the photovoltaic cell, η_{SP} indicates the spectral efficiency of the emitter, Pout represents the maximum output power, and P_{rad} is the total radiant power of the emitter. The spectral efficiency η_{SP} is defined by the equation (2.54) provided by(H. Wang, Chang, et al., 2016).

$$\eta_{sp} = \frac{\int_{in.}^{\lambda c} I_{bb}\mathcal{E}(\lambda)d(\lambda)}{\int_{in.}^{\infty} I_{bb}\mathcal{E}(\lambda)d(\lambda)} \qquad (2.54)$$

In this context, λ_c represents the cutoff wavelength, $I_{BB}(\lambda)$ denotes the emission spectrum of a blackbody, and $\epsilon(\lambda)$ is the spectral emissivity of the proposed selective emitter.

2.5 Study of W/Hfo$_2$ Thermal Emitters for Thermophotovoltaic applications

Thermophotovoltaic (TPV) cells offer an efficient method for converting thermal energy into electricity, serving as a sustainable energy source from waste heat and other thermal sources. For instance, TPV cells have been utilized in solar applications with optical concentration and selective absorbers (Gamel et al., 2021) , in portable microgenerators that incorporate photonic crystals(Kudyshev et al., 2019), and in hybrid waste-heat converters that combine TPV cells with solid oxide fuel cells (Rinnerbauer, Lenert, Bierman, Yeng, Chan, Geil, Senkevich, Joannopoulos, Wang, et al., 2014b). Designing TPV cells for specific applications is a complex optimization challenge. Previous research has focused on aspects such as near-field thermal radiation (G.Charache, C.HITCHCOCK, 1997) and global system optimization(Ghanekar et al., 2016b), along with experimental development and characterization of TPV devices (Racka-Szmidt et al., 2022).

Comprehensive reviews of the design and optimization of essential TPV components can be found in(Yangjian et al., 2019) and their references. The design of TPV cells focuses on two key components: an emitter that produces thermal radiation at high temperatures, and a photovoltaic (PV) cell that converts this radiation into electricity. Selective emitters are engineered to modify the thermal radiation spectrum, aligning the peak emittance with the absorption characteristics of the PV cell. While semiconductor junction technology for PV cells is well-established, the main potential for enhancing TPV cell conversion efficiency lies in the development and optimization of effective selective emitters. Conventional TPV cells that rely on blackbody emission require emitters to operate at elevated temperatures. For instance, Wien's displacement law indicates that a black body emitter must reach 1680 K for its peak emittance to correspond with the band gap of a GaSb PV cell (Eg = 0.72 eV). This necessitates the use of materials with high melting points. As a result, structures made from refractory metals such as tungsten (Yeng et al., 2012), tantalum(Ahmadivand & Gerislioglu, 2022) have been proposed and studied. Conversely, employing periodic structures like metamaterials (Kality et al., 2025),and photonic crystals (Gier et al., 2023) has demonstrated the ability to alter the emittance spectrum of selective emitters. Gratings, due to their simplicity and ease of fabrication, present a promising practical option. (Wu et al., n.d.) Investigated complex tungsten gratings and found that the excitation of surface plasmon polaritons (SPP) can significantly enhance thermal emittance. (Ren et al., 2011) examined tungsten pyramidal nanogratings that incorporate structures with both low and high filling ratios. This combination was found to enhance emittance and reduce sensitivity to the angle of incidence for transverse magnetic (TM) polarization. (Barkhouse et al., 2015)proposed trilayer metal-insulator-metal (MIM) gratings consisting of W-SiO2-W, while (Valipour et al., 2022) investigated more general multilayer metal-dielectric gratings.

Perfect emittance at the designed wavelength was achieved for TM polarization through the excitation of surface plasmon polaritons (SPPs) and magnetic polaritons (MP). To enhance polarization insensitivity, (Pappalardo et al., 2022) investigated a deep grating that utilizes Wood's anomalies (WA), cavity resonances (CR), and SPPs. Recently, multilayer W-HfO2 metamaterial structures have demonstrated the capability for thermal emission control via topological transitions(Millikan, 1916). Additionally, (Martínez et al., 2007)filled a 2D tantalum photonic crystal with SiO_2 or HfO_2, achieving omnidirectional and as mentioned earlier, both SPPs and MPs have been utilized to enhance thermal emittance. However, these enhancements are achieved only for TM-polarized incident radiation. In general TPV applications, the incident radiation is randomly polarized, making both the transverse electric (TE) and TM responses important. Unfortunately, the methods used for controlling TM emittance do not work for TE; instead, cavity resonances

(CRs) are needed to boost thermal emittance for TE polarization. Moreover, gratings that can excite both SPPs and CRs (Nguyen-Huu et al., 2012) typically have their emittance peak in the visible range (0.4–0.8 μm), which corresponds to very high operating temperatures. Therefore, to enhance thermal emitters for infrared TPV applications, it is essential to develop strategies that allow for efficient TPV operation at lower emitter temp eratures.polarization-insensitive thermal emitters by leveraging CRs. The HfO2 dielectric in these structures shows promise for TPV applications due to its high melting point (3031 K).

2.6 Emitter Design

Hafnia is a high permittivity oxide with advantageous characteristics for selective emitters. HfO2 exhibits a very high refractive index (n ∼ 4) at short wavelengths and remains relatively stable, around n = 2, for wavelengths longer than 0.4 μm. Furthermore, the absorption coefficient—linked to the imaginary part of the refractive index is minimal in the optical and near-infrared ranges where TPV systems are expected to function (Yi Xiang Yeng, 2014). Additionally, hafnia has a large energy bandgap (Eg ∼ 6 eV) and, importantly for thermal emitters, a very high melting point of 3031 K, ensuring good thermal stability (Kar, 2013). Its thermal expansion coefficient is also compatible with tungsten (Knibbs, 1969), which is crucial for high-temperature operations. Recently, hafnia layers have been applied to photonic crystals to prevent degradation at elevated temperatures, providing experimental evidence of its potential for high-temperature applications.

The gratings examined in this study consist of a tungsten substrate, a hafnia spacer layer, and a tungsten grating, similar to the design proposed by (Kaur et al., 2023). Additionally, to better understand the underlying physics, a tungsten grating without the HfO2 spacer layer has also been simulated for comparison. To simulate the selective emitter discussed here, Helmholtz's equation is solved using the FEM method to determine the reflectance (ρ) and transmittance (τ). The absorptance (α) is calculated indirectly using energy conservation with the formula $\alpha = 1 - \rho - \tau$. Finally, the emittance is derived from Kirchhoff's law, which asserts that in thermal equilibrium, absorptance equals emittance ($\alpha = \varepsilon$). To achieve more accurate estimates of thermal emittance for selective emitters operating at high temperatures, we employed a temperature-dependent Drude model for tungsten (Minissale, Pardanaud, Bisson, & Gallais, 2017; Alabastri et al., 2013). The properties of HfO2 are sourced from (Padma Kumar et al., 2015). Additionally, both the electric and magnetic fields within the structures are determined using the finite element method.

2.7 Radiation emiter for photovoltaicell

A photovoltaic cell converts photons into electrical energy using semiconductor materials and the photovoltaic effect. When energy at least equal to the band gap energy (Eg) is supplied such as from a sufficiently energetic photon an electron or hole may cross the energy band gap. In designing a TPV emitter, it's essential to consider the energy band gap of the TPV cell, as each TPV cell has its unique band gap. In this context, researchers have focused on TPV cells with lower energy band gaps, corresponding to longer cut-off wavelengths, such as GaSb, InGaSb, and InGaAsSb, as indicated in Table 2.2.

Photovoltaic cells come in several types, each with distinct materials, structures, and efficiencies. The most common type is monocrystalline silicon cells, which are made from a single crystal structure of silicon. These cells are known for their high efficiency, typically ranging from 15% to over 22%, and their longevity, often lasting more than 25 years. They occupy less space compared to other types due to their higher power output, making them ideal for residential and commercial applications where space is limited. However, the manufacturing process is more complex and costly, which can increase the overall price of the systems. Another popular type is polycrystalline silicon cells, which are made from multiple silicon crystals. These cells are generally less efficient than monocrystalline cells, with efficiencies typically around 13% to 16%. The manufacturing process for polycrystalline cells is simpler and less expensive, leading to lower costs for consumers. While they require more space to produce the same amount of power as monocrystalline cells, they are a popular choice for larger installations, such as solar farms, where space is less of a concern. Their performance can be slightly affected by high temperatures, but they still provide a reliable option for solar energy generation.

Thin-film photovoltaic cells represent another category, made from layers of semiconductor materials such as cadmium telluride or amorphous silicon. These cells are lightweight, flexible, and can be produced in large areas, making them suitable for applications where traditional rigid panels may not be practical. However, their efficiency is generally lower, ranging from 10% to 12%, and they require more space to produce equivalent power output compared to crystalline silicon cells. They are particularly useful for building-integrated photovoltaics (BIPV) and portable solar applications. Additionally, TPV cells can vary in band gap energies, with examples like Ge (0.66 eV) and Si (1.1 eV).

The InGaAsSb cell is being considered as a potential replacement for GaSb cells in low-temperature TPV generators (H. Wang, Wang, et al., 2016). The proposed cut-off wavelength for the TPV cell under consideration ranges from 0.3 µm to 2.3 µm, making it broadband. This study specifically targeted three different PV cells: GaSb (1.8 µm), InGaAs (2.1 µm), and InGaAsSb (2.3 µm).

Table2.2: Thermophotovoltaic cells and cut-off wavelength

Cut-off wavelength/energy bandgap	TPVcells
InAsSbP	3 µm/0.4 eV
Si	1.1 µm /1.0 eV
InGaAs	2.1 µm /0.60 eV
GaSb	1.85/0.67 Ev
Ge	1.9 µm /0.66 eV
InGaAsSb	4 µm/0.4 eV

3. MATERIALS AND METHODS

This chapter discusses the materials and methodologies utilized. Section 3.1 outlines the materials, data analysis techniques, databases, and software employed. Section 3.2 details the methods used, including the finite element method (FEM), emphasizing design, optical calculations, and performance analysis.

3.1 Materials

This dissertation examines a range of metal and dielectric materials used in both experimental and computational data sofar used. Metals such as tungsten (W), molybdenum (Mo), and tantalum (Ta) are selected for computational analysis due to their exceptional optical and electrical properties, including high melting points, elevated emissivity at relevant wavelengths, and temperature stability. In contrast, hafnium oxide (HfO_2), aluminum nitride (AlN), and magnisiumdifloride (MgF_2) are identified as dielectric materials, while indium galium antimonide (InGaSb) and indium galium arsenide antimonide (InGaAsSb) serves as a semiconductor. These materials were chosen for their high dielectric constants, excellent thermal stability, minimal optical losses, high emissivity for thermal radiation, and insulating characteristics. The structure is designed as a metal-dielectric-metal configuration. The metamaterial model consists of refractory metal tungsten (W) at both the top and bottom layers, with hafnium dioxide (HfO_2) and aluminum nitride (AlN) serving as the dielectric spacer. Tungsten is chosen for high-temperature applications due to its melting point of approximately 3722 K, hafnium oxide has a melting point of around 3031 K and aluminum nitride has melting point of 3273K exhibits good oxidation resistance. Additionally, aluminum (A) and molybdenum (Mo) are used as substitutes for tungsten (W), while aluminum nitride (AlN) and magnsium floride (MgF_2) replace HfO_2 for comparison purposes.

3.2. Numerical Simulation

Numerical simulations were conducted using COMSOL Multiphysics software. This software is designed to help engineering, manufacturing, and scientific research organizations manage physics-based modeling by verifying and optimizing processes and devices. The platform allows users to develop custom modeling workflows and supports data exchange between various models, including those related to electromagnetics, heat transfer, structural mechanics, and fluid flow. COMSOL Multiphysics offers geometry modeling tools, including solids, curves, surfaces, and Boolean operations, along with the ability to define process sequences for data editing and parametric studies. The software provides a variety of features such as virtual operations, CAD data import, predefined physics interfaces, both automated and manual meshing, and 2D/3D modeling capabilities. Additionally, it includes visualization and post-processing tools that allow researchers to view simulation data through interactive graphics, charts, and figures, and to export results in formats like text, DAT, CSV, and Excel. Research professionals can also create custom modeling applications and share them with process operators, testing labs, manufacturing departments, or clients.

The design parameters include w (width of the unit cell), h_1 (height of the top tungsten layer), h_2 (thickness of the dielectric), h3 (thickness of the ground tungsten layer), b_1 (base length), and b_2 (base width). The optical properties of air are given as n = 1, while tungsten (W) and hafnium oxide (HfO_2) have melting points of 3695 K and 2883 K, respectively. A nano-MDM was created with a tungsten base and top, forming a metal-dielectric-metal structure. The COMSOL Multiphysics software was employed for three-dimensional electromagnetic wave and wavelength domain analysis. To reduce reflections, perfectly matching layers were applied to the top and bottom of the computational domains, or along the z-axis, during the simulation. Periodic boundary conditions were set at the right and left edges to simulate an infinite flat surface on the emitter and accommodate oblique incidence. It is assumed that the electromagnetic waves or incident light on the emitter are perpendicular to the x-y plane throughout the working wavelength.

The refractive index (optical properties) of tungsten (W) and aluminum nitride (AlN) at the working wavelength were obtained from the software's default material database. The following are setup of simulation for constructing the proposed geometry: 3D, Optics, Wave optics, EMWFD, Add, Study, Wavelength domain, and done. During the simulation, a Perfectly Matched Layer (PML) is applied to the top and bottom of the computational domains to reduce reflections. This virtual layer surrounding the physical area of interest employs advanced coordinate scaling through the Perfectly Matched Layer node. When properly configured, this layer absorbs all outgoing wave energy in frequency-domain problems without causing impedance mismatches at the boundary, which would lead to unwanted reflections. A Perfectly Matched Layer is created by selecting it from the Definitions toolbar. Each distinct PML area requires its own Perfectly Matched Layer node, meaning all PML domains must be connected to use the same node; otherwise, the PMLs will not operate effectively. The electromagnetic properties, including the Periodic Boundary Condition and Scattering Boundary Condition, are established through numerical simulation. The Periodic Boundary Condition creates a pattern between the specified limits. The Destination Selection sub-node can be accessed via the context menu (by right-clicking the parent node) or through the Attributes menu on the Physics toolbar. The Scattering Boundary Condition is designed to make a boundary transparent to scattered waves. It is also transparent for incoming plane waves, which is configured using the scattering boundary condition from the physics toolbar Port and scattering parameter.

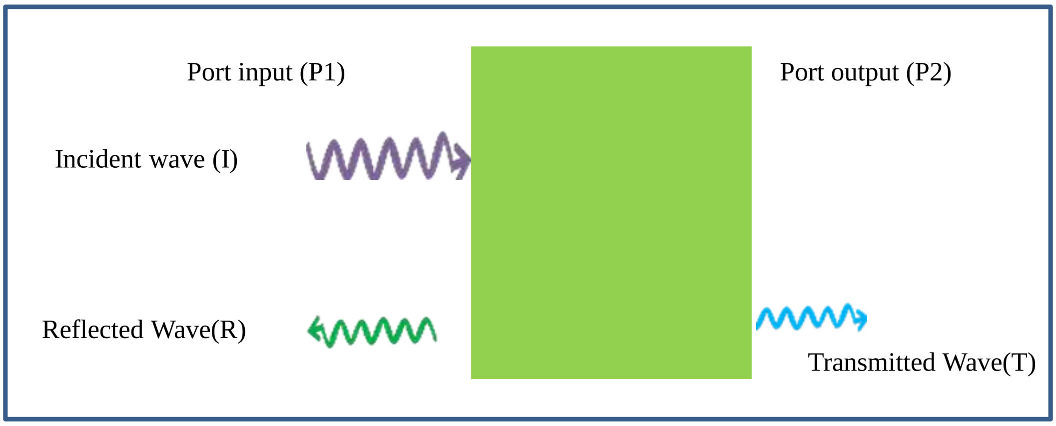

Figure 3.1: Showing port and scattering parameters. Port input (P1) the left hand side, Port output (P2) the right hand side. Incident wave (I) reflected wave (R), and transmitted wave (T)

Two ports were considered in the numerical analysis. The first, generating electromagnetic waves, was referred to as the "in-port," and the second was called the "out-port." When an electromagnetic wave strikes a plane, it can be absorbed, reflected, or transmitted. Ultimately, the simulation results were utilized to determine emissivity from absorptivity. When developing a COMSOL model, there are several factors to consider. Notably, regularity should be employed as frequently as possible, as it can significantly reduce the simulation runtime.

3.2.1 Designing Spectral Matching and Absorption Calculations

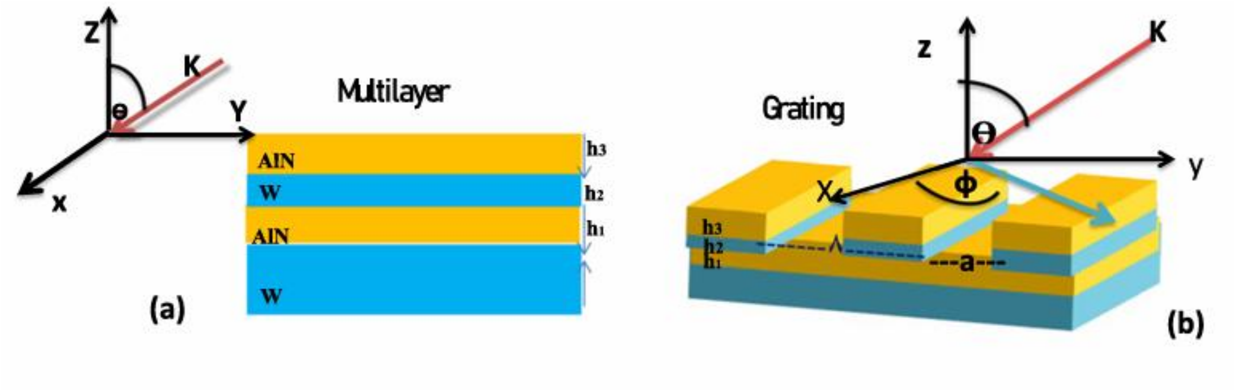

Figure 3.2: Design of metamaterial emitter for COMSOL Multiphysics simulation using (a) mult-layers and (b) grating

The ability of a material system to absorb, reflect, or transmit electromagnetic waves is influenced by structural factors as shown in Figure 3.2, 3.3 and 3.5, including the size, shape, geometry, arrangement, thickness, and composition of its elements. To simplify various complexities, such as fabrication challenges, a three-layer structure was created seen figure 3.3. Three distinct types of structures have been designed, each tailored for specific applications. The structures design includes a three-dimensional (3D) L-shaped, muit-layer and grating as illustrated in Figure 3.2 and 3.3, respectively used for the emitters TPV application; a 3D swastika shape, depicted in Figure.3.5, utilized for the detection of harmful gases.

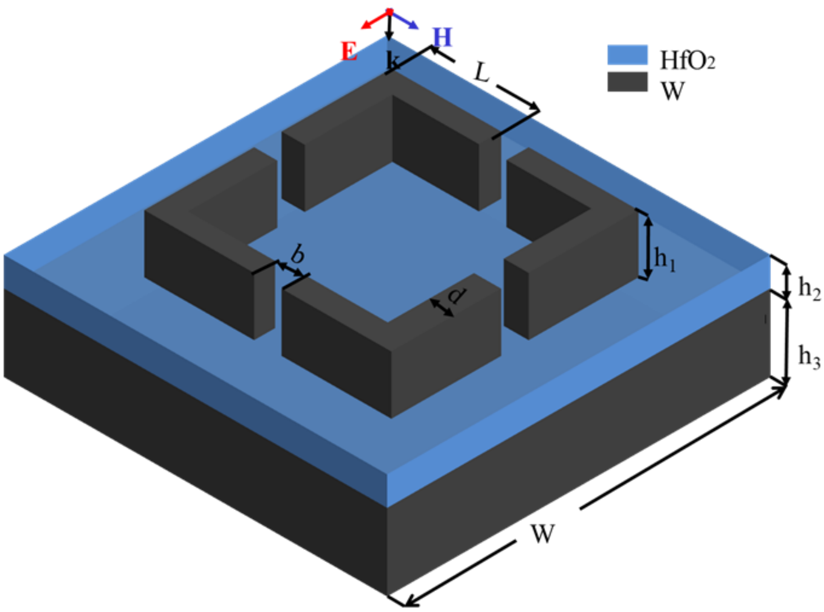

Figure 3.3: Design of metamaterial emitter for COMSOL Multiphysics simulation using three layers (tungusten-hafiniumdioxide-tungusten).

The primary goal of this method is to measure the amount of radiation absorbed by the designed structure. As illustrated in Fig. 3.4, periodic boundary conditions are implemented in both the x and y directions for the unit cell, with a plane wave of 1 W power directed along the z-axis towards the specified structures. Consequently, the incoming light is perpendicular to the x-y plane. Reflected waves (R) are captured by placing a wavelength domain field monitor above the source. To reduce reflections during numerical analysis, a perfectly matched layer is installed at both the top and bottom of the computational domain.

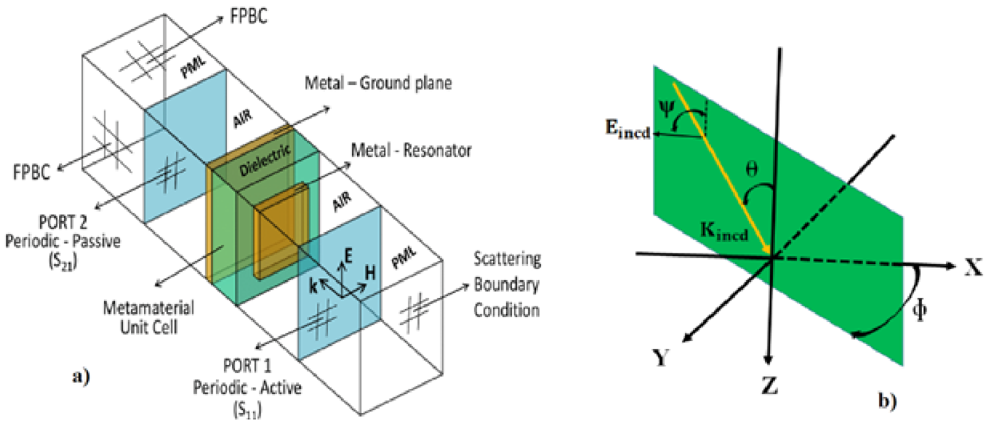

Figure 3.4: a) MDM model simulations in 3D. b) Incoming plane wave

Additionally, periodic Bloch boundary conditions were implemented on the left and right boundaries to simulate an infinitely flat surface on the absorber. The finite element method (FEM) was utilized to quantitatively analyze the differential form of Maxwell's equations. COMSOL Multiphysics and Origin software were employed for structural design, computations, and parameter analysis. In the designed structures, effective coupling between various resonant modes arising from the intended structure is essential for assessing absorbance and reflectivity across the examined range, which extends from ultraviolet to far-infrared. This method relies on electromagnetic losses, which encompass impedance-matching losses, resonance-related losses, and material-specific losses. The first theory suggests that the impedance of metamaterials can be aligned with the surrounding environment by modifying their permeability and permittivity. When electromagnetic radiation interacts with the metamaterial structure, it penetrates the dielectric layer and gradually diminishes as it approaches the metallic layer beneath. The metal layer reflects the remaining energy, resulting in further attenuation as the wave continues to travel through the structure.

Another type of resonance occurs when an electromagnetic wave travels along the interface between a metal and a dielectric material (such as air or glass), coupled with the collective oscillations of the metal's free electrons. Additionally, a resonance mode known as magnetic polariton arises when an electromagnetic wave interacts with a magnetic dipole moment in a structured material made of alternating metal-dielectric-metal layers. Some of the energy carried by electromagnetic waves is inevitably converted into heat. The primary function of the dielectric layer is to absorb these incoming waves. Within the resonator, the waves oscillate at the absorber's resonance frequency, facilitating efficient energy dissipation. Overall, in this study, the metamaterial structures are designed with three layers, and their optical properties are derived from these three resonances.

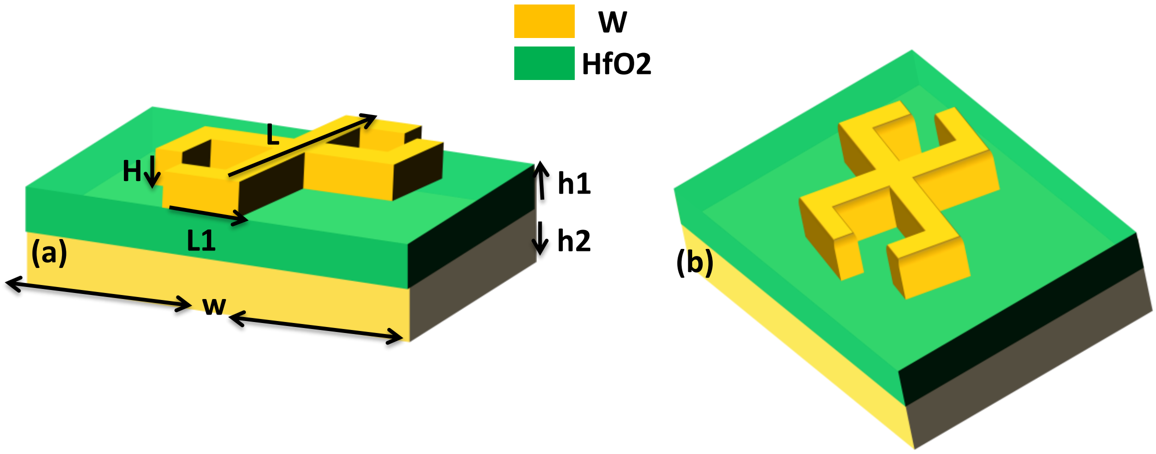

Figure 3.5: Schematic unit cell (a) side view (b) top view

The incident radiation is assumed to be linearly polarized and is characterized by the incident wave vector, defined by the polar angle θ, the azimuthal angle ϕ, and the polarization angle ψ in relation to the plane of incidence. Here, ψ indicates the angle between the electric field E and the plane of incidence, while ϕ represents the angle between the plane of incidence (which contains the z-axis and the incident wave vector) and the x z plane. The incident plane wave, whichpropagates through space, has the wave vector $K_{incd} = (K_{x,incd}, K_{y,incd}, K_{z,incd})$ where $K_{x,incd}=k_0 n_{air} \sin\theta \cos\phi$, $K_{y,incd}=k_0 n_{air} \sin\theta \cos\phi$ and $K_{z,incd}=k_0 n_{air} \cos\theta$. In this context, λ_0 refers to the wavelength in a vacuum, and nair represents the refractive index of air. The radiation source travels through the air, with the free-space wave vector defined as $K_0 = 2\pi\lambda_0$. An incident wave at a polarization angle ψ can produce transverse magnetic (TM) waves when ψ = 0° and transverse electric (TE) waves when ψ = 90°. These two polarizations are fundamental components from which all other polarizations can be derived. Ultimately, after collecting the reflected waves (R), the directional absorbance can be calculated using Equation (2.46).

4. RESULTS AND DISCUSSION

Section 4.1 focuses multilayer and gratting metamaterial structure for light control in thermophotovoltaics using tungsten aluminum nitride metamaterials. Section 4.2 addresses the Optimizing light control in thermophotovoltaics using W-HfO2 Metamaterials considering factors such as structure, incident angle, and conversion efficiency. Section 4.3 explores the efficient gas sensor based on a narrow-band IR metamaterial. Finally, Section 4.4 covers validation and verification processes. This research explores how a special layered structure made of tungsten and hafnium dioxide / aluminium nitride can bo ost light absorption and emission for thermophotovoltaic (TPV) devices. The goal is to help convert thermal energy into electricity more efficiently by tuning the materials to emit and absorb light at specific wavelengths that match the photovoltaic cells used. The main goal of the study was to assess the electromagnetic and thermal emission characteristics of a newly designed multilayer W/HfO_2 or AlN /W metamaterial intended for thermophotovoltaic (TPV) applications. Through numerical simulations employing finite element methods, this study's primary contribution is its novel emitter designs and o ptimization methods, which work in concert to improve the performance and scalability of Thermophotovoltaic systems.

4.1 Multilayer and grating designs of W-AlN emitters for optimal Performance in TPV systems

This study reveals that some cool designs for tungsten–aluminum nitride emitters aimed at boosting thermophotovoltaic (TPV) systems. TPVs turn heat into electricity, which is awesome for grabbing energy from waste heat or renewable sources. The study looks at two designs: a layered stack and a grating structure, using smart optimization and simulations to get the best thermal emission match for InGaSb solar cells as shown in figure 4.1. The results show high thermal emission with little directional variation, meaning better power output and efficiency. Aluminum nitride (AlN) is selected as a dielectric material due to its exceptional properties, including high thermal stability and thermal conductivity, which make it suitable for high-temperature applications like thermophotovoltaic systems. These characteristics enable efficient heat dissipation and durable performance under extreme conditions. finite element method (FEM) were employed to optimize the design of thermal emitters and perform detailed comparative analysis of their performance. Concurrently, the FEM approach was used to accurately simulate the thermal emittance and radiative properties of these designs, ensuring reliable evaluation of their performance. This combined methodology allowed for the strategic refinement of emitter architectures, balancing practical manufacturability with enhanced energy conversion efficiency in thermophotovoltaic applications.

4.1.1 Comparative Spectral emittance for the grating and multilayer structure

In the results presented in Figure 4.1, the typical emittance profiles for the grating structure are shown for both transverse electric (TE) and transverse magnetic (TM) polarizations, represented by the green dashed and blue dotted lines, respectively

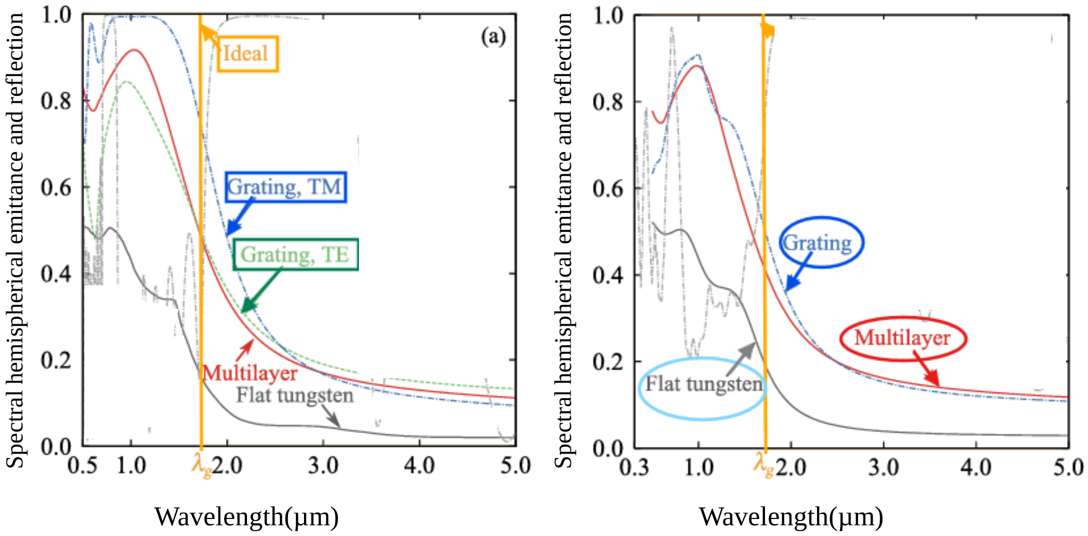

Figure 4.1: (a) Typical emittance of the grating for transverse electric (TE) polarization (green dashed line) and transverse magnetic (TM) polarization (blue dotted line) of the incident radiation, along with the emittance of the planar multifacet structure (red solid line) (b)

Comparison of the hemispherical emittance for the grating (blue) and planar multifacet (red solid line) structures. In both figures, the optimal emitter (orange solid line) with λg = 1.72 μm, as well as the planar tungsten emitters (black solid line) and the reflectance of the photovoltaic (PV) channel (light gray dotted line), are included for comparison. These profiles indicate that the grating exhibits broad spectral response with high emittance values across a wide range of wavelengths, which enhances its ability to efficiently emit thermal radiation. When compared to the planar multifacet structure (red solid line), the hemispherical emittance (Figure. 4.1b) reveals that the grating achieves superior broadband emission, approaching the optimal emitter performance (orange solid line) with a characteristic cut wavelength = 1.72 μm. Notably, both structures demonstrate high emittance near the target wavelength of the photovoltaic (PV) cell, aligning well with the spectral response. The black solid line representing planar tungsten emitters and the light gray dotted line showing the PV reflectance serve as important benchmarks; these comparisons validate that the grating design offers significant improvements over simple planar configurations. Overall, the analysis confirms that the engineered grating structure effectively harnesses resonance mechanisms, such as surface plasmon polaritons and Fabry–Perot resonances, to maximize hemispherical emittance, thereby optimizing the emitter's performance for thermophotovoltaic applications.

4.1.2 Comprehensive analysis of the angular emittance behavior for the multi-layer emitter structure

The results depicted in Figure 4.2 provide a comprehensive analysis of the angular emittance behavior for the multi-faceted emitter structure under both TE (a) and TM (b) polarizations across various angles of incidence.

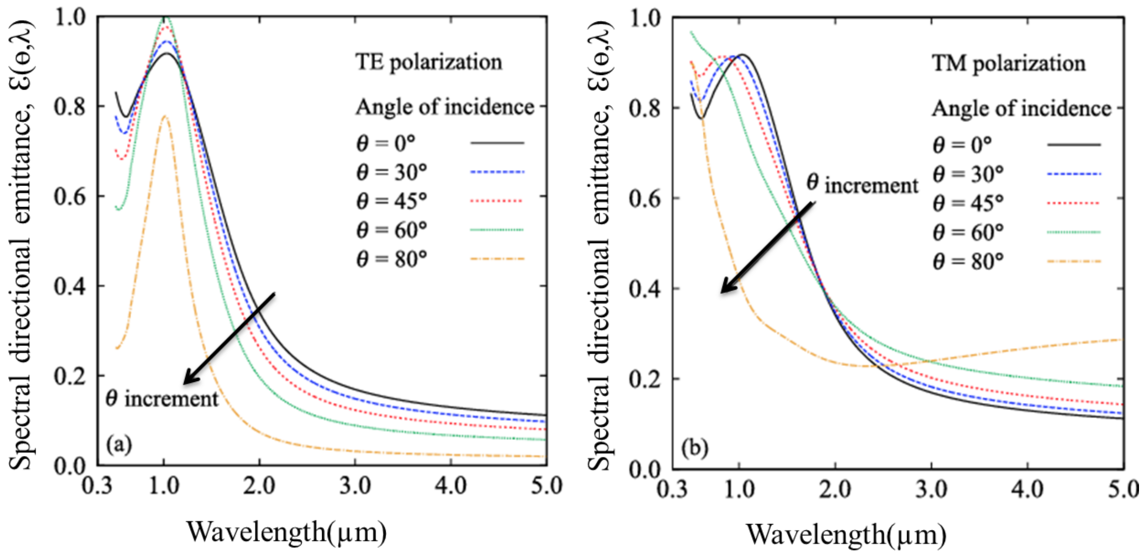

Figure 4.2: Angular emittance for multiple facets for both transverse electric TE (a) and transverse magnetic TM (b) polarizations for five unique points of rate (θ = 0°, 30°, 45°, 60°, and 80°).

The plots illustrate that the emittance remains exceptionally high above 90% for TE polarization and similarly robust for TM polarization up to approximately 60°, indicating that the emitter maintains near-omnidirectional emission performance over a broad angular range. This angular independence is critically important for thermophotovoltaic (TPV) applications, where incident radiation may arrive from multiple directions. Notably, at higher angles approaching 80°, a slight decrease in emittance is observed, yet the values still remain significantly elevated, suggesting minimal sensitivity to angular variations. The consistency of high emittance across these diverse angles underscores the effectiveness of the multi-faceted design in promoting omnidirectional thermal emission, which can enhance overall device efficiency by capturing and emitting radiation more uniformly. Additionally, the comparative analysis between TE and TM polarizations reveals that the structure sustains high emittance regardless of polarization state, further affirming its suitability for practical TPV systems where polarization effects may fluctuate. Overall, these findings highlight the multi-faceted emitter's capability to deliver stable, broad-angle high emittance, a desirable trait that can lead to improved energy conversion efficiency in thermophotovoltaic devices.

4.1.3 Electric and magnetic field distribution

The results presented in Figure 4.4 illustrate the electric and magnetic field distributions, specifically the magnetic field components Hy and Hz, within the grating structure for TE polarization at three significant incident angles: 0°, 60°, and 80°. These field profiles are critical for understanding the resonance mechanisms underlying the high emittance behavior observed .At $\theta = 0°$ (Figures 4.4a and 4.4d), the field distribution reveals strong confinement and pronounced electric field enhancement within specific regions of the grating. These localized field intensities are indicative of resonant modes, such as surface plasmon polaritons (SPPs) or Fabry–Pérot (FP) resonances, which facilitate efficient electromagnetic coupling and lead to elevated emissivity at this frequency. The magnetic field Hy shows a concentrated distribution, supporting the existence of standing wave patterns associated with these resonances.When examining $\theta = 60°$ (Figures 4.3b and 4.3e), a noticeable shift in the field localization occurs, with the fields spreading over broader regions, suggesting the excitation of different resonance modes or a change in mode confinement due to the oblique incidence. Despite this shift, the fields still significantly interact with the grating structure, maintaining high emission efficiency. At $\theta = 80°$ (Figures 4.3c and 4.3f), the field patterns demonstrate further lateral spreading and reduced intensity within the grating's features. Nevertheless, the fields remain sufficiently strong to sustain high emittance, confirming the structure's robustness across a wide angular range. The persistence of resonant field distributions at this angle underscores the design's effectiveness in producing omnidirectional emission. Overall, these field profiles elucidate how the grating's resonances primarily driven by electric and magnetic field interactions are responsible for the broadband and angle-insensitive high emittance observed. The detailed visualization of Hy and Hz at various incident angles supports the conclusion that carefully engineered resonances can enable omnidirectional thermal emission, which is essential for optimizing TPV system performance.

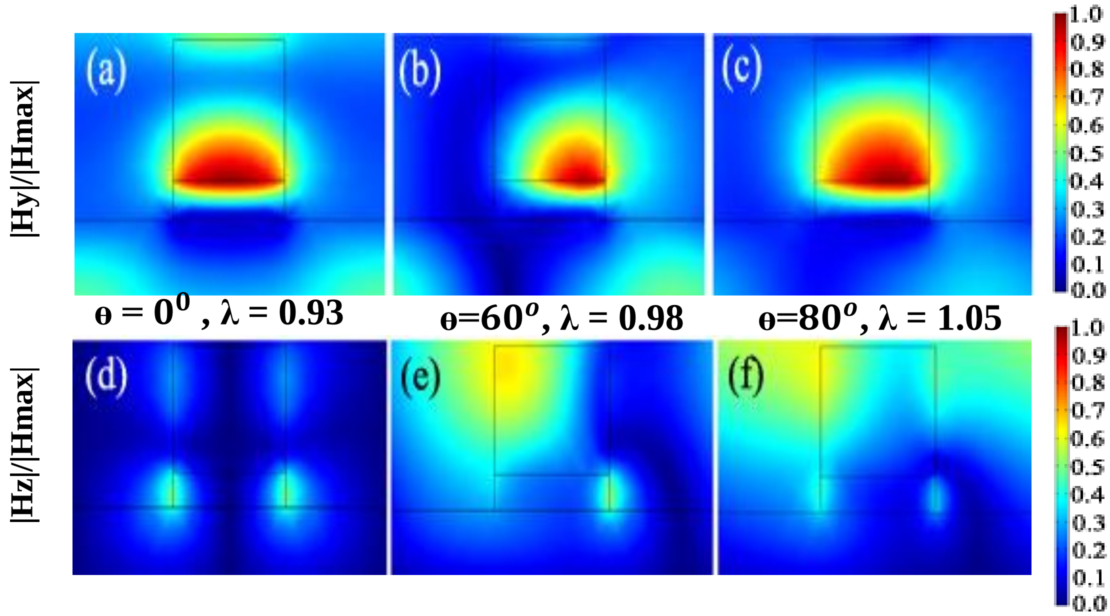

Figure 4.3**:** Standardized attractive field parts (H_y and H_z) in the grating structure for transverse electric TE polarization. Three (3) points of angles are considered θ = 0° for (a) and (d), θ = 60° for (b) and (e), and θ = 80◦ for (c) and (f) for the frequencies that fit the pinnacles of Fig. 4.2 (a).

Figure 4.4 illustrates the distribution of the electric field components Ez and Ey within the grating structure under transverse magnetic (TM) polarization at three distinct angles of incidence: 0°, 60°, and 80°, corresponding to the points explored in the study. At θ = 0° (Figures 4.4a and 4.4d), the electric fields exhibit a strong concentration within the top AlN layer, indicating dominant resonance activity at normal incidence, which facilitates efficient photon coupling and enhances hemispherical emittance. As the incidence angle increases to 60°, the field distributions reveal shifts in resonance patterns, with Ez and Ey components adapting to the change in wavevector orientation, leading to more complex interference effects. At 80° (Figures 4.4c and 4.4f), the electric fields demonstrate localized resonance modes near the grating features, with pronounced field intensities indicating strong surface interactions and potential excitation of surface plasmon polaritons (SPPs). These observations underscore how the electric field behavior dynamically adapts with incident angle, contributing to the broadband and omnidirectional emission characteristics of the grating. The detailed field profiles at resonant frequencies reveal critical insights into the underlying physical mechanisms such as FP resonances and

SPP excitation that enable the high emittance and spectral selectivity essential for efficient TPV applications

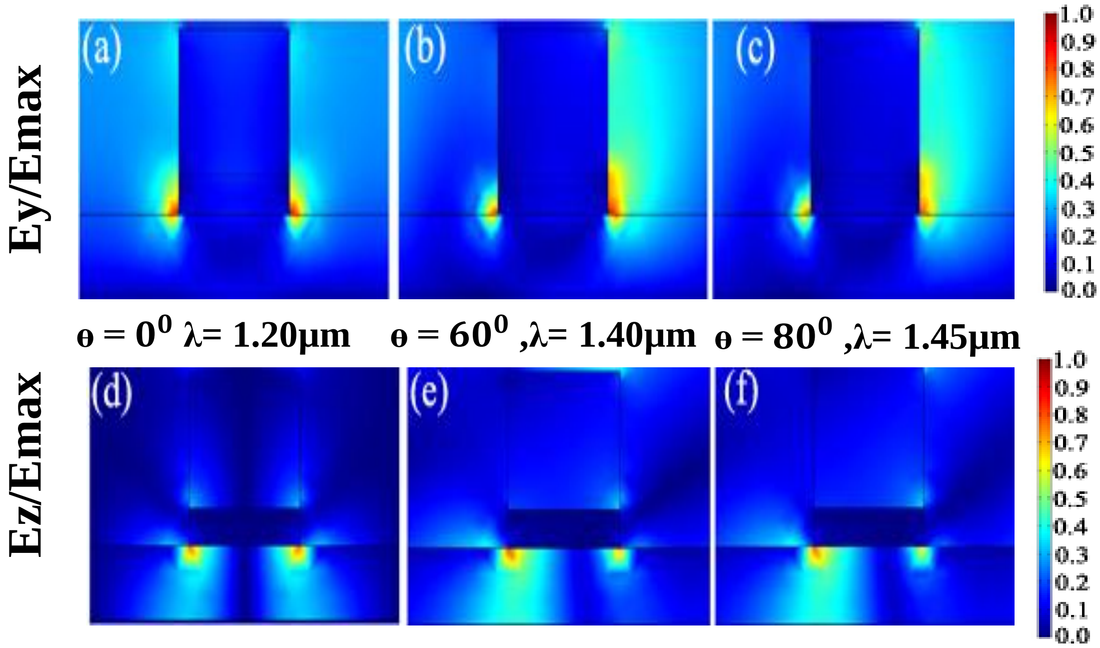

Figure 4.4**:** Standardized electric field parts (Ey and Ez) in the grating structure for transverse magnetic TM polarization. Three (3) points of the rate are considered θ = 0° for (a) and (d), θ = 60° for (b) and (e), and θ = 80◦ for (c) and (f) for the frequencies that fit the pinnacles.

Generally, the study demonstrates the successful design and optimization of tungsten–aluminum nitride (W-AlN) based thermal emitters, specifically a planar multifaceted stack and a grating structure, aimed at enhancing thermophotovoltaic (TPV) system performance. Through rigorous numerical simulations and genetic algorithm-based optimization, both designs achieved high hemispherical thermal emittance that closely matches the spectral response of InGaSb photovoltaic cells, while maintaining minimal angular dependence, particularly in the grating structure. The results reveal that the grating emitter not only exhibits superior broadband resonance behavior driven by surface plasmon polaritons and Fabry–Pérot resonances but also delivers higher output power, efficiency, and power density across various temperatures and material thickness variations. These findings underscore the potential of engineered W-AlN emitters to significantly improve TPV energy conversion efficiency, offering scalable, thermally stable, and fabrication-friendly solutions for advanced energy harvesting applications.

4.2 Optimizing light control in thermophotovoltaics using W-HfO2 Metamaterials

This study explores how tungsten–hafnium dioxide metamaterials can be engineered to enhance light absorption and emission in thermophotovoltaic (TPV) systems. By tailoring the optical properties of these materials, the research aims to improve energy conversion efficiency, enabling more effective harvesting of thermal radiation. The focus is on optimizing spectral selectivity and thermal stability, making these metamaterials promising candidates for high-performance TPV applications. Figure 3.3 illustrates a metamaterial emitter composed of tungsten and hafnium oxide (HfO_2), created using COMSOL Multiphysics software. A 3D spatial dimension was employed for the working environment. The optical interface was used to calculate the electric and magnetic fields for our system, which operates at wavelengths comparable to or smaller than the analyzed device. The EMWFD interface was selected to solve for time-harmonic electromagnetic field distributions. The Wavelength Domain study calculated the model's response to harmonic excitation at one or more wavelengths, determining the structure's transmission and reflection characteristics in relation to wavelength during electromagnetic wave propagation through the designed structure.

The numerical simulations revealed that the W/HfO_2/W multilayer metamaterial demonstrates outstanding emissivity characteristics within the desired wavelength range of 0.3–2.2 μm. The average emissivity exceeds 96%, peaking at 99.9% specifically in the 1.5–2.0 μm range, which aligns with the spectral needs of high-efficiency InGaAsSb TPV cells. This high level of emissivity is mainly due to resonant absorption mechanisms, such as surface plasmon polaritons (SPPs) and magnetic polaritons, which are precisely optimized through careful adjustments of geometry and materials. Additionally, the metamaterial exhibits stable emissivity profiles across incident angles from 0° to 60°, showing resilience under diverse operational conditions and insensitivity to the polarization states of incoming radiation. This independence from polarization is due to its symmetric and periodic design, which guarantees consistent electromagnetic interactions regardless of the polarization orientation.

4.2.1 Effect of Structural Height on the Emissivity of designed Metamaterials

The electromagnetic and thermal radiative properties of metamaterials are intricately linked to their geometric configurations. Particularly, the height of metallic and dielectric layers parameters such as h_1 play a crucial role in tailoring the resonance mechanisms and, consequently, the spectral emissivity of metamaterial structures designed for thermophoto voltaic (TPV) applications. Figure 4.5 in the current study visually encapsulates the relationship between the height h_1 of the W (tungsten) component in the multilayer MDM structure and the resulting emissivity profile, offering insights into how variations at the nanoscale influence macroscopic optical properties.

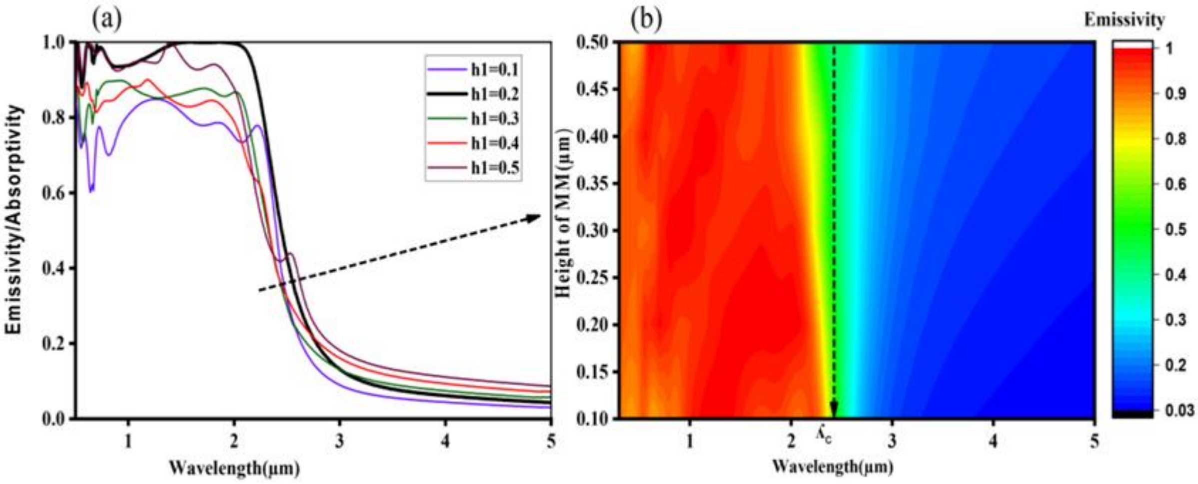

Figure 4.5: (a) Impact of height (h_1) on the spectral emissivity of the proposed nano-MDM metamaterial with h1 = (0.2–0.6) µm. (b) Emissivity of MDM by using a contour fill counterpart.

This section provides an in-depth analysis of the impact of h_1 on the broadband emissivity characteristics of the proposed structure, supported by simulation data and physical reasoning. The height h_1 refers to the thickness of the tungsten (W) layer adjacent to the dielectric spacer (HfO_2) in the nano-MDM stack. This parameter significantly affects the electromagnetic response, particularly the excitation and coupling of surface plasmon polaritons (SPPs) and magnetic polaritons (MPs). These modes are responsible for the enhanced absorption and emission at specific wavelengths due to their resonant nature.

4.2.2 Effect of Spacer Thickness (h_2) on Spectral Emissivity and Reflectivity of the Designed MDM Metamaterial

As dippicted in figure 4.6 a comprehensive analysis of how varying the spacer thickness (h_2) influences the electromagnetic response of the designed metal-dielectric-metal (MDM) metamaterial, specifically focusing on spectral emissivity and reflectivity across the relevant wavelength range. The figure is divided into two parts: (a) illustrating the effect on emissivity and (b) depicting the impact on reflectivity. Such a study is fundamental in tailoring the optical properties of metamaterials for applications like thermophotovoltaic (TPV) devices, where precise control over emissivity and reflectivity properties directly correlates with device efficiency.

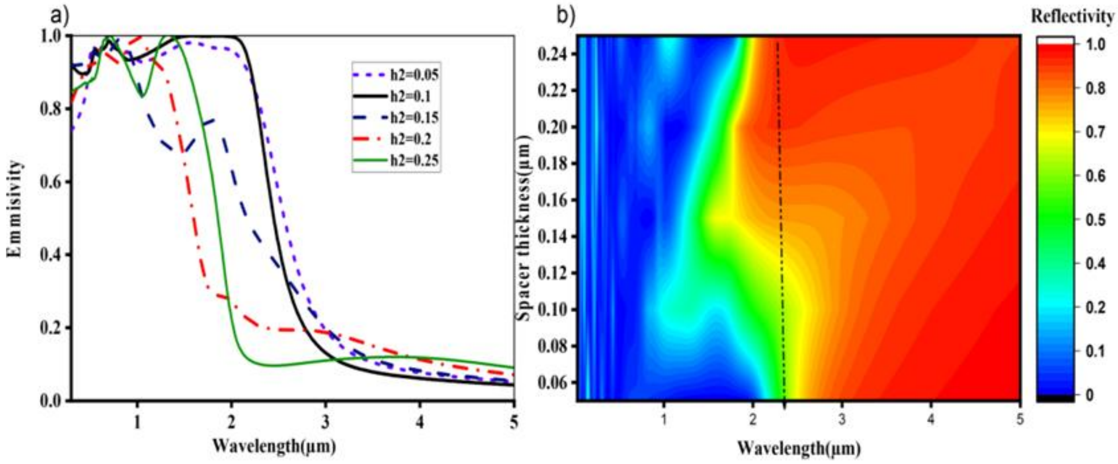

Figure 4.6: Effect of spacer thickness (h2) on the spectral (a) emissivity and (b) reflectivity of the designed MDM metamaterial.

The variation of spacer thickness h_2 significantly influences the emissivity profile of the metamaterial. As h_2 increases from 0.1 μm to 0.25 μm, the spectral emissivity within the wavelength range below the cutoff (~2.2 μm) exhibits notable changes. When h_2 is at the lower end of this range (around 0.1 μm), the emissivity profile shows relatively high and stable values across the spectrum, nearing broadband emissivity above 0.05 μm. This indicates strong resonant absorption facilitated by surface plasmon polaritons and magnetic polaritons associated with the thin spacer layer. The resonance modes are efficiently excited owing to the tight coupling between the metal and dielectric layers, leading to enhanced thermal emission in the targeted spectral range.

As the spacer thickness increases, the peak emissivity within the spectrum tends to diminish. Specifically, at h_2 = 0.15–0.25 μm, the overall emissivity reduces gradually. This trend suggests that thicker dielectric spacers weaken the electromagnetic coupling between the metallic layers, causing a detuning of the resonance modes that underpin high emissivi ty. Consequently, the spectral absorption and thus the thermal emission characterized by the emissivity becomes less effective.This behavior underscores the importance of the spacer thickness in optimizing the resonance conditions critical for high emissivity. Thinner spacers serve to sustain strong magnetic and surface plasmon resonances, resulting in enhanced electromagnetic field confinement and absorption. Conversely, increasing the spacer thickness shifts the resonance conditions away from the optimal, degrading the broadband emissivity essential for efficient TPV energy conversion. The reflectivity spectrum exhibits trends complementary to the emissivity profile, consistent with Kirchhoff's law of thermal radiation, which states that emissivity and absorptivity are equal at thermal equilibrium. When h_2 is minimal (~0.1 μm), the reflectivity remains relatively low across the wavelength spectrum, indicating high absorption and emissivity.

This low reflectivity corresponds to the effective excitation of resonant modes that trap incident electromagnetic energy within the metamaterial. As the spacer thickness increases, the reflectivity in the relevant spectral band progressively rises, coinciding with the decrease in emissivity. This rise in reflectivity results from the weakened resonant coupling, reducing the absorption efficiency. At higher h_2 values (~0.25 μm), the reflectivity peaks, signifying that a larger portion of incident radiation is reflected rather than absorbed and emitted. The increase in reflectivity agrees with the diminished electromagnetic fields at the resonant frequencies, as the thicker dielectric spacer hampers the formation of localized modes like magnetic polaritons that are responsible for high absorption.Furthermore, understanding the sensitivity of optical properties to h_2 allows for precise engineering of the electromagnetic response, enabling the development of tailored metamaterials with desired emissivity spectra. Small variations in spacer thickness can lead to significant changes in performance, emphasizing the need for accurate fabrication processes. In conclusion, Figure 4.6 underscores that spacer thickness h_2 is a vital control parameter in the electromagnetic design of MDM metamaterials. A thinner spacer enhances field confinement, resonant absorption, and broadband emissivity, while a thicker spacer tends to diminish these effects, increasing reflectivity and decreasing emissivity. The insights gained from this analysis facilitate the systematic tuning of metamaterial parameters to achieve optimal thermal emission characteristics for high-efficiency TPV systems or other photonic applications. Future research may explore the combined effects of spacer thickness with other geometrical and material parameters to further refine and optimize the spectral response of such metamaterials.

4.2.3 Influence of Periodic Unit Cell Widths on Spectral Absorptivity and Emissivity of the Metamaterial Emitter

A detailed examination of how variations in the periodic unit cell width influences the optical properties specifically the absorptivity and emissivity—of the proposed metal-dielectric-metal (MDM) metamaterial emitter provided in figure 4.7. The figure is divided into two parts: (a) presents the absorptivity/emissivity spectra for different unit cell widths, and (b) visualizes the emissivity distribution across the spectral range using contour mapping, comparing regions below and above the cutoff wavelength (~2.2 μm). This analysis is pivotal to understanding the role of geometric scaling in tailoring the spectral characteristics essential for applications such as thermophotovoltaic (TPV) devices.

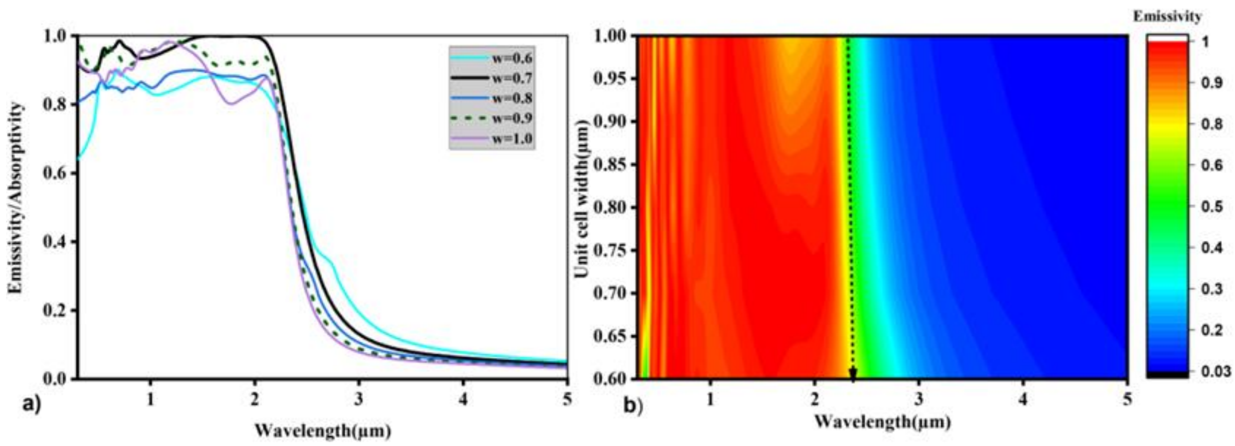

Figure 4.7: (a) Absorptivity/emissivity of the emitter with various unit cell widths and (b) emissivity of the emitter using a contour fill counterpart below and above the cutoff wavelength.

Absorptivity and emissivity are intrinsically linked through Kirchhoff's law of thermal radiation, stipulating that, at thermal equilibrium, these two properties are equal and wavelength-dependent. Consequently, manipulating the unit cell width directly affects the resonant electromagnetic modes supported by the metamaterial structure, thereby shaping the spectral distribution of thermal emission. In Figure 4.7(a), the spectral absorptivity/emissivity is plotted for unit cell widths ranging between 0.6 μm to 1.0 μm. An increase in the unit cell width initially correlates with an improvement in average emissivity below the cutoff wavelength (~2.2 μm). Specifically, as the periodicity increases from 0.6 μm to approximately 0.7 μm, the spectral features become more pronounced, and the broadband emissivity approaches an optimal level within the targeted spectral window. This enhancement is attributable to the augmentation of resonant electromagnetic modes, notably magnetic polaritons (MPs) and surface plasmon polaritons (SPPs), which are highly sensitive to the geometric dimensions of the structured surfaces. However, beyond the 0.7 μm threshold, a reversal in trend occurs. The average emissivity begins to decline as the unit cell width approaches 0.9 μm. This reduction is related to the dispersive properties of the resonant modes, which are strongly dependent on the periodicity. Larger periodicities tend to shift the resonance frequencies to longer wavelengths, potentially outside the desired spectral window, thereby diminishing the spectral match with the targeted emission range.

Additionally, broadening of the spectral features and decreased coupling efficiency at larger periods can lead to lower overall absorption and emissivity in the critical wavelength range.The interplay between periodicity and resonance excitation underscores the importance of optimal structuring. For the designed MDM emitter, a unit cell width around 0.7 μm appears to maximize broadband emissivity, facilitating enhanced electromagnetic confinement and mode excitation within the desired spectral region. These results align with the theoretical understanding that periodic structures can be engineered to support specific photonic modes, which strongly influence the thermal emission characteristics.

4.2.4 Correlation of Spectral Emittance, Reflectance, and Transmittance in MDM Emitters

The term "spectral emittance" refers to an effective measure of the confident emissive capacity of the metamaterial, accounting for absorptive and reflective contributions. A comprehensive analysis of the optical electromagnetic response of the proposed metal-dielectric-metal (MDM) metamaterial emitter, central to understanding its spectral emissive properties are provides in figure 4.8. It elucidates the intricate interplay between spectral emittance, reflectance, and transmittance, and further distinguishes the polarization dependence of these characteristics through processed spectral emittance data for Transverse Magnetic (TM) and Transverse Electric (TE) polarizations. Such a detailed examination is pivotal within the context of designing metamaterials for thermophotovoltaic (TPV) applications, where spectral selectivity, polarization insensitivity, and high emissivity are critical performance parameters.

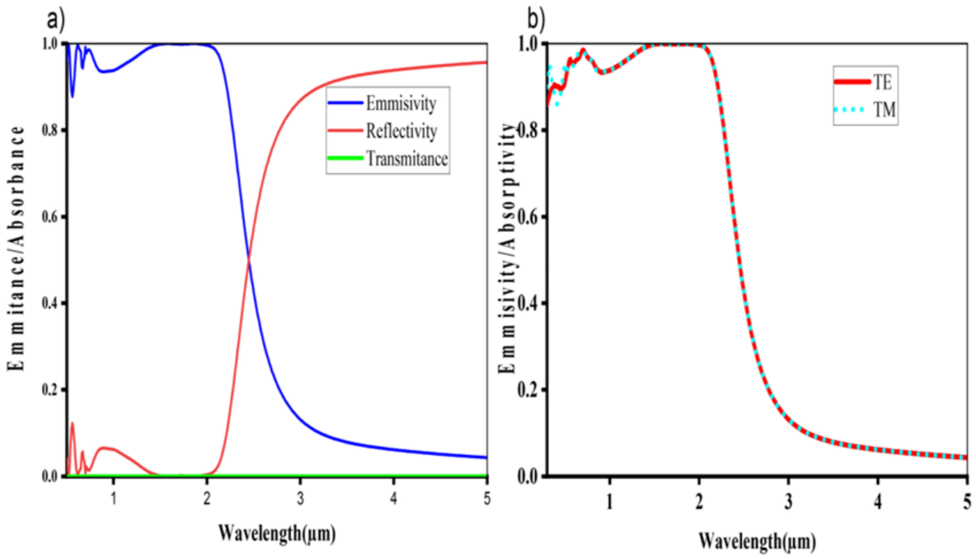

Figure 4.8: (a) Relationship between Spectral emittance, reflectance, and transmittance for a designed MDM emitter (b) Analyzed spectral emittance for TM and TE polarizations

4.2.5 Analysis of electricomagnetic field distribution

To support the claim that magnetic polaritons play a role in the broad absorption seen in the W/HfO2/W metamaterial, we examined the electromagnetic field distributions within the structure across various wavelengths. Utilizing numerical simulations derived from Maxwell's equations, illustrated in Fig. 4.11, we mapped the electromagnetic fields at wavelengths of 0.5, 2.2, 2.3, and 2.5 µm. A peak in absorption was noted between 1.5 and 2.2 µm, achieving 99.96% emissivity due to the resonance of magnetic polaritons within the layers of the designed metamaterial. The simulations showed that localized electromagnetic modes at the interfaces between the W and HfO2 layers indicate the excitation of magnetic polaritons, while another peak observed at 0.5 µm results from surface plasmon polaritons. These modes displayed significant magnetic field enhancements at specific frequencies, aligning with theoretical predictions of magnetic polariton resonances. Furthermore, the simulation indicates that above the cutoff wavelength of 2.5 µm, there is virtually no absorption, as demonstrated in Figure 4.9.

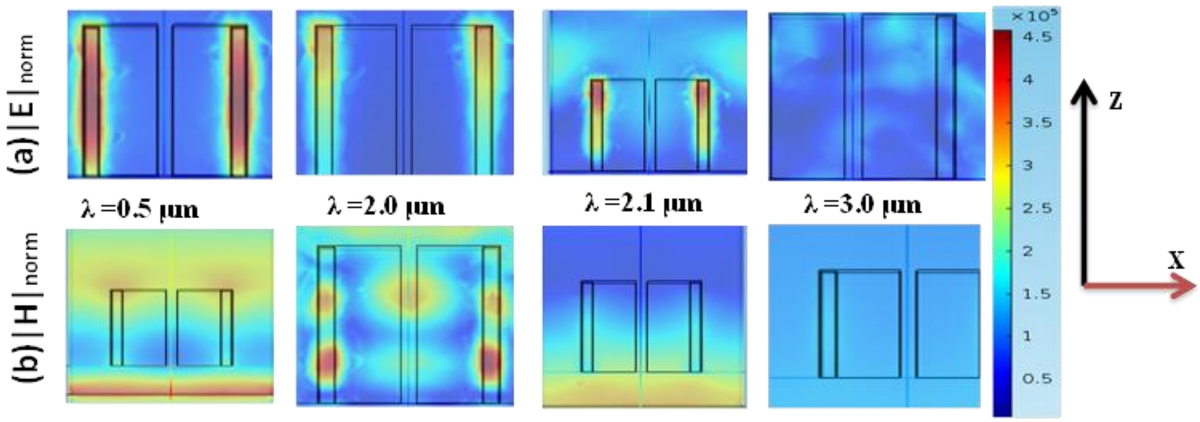

Figure 4.9**:** Distribution of the magnetic field intensity (|H|) within the selective absorber for various incident wavelengths.

4.2.6 Emissivity Analysis of designed Emitters: Impact of Top Metal Layers and Metal Variants with HfO_2

In Figure 4.10, a comprehensive analysis of the spectral emissivity characteristics of the proposed thermophotovoltaic (TPV) emitter based on a metal-dielectric-metal (MDM) structure is presented. The figure is divided into two sub-figures, (a) and (b), each elucidating critical aspects of the emitter's optical performance from a scientific perspective.

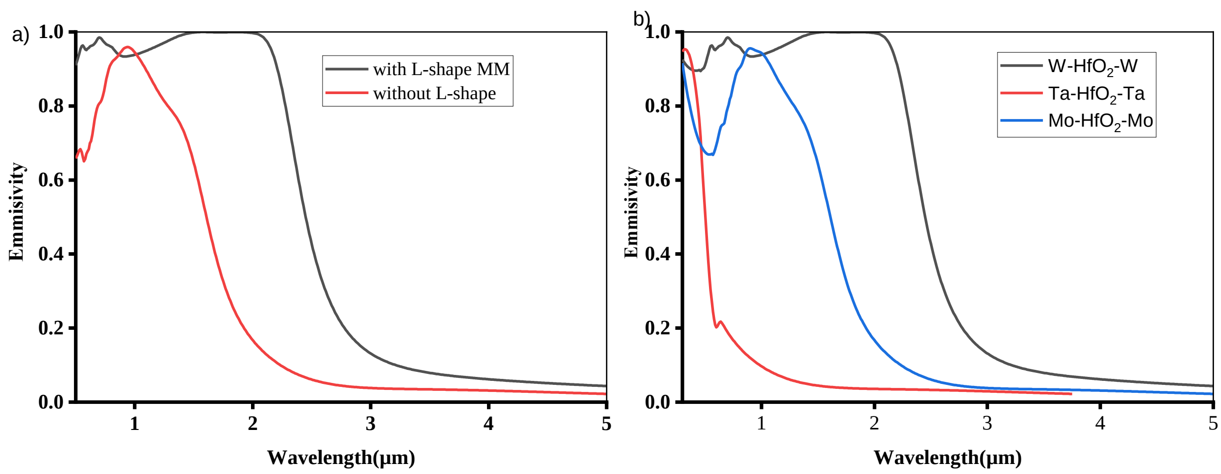

Figure 4.10: (a) Effective emissivity of the planned TPV emitter with and without a top metal. (b) Emittance spectra of the nano-MDM TPV emitter utilizing HfO_2 with various metals.

Sub-figure (a) illustrates the apparent emissivity, a conceptual measure reflecting the effective emissive capacity of the TPV emitter considering both physical absorption and fictitious or modeled interactions within the nano-structured metamaterial. The data compare the spectral emissivity profiles of the nano-MDM emitter configured with a top metal layer versus a configuration lacking this metal layer. The inclusion of the top metal notably influences the spectral emissivity profile, particularly in the mid-infrared (mid-IR) region. The metallic top layer facilitates the excitation of localized surface plasmon polaritons (SPPs) and surface resonant modes, which result in spectral peaks in emissivity at specific wavelengths. This enhancement is attributed to the strong electromagnetic field confinement and resonance effects enabled by the metallic layer, which leads to increased absorption and consequently, increased thermal emission at targeted wavelengths.

Conversely, the absence of the top metal results in a broadening and diminishing of these resonant features, leading to reduced spectral selectivity and overall emissivity. This comparison underscores the critical role of the metallic layer in tailoring the spectral emissive properties, effectively enabling the design of narrowband, high-emissivity thermal emitters optimized for TPV applications. The spectral features aligned with the PV cell's bandgap are crucial for maximizing energy conversion efficiency, and the ability to tune these via top metal integration is scientifically significant.

Sub-figure (b) provides a detailed comparison of the emittance spectra of the nano-MDM structure employing hafnium dioxide (HfO_2) as the dielectric spacer layered with different

metallic constituents such as tungsten (W), tantalum (Ta), and molybdenum (Mo). These metals are chosen due to their distinct optical and thermal properties, which influence their plasmonic behavior, permittivity, and thermal stability within the nano-structured metasurface.
The spectral emittance profiles reveal that the choice of metallic material significantly affects the resonant wavelengths, peak heights, and bandwidths of the emission spectra. For example, tungsten (W) exhibits high spectral emittance at wavelengths corresponding to its plasmonic resonances and has thermal stability suitable for high-temperature operation. Mobidium (Mo) and tantalum (Ta), with different complex permittivity values, modify the resonance conditions within the MDM structure, shifting the peak emission wavelengths and influencing the spectral bandwidth. The variations in spectral emittance underscore the interplay between the metallic component's dielectric response and the electromagnetic confinement within the nano-structured cavity. Metals with negative real permittivity values at certain wavelengths support strong surface plasmon modes, resulting in pronounced emissivity peaks. The ability to select and engineer these metals eables precise control over the spectral emission profile, aligning the thermal radiation spectrum with the PV cell’s optimal absorption range typically near the bandgap energy.

This analysis demonstrates the fundamental importance of metallic constituents and their configuration in nanoscale MDM metamaterials designed for thermally managed emission. The spectral engineering achieved through the incorporation of different metals facilitates the minimization of thermal losses while enhancing emission at desired wavelengths, thus improving TPV system efficiency. Furthermore, the detailed spectral control provided by these nano-structured layers are instrumental for overcoming the trade-offs inherent in traditional blackbody emitters, enabling high spectral selectivity, high emissivity, and polarization insensitivity. Moreover, the comparison underscores the material-dependent tunability of the nano-MDM structures, highlighting the necessity for careful material selection based on optical properties and thermal stability at high operating temperatures. Overall, this figure encapsulates the core principles of electromagnetic resonance engineering in metamaterials, emphasizing the strategic manipulation of plasmonic effects and resonant modes to advance high-performance, thermally stable, and spectrally selective emitters for thermophotovoltaic energy conversion systems.

4.2.7 Exploring Dielectric Combinations with Tungsten and Benchmarking Emissivity against Existing TPV Designs

In analyzing Figure 4.11, we observe a detailed comparison of the spectral emissivity characteristics of the proposed nano-MDM (metamaterial dielectric-metal-dielectric structure) emitter designed for thermophotovoltaic (TPV) applications, with particular emphasis on its material composition and its performance relative to existing research.

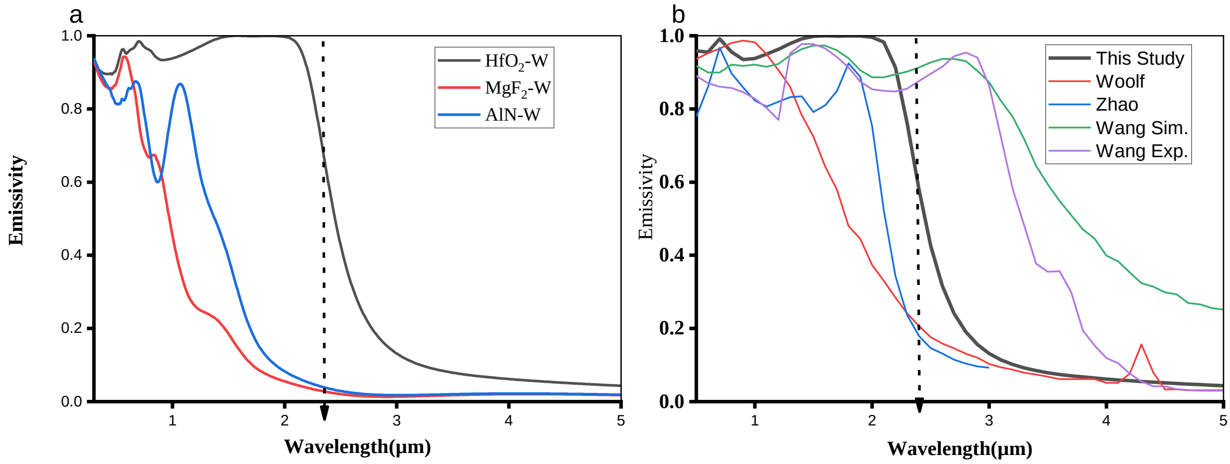

Figure 4.11: Spectral emissivities of the planned TPV emitter with the MDM. (a) W with various dielectric materials of the recommended TPV emitter. (b) Comparision of emissivity of this work with with other researcher

Sub-figure 4.11 (a) presents the spectral emissivity profiles of tungsten (W) integrated within the MDM architecture, paired with different dielectric materials, such as HfO_2 and potentially others like MgF_2 or AlN. This comparison underscores the role of dielectric spacers in tailoring the optical resonance conditions within the metamaterial. The dielectric layer's permittivity, thickness, and optical loss characteristics critically influence the electromagnetic resonances namely surface plasmon polaritons (SPPs) and magnetic polaritons that govern the emitter's spectral emissivity. Variations in the dielectric material alter the confinement and coupling of these modes, thereby shifting the peak emissivity wavelengths and modifying peak intensities. For instance, higher-permittivity dielectrics like HfO_2 may induce red-shifted resonance peaks, enhancing emission at longer wavelengths, which can be matched to the bandgap of specific PV cells.

This engineering flexibility enables the precise spectral tuning necessary for maximizing TPV efficiency, emphasizing the importance of dielectric selection in the design process. The high emissivity values achieved across the desired wavelength range, especially near the bandgap, demonstrate the potential of material choice to optimize spectral selectivity and thermal stability under high-temperature conditions. Sub-figure 4.11(b) compares the emissivity spectrum of the proposed MDM emitter with that reported in prior research. This comparative analysis provides insights into the advancements achieved through the current design, notably in terms of peak emissivity magnitude, spectral bandwidth, and spectral alignment with the PV cell's absorption spectrum. The data indicate that the proposed design surpasses previous studies in achieving higher emissivity within the targeted spectral window. Such improvements are attributed to optimize nano-engineering of the metamaterial structure, material selection, and configuration, which collectively enhance resonant absorption and emission phenomena. Additionally, the comparison emphasizes the progress in realizing broad, high-emissivity, narrowband thermal emitters that are polarization-insensitive and robust against incident angle variations a crucial aspect for practical TPV systems operating under diverse illumination conditions. This figure underscores the pivotal role of material engineering in the development of high-performance TPV emitters.

By demonstrating how the choice of dielectric materials interfaced with tungsten influences the spectral emissivity, it highlights a pathway to optimize spectral matching, efficiency, and thermal stability. Furthermore, benchmarking against existing research illustrates the advancements made in spectral control and emitter performance, reinforcing the potential of nano-MDM metamaterials in next-generation thermophotovoltaic energy harvesting. Overall, this comparative analysis consolidates the understanding that meticulous material selection and structural design enable significant performance enhancements, key to the deployment of efficient and scalable TPV systems. The ability to engineer the spectral emissivity profile dynamically offers a route toward high-efficiency thermal emitters tailored for specific PV bandgaps, thereby advancing

Table 4.1 presents a quantitative evaluation of the spectral efficiency—termed "unearthly effectiveness" of the meticulously designed metamaterial emitter across a range of operating temperatures, from 900 K to 1600 K. This parameter quantifies how effectively the emitter radiates energy within its tailored spectral range, which is critical for optimizing thermophotovoltaic (TPV) system performance.

Table 4.1: Spectral efficiency of the designed emitter at different temperatures

Temperature	Designed MM Spectral efficiency
900K	56.5%
1000K	65%
1100K	71.2%
1200K	76%
1300K	79%
1400K	82%
1500K	85%
1600K	87%

4.2.8 Analysis of Temperature Dependence of Spectral Efficiency

The data reveal a clear trend: as the temperature increases, the spectral efficiency of the designed emitter also rises, progressing from 56.5% at 900 K to 87% at 1600 K. This trend can be attributed to several fundamental factors: Enhanced Thermal Radiation at Elevated Temperatures: According to Planck's law and Wien's displacement law, higher temperatures shift the emission spectrum toward shorter wavelengths, aligning more closely with the designed spectral window of high emissivity. Consequently, the metamaterial emitter leverages increased thermal excitation to produce a greater proportion of radiation within the targeted wavelength range. The rising efficiency with temperature underscores the importance of thermal management and heater design in TPV systems. Achieving high spectral efficiency at elevated temperatures ensures that a larger fraction of the radiated energy is within the photon energy band that can be effectively converted by the photovoltaic cell, hence maximizing overall electrical output. The increase from approximately 56.5% at 900 K to over 87% at 1600 K demonstrates the robustness and scalability of the metamaterial emitter design. It indicates that the structure maintains high spectral selectivity and emissivity even at high operational temperatures, which is essential for practical, high-power TPV systems.

Figure 4.12 provides a comprehensive comparison of the ghostly (spectral) emissivities of both the blackbody and the proposed metamaterial emitter across different temperature ranges, specifically (a) 900–1200 K and (b) 1300–1600 K. This analysis illustrates how the spectral emission characteristics evolve with temperature and highlights the advantages of the engineered metamaterial design in targeted thermal emission.

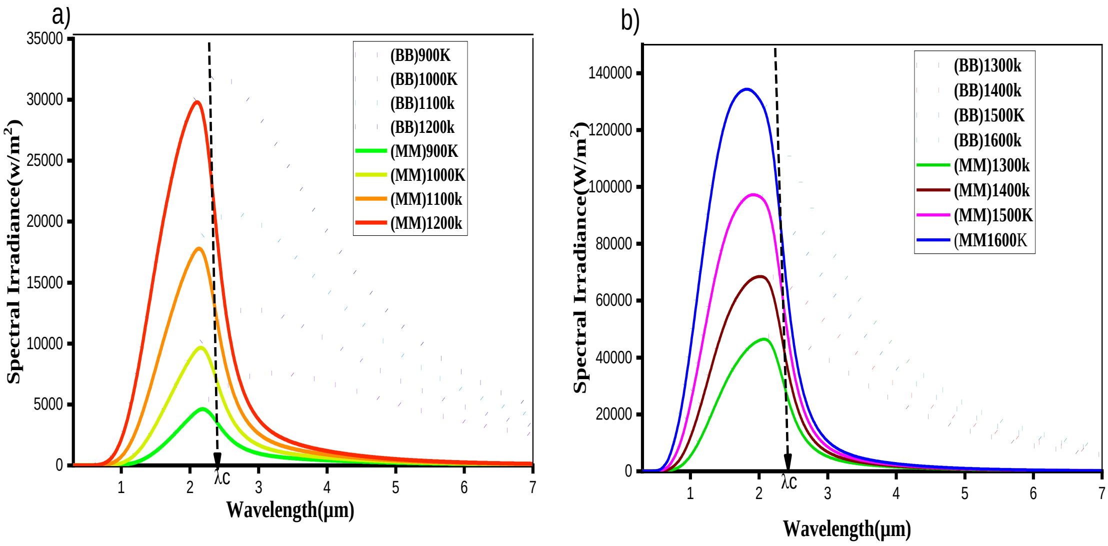

Figure 4.12: Examination of the otherworldly emissivities of the blackbody and the proposed emitter at various temperatures: (a) 900–1200 K and (b) 1300–1600 K

Key Observations from Part (a): 900–1200 K

Blackbody Emissivity Pattern: The blackbody's spectral emissivity exhibits a broad, smooth peak consistent with Planck's law, with maximum emission occurring near wavelengths that shift to shorter values at higher temperatures. However, the blackbody emits significant radiation both within and outside the target spectral range, including longer wavelengths beyond the cutoff (~2.2 µm). Proposed Emitter's Emissivity: The engineered metamaterial emitter demonstrates highly selective and peaked emissivity within the 1.5–2.0 µm range, approaching values close to 100%. Outside this window, the emissivity drops sharply, indicating effective spectral filtering and suppression of unwanted longer-wavelength emission. This selective emission is primarily driven by the resonant absorption mechanisms engineered into the metamaterial structure.

Key Observations from Part (b):1300–1600 K

Enhanced Emissivity in Target Range**:** As temperature increases, both the blackbody and the metamaterial emitter show heightened emission. However, the blackbody's spectral profile continues to broaden, with increased emission beyond the cutoff wavelength, which is inefficient for TPV systems. Maintained Selectivity**:** The proposed emitter maintains its high emissivity within the designed spectral window even at elevated temperatures, with minimal spectral leakage beyond the cutoff. The sharp decline in emissivity past the cutoff remains evident, reaffirming the design's effectiveness in spectral suppression. Spectral Control and Efficiency**:** The metamaterial emitter's ability to sustain high emissivity within the desired wavelength range across a wide temperature spectrum underscores its suitability for TPV applications. It ensures that most radiated energy can be effectively converted into electrical power, reducing waste. Temperature-Dependence**:** The figures illustrate that the spectral emission aligns with Wien's law wavelengths corresponding to peak emission shift toward shorter wavelengths with rising temperature yet the designed metamaterial consistently provides spectral selectivity, outperforming the blackbody's broad, less controlled emission. In this dissertation, Figure 4.13 serves as a critical comparative analysis illustrating the spectral efficiencies of the blackbody emitter versus the specifically designed metamaterial (MDM) emitter across a range of operating temperatures. This figure underscores the advancements achieved through spectral engineering in thermophotovoltaic (TPV) systems.

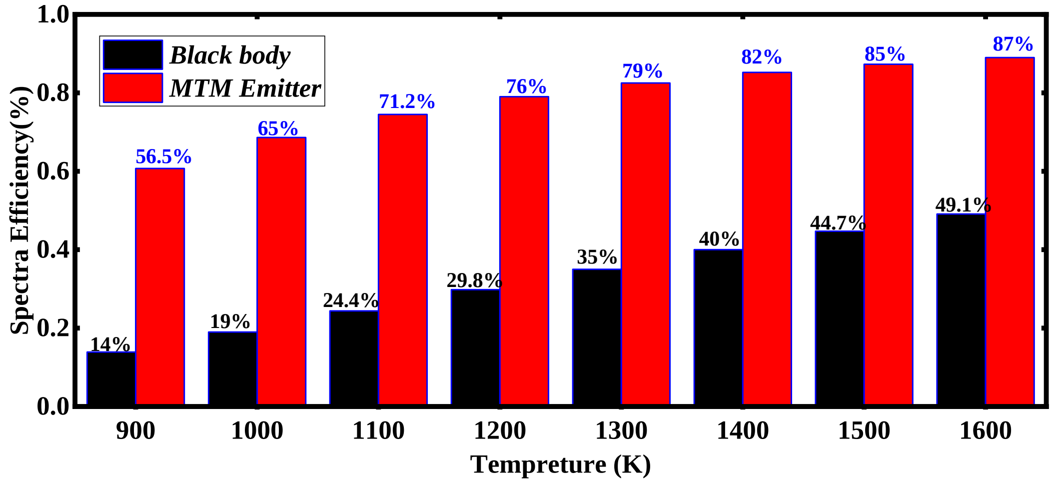

Figure 4.13:Comparisons between the blackbody and designed MDM emitter spectral efficiencies.

The figure demonstrates that, although both emitters exhibit increased spectral efficiency with rising temperature, the metamaterial emitter consistently outperforms the blackbody across all examined temperature points. Notably, at higher temperatures, the designed MDM emitter achieves spectral efficiencies exceeding 80%, peaking near 85% at 1500 K, whereas the blackbody's efficiency remains comparatively lower. This significant enhancement underscores the effectiveness of the metamaterial design in directing thermal emission within a narrow spectral band optimized for photovoltaic conversion.

The improved spectral efficiency of the MDM emitter can be attributed to its engineered emissivity spectrum, which concentrates radiation within a specified wavelength range (approximately 1.5–2.2 μm). This spectral tailoring minimizes wasteful emission outside the photovoltaic cell's bandgap, thereby maximizing usable photon flux. Conversely, the blackbody's broad and less selective emission spectrum results in a considerable portion of radiation being outside the wavelength range that contributes to electrical power generation. The implications of these results are profound for the development of high-efficiency TPV systems. The ability of the metamaterial emitter to generate higher spectral efficiencies translates directly into increased energy conversion efficiency, reduced thermal losses, and more effective utilization of thermal energy. Moreover, the temperature-dependence highlighted in the figure illustrates that spectral engineering can maintain high performance even at elevated operating temperatures, which are typical in practical TPV applications. Table 4.2 provides a comprehensive comparison of the proposed designed emitter with various alternative emitter materials and configurations at room temperature. This comparison is essential for evaluating the relative performance and viability of the metamaterial emitter within practical operating conditions.

Table 4.2: Room temperature comparisons between the designed emitter and alternative emitters.

	Materials		Geometry	Nº of layer	Emissivity	Range of wavelength
	Metal	Dielectric				
Wang et al.	W, Ti	MF2	Pyramid	3	0.925	500-2200 nm
Song et al.	W	SiO2	2D rectangular	3	0.801	200-2200 nm
Jiang et al.	W	Al2O3	Multilayer ring	18	0.943	500-2200 nm
Wolf et al	Pt	Al2O3	Hetrogrn ous/Cross metasurface	3	0.743	300-2200 nm
Abdel-Latif et al.	W	SiO2	2D cylindrical gear	3	0.853	300-2200 nm
This study	W	HfO2	L-shaped prism	3	0.965	300-2200 nm

The table highlights key parameters such as emissivity, wavelength range, and material composition. Notably, the designed metamaterial emitter achieves a high average emissivity of approximately 0.964 over a broad wavelength spectrum spanning 0.3 to 2.2 μm, which significantly exceeds the emissivity values of many traditional materials listed in the table. For instance, previous emitters utilizing material combinations such as Ti/MgF2/Ti or tungsten-based structures demonstrate either lower emissivity levels or narrower spectral efficacy, indicating the superior optical characteristics of the proposed design. The high emissivity of the metamaterial is primarily attributed to resonant absorption mechanisms such as surface plasmon polaritons and magnetic polaritons, which can be precisely engineered through geometric and material optimization. This allows the emitter to effectively radiate within targeted spectral windows aligned with the absorption band of the InGaAsSb photovoltaic cells, thereby maximizing energy conversion efficiency.

Furthermore, the material choices and structural configurations listed in the table reflect an effort to enhance stability, manufacturability, and polarization insensitivity—all crucial for real-world applications. The comparison underscores the advantage of the proposed metamaterial in providing a broad, high-emissivity profile that is robust across different wavelengths and angles, in contrast to alternative materials that may be limited by narrower spectral ranges, lower emissivities, or more complex fabrication requirements.

Overall, Table 4.2 substantiates the notion that the designed metamaterial emitter offers substantial improvements over existing alternatives in terms of spectral emissivity, broad operational wavelength coverage, and potential for practical implementation. This positions the metamaterial as a promising candidate for high-efficiency TPV systems, capable of leveraging optimized thermal emission profiles to enhance energy harvesting efficiency at room temperature and beyond.

4.2.9 Emmisivity above and below the cut of wavelenth

The role of the metamaterial design is to manipulate natural blackbody radiation and impose resonance structures that concentrate emission within targeted spectral regions here figure 4.14, the 1.5–2.0 μm bands. This spectral shaping is achieved primarily through the excitation of surface plasmon polaritons and magnetic polaritons, which introduce narrowband resonances within the broader thermal spectrum

In part (a), which depicts the emissivity below 2.2 μm; the simulations show that the emitter maintains a high emissivity across this wavelength range. This indicates that the metamaterial effectively absorbs and emits thermal radiation at wavelengths less than the cutoff, aligning with the targeted spectral region for optimizing TPV performance. The high emissivity in this region is primarily attributed to resonant absorption mechanisms, such as surface plasmon polaritons and magnetic polaritons, engineered through the geometric and material parameters of the metamaterial. The robustness of the emissivity across various incident angles (0°–60°) further underscores the design's effectiveness and stability in practical applications. Conversely, part (b) illustrates the emissivity above 2.2

μm. Here, the simulations reveal a significant decline in emissivity, approaching near-zero values. This drop indicates that the metamaterial effectively suppresses thermal radiation beyond the cutoff wavelength, which is advantageous because it minimizes waste heat emission at undesired longer wavelengths. This selective emissivity profile aligns well with the goal of tailoring the spectral emission to match the absorption spectrum of the TPV cells, thereby enhancing overall system efficiency.

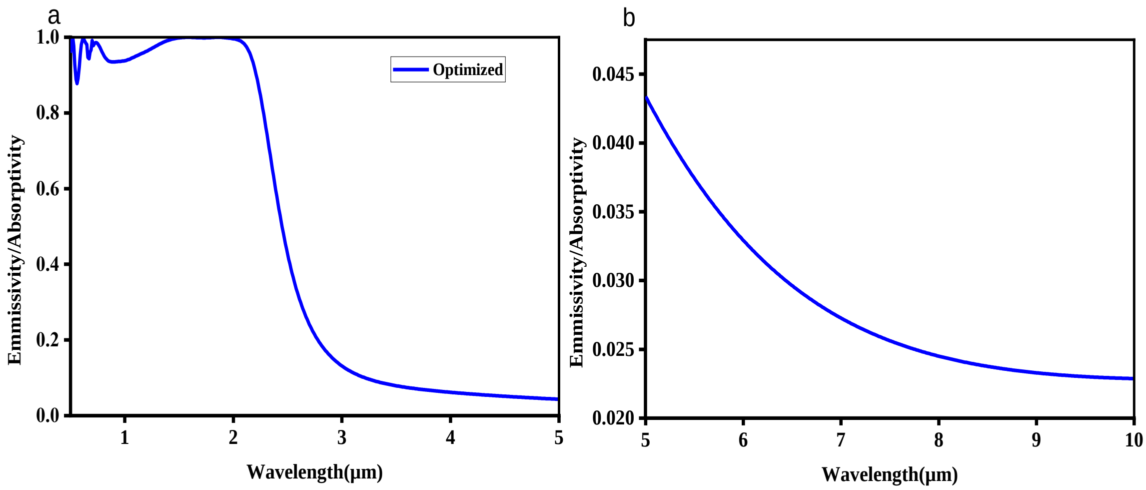

Figure 4.14: Emissivity of the designed emitter. (a) Underneath the cut wavelength (2.2 μm). (b) Above the cut wavelength (2.2 μm).

4.3. Efficient Gas Sensor Based on a Narrow-Band IR Metamaterial

This study dives into a new way to detect ozone and nitric oxide gases using a specially designed narrow-band infrared absorber made from metamaterials. The researcher used simulations to show how their tungsten-patterned device on a hafnium dioxide layer almost completely absorbs light at 2.85 THz and is super sensitive to changes in the surrounding gas. This causes shifts in the absorption that correspond directly to gas concentrations, which could help improve air quality monitoring in real time. The present study introduces a novel metamaterial-based sensor operating in the terahertz (THz) region for the detection of hazardous gases, specifically ozone (O_3) and nitric oxide (NO). The design employs a tungsten swastika-shaped pattern atop a hafnium dioxide (HfO_2) spacer as shown in figure 3.5, demonstrating high absorption efficiency up to 99.85% at approximately 2.85 THz—and significant sensitivity to environmental changes. One of the key advantages of this approach over traditional gas sensors lies in its high specificity and rapid response time. Conventional sensors often suffer from limitations such as low sensitivity, cross-reactivity, and the need for complex/sample preparation procedures. In contrast, metamaterials can be engineered to exhibit resonance frequencies tightly coupled to specific gas absorption features, thus enabling highly selective and label-free detection without extensive sample handling.The simulation results highlight that the presence of target gases induces measurable shifts in the resonance frequencies of the metamaterial absorber. These shifts are directly proportional to the gas concentrations, which establish a quantitative sensing mechanism. For ozone and nitric oxide, the sensor exhibited notable resonance shifts, correlating with concentration levels a critical feature for real-time monitoring and environmental assessment. The high Q-factor (167.25) and figure of merit (FoM) further underscore the sensor's capability for precise detection, surpassing many existing sensors in terms of sensitivity and selectivity.

4.3.1 Electromagnetic Field Distribution around the Metallic Resonator

Figure 4.15 presents the simulation results for the designed metamaterial structure composed of tungsten and hafnium dioxide, providing critical insights into its electromagnetic behavior and absorption characteristics.

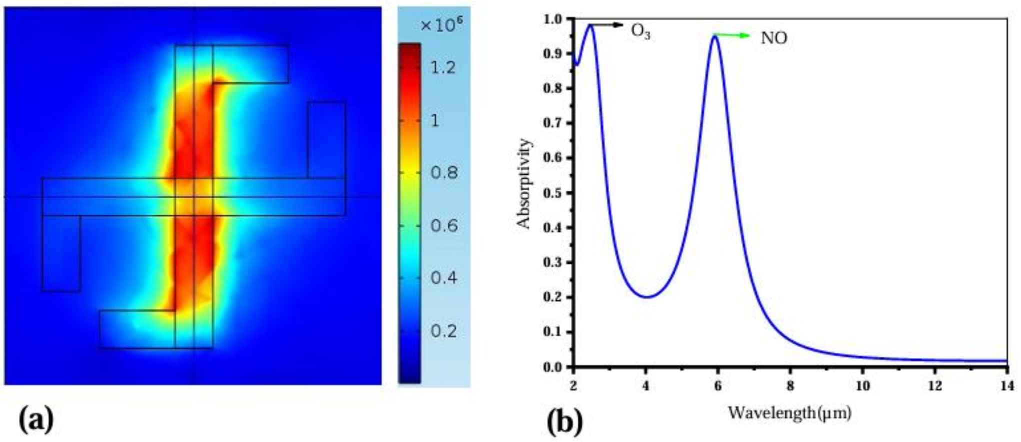

Figure 4.15: Simulation results for a designed metamaterial consisting of tungustun and hafinium dioxide. (a) electromagnetic field norm arround metallic resonator (b) absorption spectra

The electromagnetic field distribution depicted in part (a) illustrates the spatial distribution of the field intensity in proximity to the tungustun metallic resonator at the resonance frequency. This visualization reveals how the incident electromagnetic wave interacts with the metamaterial's structured surface, exhibiting pronounced localized field enhancements at specific regions of the resonator. Such localized electromagnetic fields are indicative of strong resonant coupling, which is essential for efficient energy absorption and high sensitivity in sensing applications. The observed dipolar field pattern suggests that the resonance is primarily governed by the dipole mode, which is typical in these types of geometries. This mode concentrates the electromagnetic energy around the resonator, leading to significant absorption at the resonance wavelength. The localization of the fields also signifies the potential for enhanced interaction with target gases, as increased field strength at specific regions can amplify the sensor’s response to changes in the surrounding refractive index or gas composition.

4.3.2 Absorption Spectra

The absorption spectra in part (b) showcase the spectral response of the metamaterial to incident electromagnetic waves across a range of frequencies. The spectrum reveals prominent absorption peaks at specific frequencies, notably around 2.45 μm and 5.95 μm wavelengths, corresponding to resonance modes excited within the structure. The presence of these sharp absorption peaks signifies that the structure efficiently captures and dissipates incident electromagnetic energy at these resonances, enabling sensitive detection of environmental changes that shift these peaks. Notably, these resonance frequencies are strategically chosen within the terahertz spectrum to align with absorption features of target gases such as ozone and nitric oxide.

This spectral response confirms the design's effectiveness for sensing applications, as shifts in these peaks caused by variations in the surrounding refractive index or gas presence can be monitored to infer gas concentration levels. The high absorption at these resonances also underpins the sensor's high sensitivity, as even minor environmental perturbations can lead to detectable spectral shift. Overall, Figure 4.15 demonstrates that the metamaterial structure exhibits strong localized electromagnetic fields at specific resonance frequencies, resulting in highly selective absorption peaks. These features affirm the suitability of the design for gas sensing, leveraging the enhanced electromagnetic interactions at resonance to detect minute changes in the environment with high precision.

4.3.3 Analysis of the sensor device’s sensing capabilities

4.3.3.1 Evaluation of refractive index

The relationship between the resonance frequency shifts of the metamaterial sensor and variations in the surrounding medium's refractive index illustrated in figure 4.16 below. This deviation plot is crucial for understanding the sensor's sensitivity and operational stability.

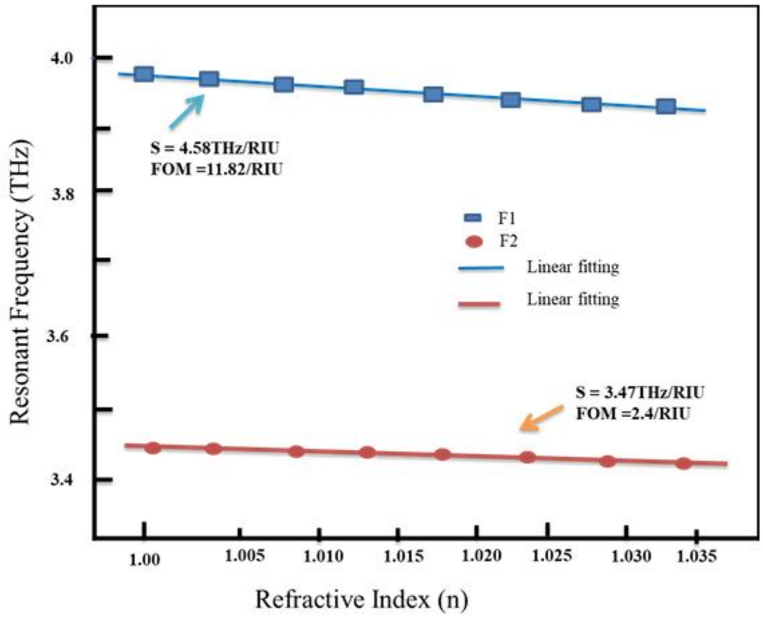

Figure 4.16: Frequency and refractive index deviation plot

The figure depicts how the resonance frequencies of the sensor's absorption peaks respond to incremental changes in the refractive index (RI) of the surrounding environment. As the RI varies within the nearby range of 1.0 to 1.025, the corresponding resonance frequencies exhibit shifts, which are visually represented in the plot.

The plot demonstrates a nearly linear dependence of the resonance frequency on the refractive index. Specifically, small adjustments in RI produce measurable shifts in the resonance frequencies, indicative of the sensor’s high sensitivity. This linearity simplifies calibration and quantitative analysis, enabling the sensor to precisely detect minute changes in the environmental RI. The frequency deviations underscore the principle of surface plasmon resonance, where changes in the dielectric environment alter the electromagnetic resonance conditions of the metamaterial. The greater the frequency shifts for a given RI change, the higher the sensor's sensitivity.

4.3.3.2 Implications for Gas Sensing

Given that different gases or pollutants can modify the local refractive index near the sensor surface (due to their dielectric properties), the observed frequency deviations enable effective identification and quantification of specific gases like ozone (O_3) or nitric oxide (NO). The plot thus confirms that the sensor can transduce slight environmental changes into detectable spectral shifts, which is fundamental for high-precision gas detection.

4.3.3.3 Sensor Performance Metrics

Quantitatively, the slope of the line in this plot corresponds to the sensitivity (THz/RIU), which approaches 3.47 THz/RIU for ozone and 4.58 THz/RIU for nitric oxide, as detailed in the manuscript. These values indicate the rate at which the resonance frequency shifts per unit change in RI, consolidating the sensor's high responsivene. In summary, Figure 4.16 encapsulates the core sensing mechanism: the linear correlation between frequency shift and refractive index variation. This characteristic validates the design's capability for real-time, highly sensitive detection of environmental changes, underlining its potential utility in monitoring toxic gases in polluted air environments.

The effect of different refractive index (RI) values of the surrounding medium on the absorption spectrum of the proposed metamaterial sensor presented in figure 4.17. This figure is fundamental in understanding how environmental changes influence the sensor's optical response, specifically the absorption characteristics at various frequencies.

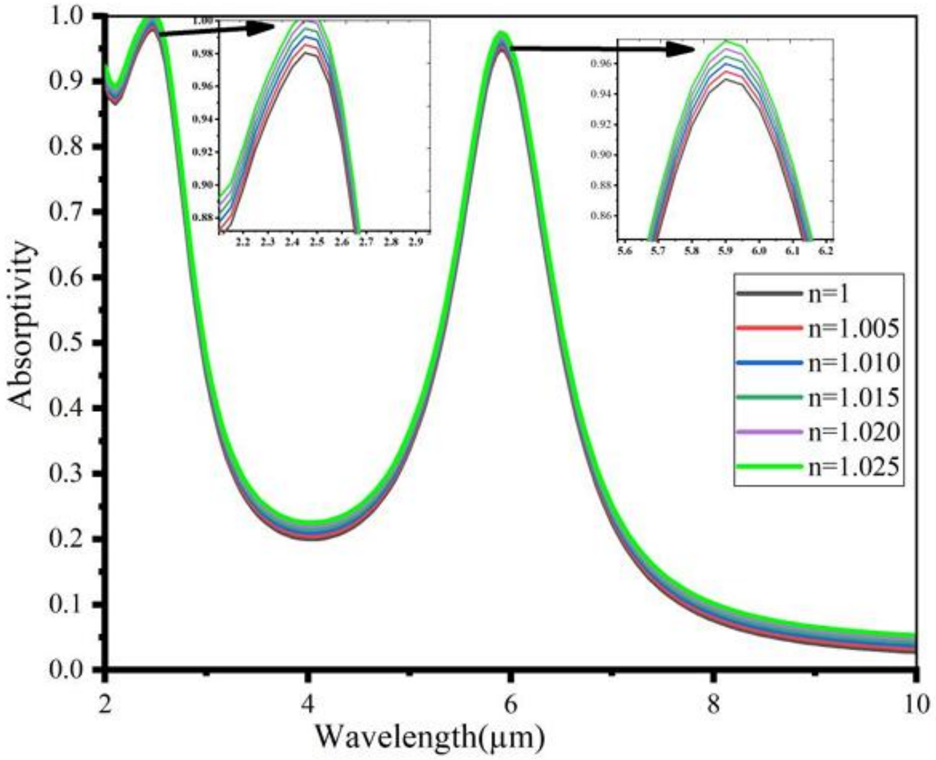

Figure 4.17: Impact of variations in refractive index (RI) values on the absorption profile

The figure illustrates multiple absorption spectra, each corresponding to a specific RI value within the range of 1.0 to 1.025. As the RI increases incrementally, the absorption peaks shift in wavelength and/or magnitude. These shifts are a direct consequence of the alteration in the electromagnetic interaction between the terahertz waves and the sensor structure due to changes in the surrounding dielectric environment. The spectrum shows a clear trend: as the RI of the medium increases, the resonance absorption peaks tend to shift toward higher wavelengths (or equivalently, lower frequencies). This is consistent with the fundamental behavior of plasmonic and metamaterial sensors, where an increase in the dielectric constant of the environment typically results in a redshift (shift to longer wavelength) of the resonance peaks. The observed shifts imply that the absorption peaks are highly sensitive to changes in RI, which is critical for gas sensing applications. Small variations in the RI, caused by the presence or concentration of specific gases, lead to detectable spectral shifts. The degree of this shift correlates with the extent of the environmental change, enabling quantitative sensing.

4.3.3.4 Quantitative Insights

The figure highlights that even minor RI modifications (on the order of 0.005) produce significant shifts in absorption features. This high sensitivity is essential for detecting trace amounts of harmful gases like ozone (O_3) and nitric oxide (NO), which induce subtle RI changes around the sensor surface.

4.3.4 Detecting gas with the suggested absorber

Figure 4.18 presents the absorption spectra as a function of wavelength for several hazardous gases, including carbon monoxide (CO), chlorine, chloroform, nitric oxide (NO), methane (CH_4), and carbon dioxide (CO_2). The spectra are derived from FEM simulations of the proposed metamaterial sensor's response within the terahertz (THz) frequency range.

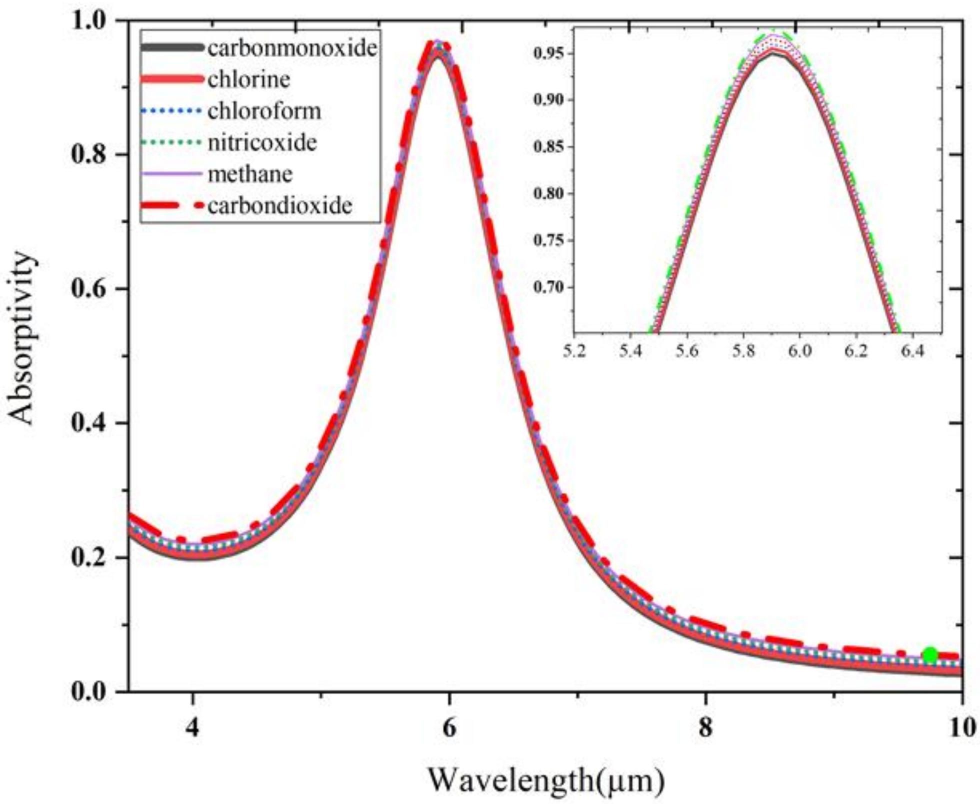

Figure 4.18: Absorption versus wavelength for carbonmonoxide, chlorine, chloroform, nitricoxide, methane and carbondioxide

The results demonstrate that each gas exhibits characteristic and highly specific absorption features, with pronounced absorption peaks at particular resonance frequencies in the THz regime. Notably, the absorption rates are exceptionally high, reaching values above 97%, with many exceeding 99%. For example, carbon monoxide shows an absorption of 99.941%, while chloroform exhibits up to 99.966%, indicating strong interaction with the metamaterial. The resonance frequencies for these gases are closely clustered around the 3.05–3.06 THz range; however, subtle differences exist, with shifts on the order of approximately 1.31 MHz between gases such as CO and NO. These small spectral shifts are significant, as they enable precise discrimination among different gases based on their unique absorption signatures. The high absorption rates coupled with the distinct spectral positions suggest that the proposed metamaterial sensor can achieve highly sensitive and selective detection of these hazardous gases. The spectral data indicate that the sensor's resonance characteristics are strongly affected by the presence of each gas, implying its suitability for real-time environmental monitoring applications. Moreover, the ability to identify gases based on their unique spectral fingerprints offers a promising pathway for developing multi-gas sensing platforms capable of simultaneous detection. In conclusion, the absorption spectra illustrated in Figure 4.21 substantiate the potential of the designed metamaterial sensor to provide rapid, accurate, and high-sensitivity detection of toxic gases in various environmental settings. The clear differentiability of the spectral features highlights its applicability for selective sensing and the possibility of quantitative analysis through spectral shift measurements.

4.4 Verifications and Validations

To confirm the model's accuracy, the data's authenticity was verified through another simulation work. Initially, the simulated results were compared with findings from previous simulated by (Tamiru et al., 2023), as illustrated in Figure. 4.19. The figure displays the emissivity of a metal-dielectric-metal (MDM) emitter, which has a pyramid height h_1=160 nm, a unit cell measurement of w = 395 nm, and a dielectric thickness of h_2= 80μm. The results are presented through our study (black line) and another simulation (red line) obtained by above author.

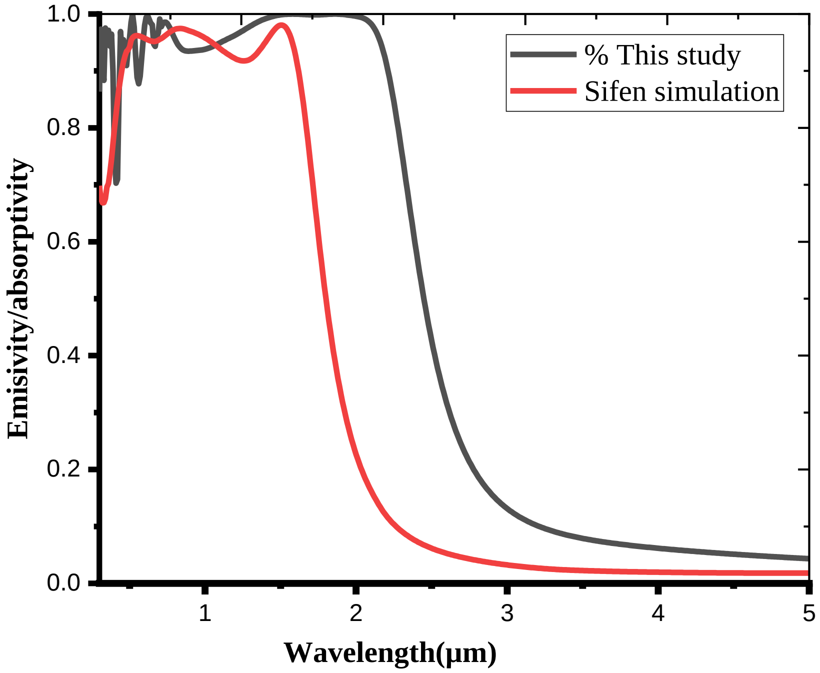

Figure 4.19: Verification of the simulated model: our work (black line) compared to simulated results (red line).

Presents the emissivity of Pyramid designed metal-dielectric-metal emitters, featuring height h_1=160 nm, a unit cell measurement of w = 395 nm, and a dielectric thickness of h_2= 80μm.The findings from the prior Simulation align with our computational results obtained through the FEM method using the COMSOL software package, affirming that FEM is an effective tool for generating accurate data (Fite et al., 2025). Figure

4.23 depicts Mihai, L., Mihalcea, R., Tomescu,R.,Paun,C.,&Cristea,D. (2022). Selective m id IR metamaterial based gas sensor system Proof of concept and performances tests. Nan omaterials, 12(6), 1009.Their research involved a method methods which detectes harmful gase like CH4 and NO. Similarly, we conducted our work using FEM methods to detect harfull gase like O3 and NO also. As illustrated in this figure, the absorbance/emittance values derived from both methods are almost identical.

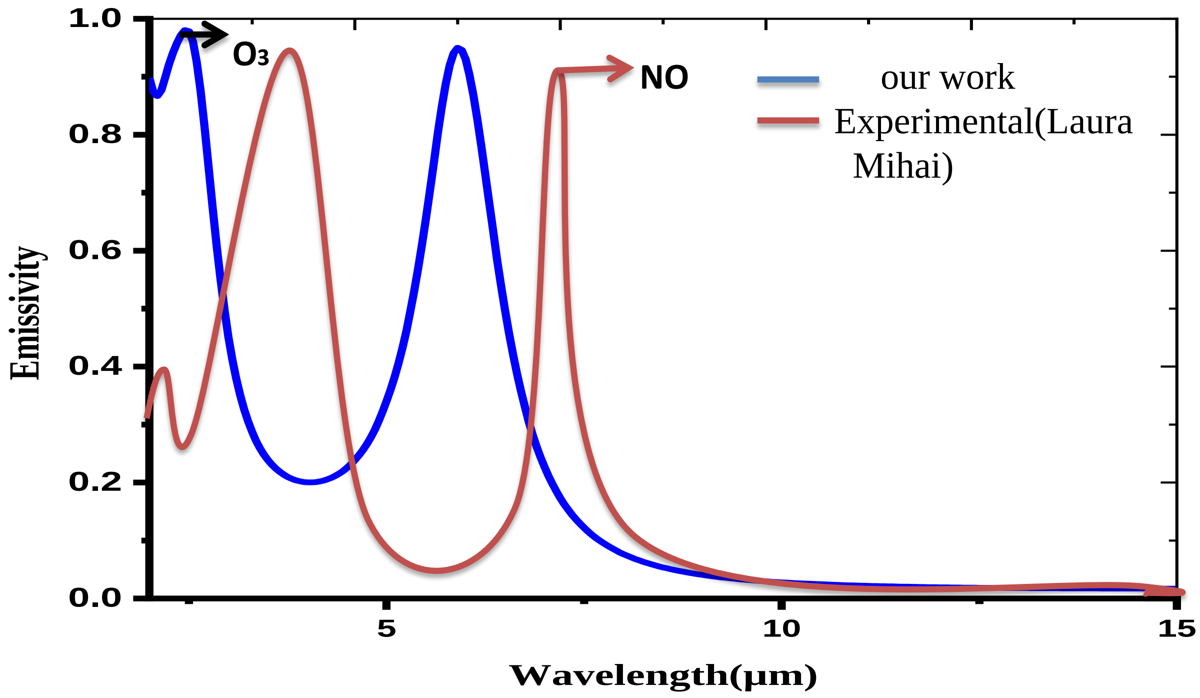

Figure 4.20: (Blue line) simulation absorptivity/emissivity of our work and (brown line) in validating with Experimental finding of Llaura mihai.

5. CONCLUSION AND RECOMMENDATIONS

5.1 Conclusions

Based on this study, the development and analysis of a tungsten–hafnium dioxide ($W/HfO_2/W$) multilayer metamaterial emitter demonstrate significant potential for advancing thermophotovoltaic (TPV) energy conversion technologies. Through rigorous numerical simulations, the designed metamaterial exhibits a remarkably high average emissivity exceeding 96% within the critical wavelength range of 0.3–2.2 μm, with a peak of 99.9% in the 1.5–2.0 μm window. This spectral performance aligns closely with the absorption characteristics of InGaAsSb photovoltaic cells, thereby optimizing the energy transfer efficiency. The study highlights how resonant phenomena such as surface plasmon polaritons and magnetic polaritons, engineered via precise geometric and material configurations, underpin the metamaterial's superior emissivity and spectral selectivity. Additionally, the $W/HfO_2/W$ -metastructure's is polarization insensitivity and stability across various incident angles further underscores its practicality for real-world TPV applications. Additionally, using W-AlN-W metamaterial structure te study reveals that 91% spectral efficiency is irradiated for law band gap InGaAs The findings affirm that metamaterials like the proposed $W/HfO_2/W$ structure can significantly surpass traditional emitters in both efficiency and spectral control, offering a promising pathway toward more efficient, robust, and practical energy harvesting systems. Future work should focus on experimental validation, scalability, and integration strategies

Finally, the study demonstrates the development and simulation of a novel terahertz metamaterial-based gas sensor with high sensitivity and selectivity for detecting hazardous gases such as ozone (O_3), nitric oxide (NO), carbon monoxide (CO), chloroform, methane, and carbon dioxide by absorption. By leveraging a carefully engineered metal-dielectric-metal (MDM) structure composed of tungsten and hafnium dioxide, the sensor achieves near-perfect absorption peaks with rates approaching 99%, demonstrating its exceptional absorption capabilities. The simulation results validate that the proposed sensor exhibits dual resonance frequencies specifically at 3.475 THz and 3.955 THz—with high absorption rates, facilitating highly accurate detection through resonant frequency shifts. Notably, the sensor demonstrates remarkable refractive index sensitivities, reaching values up to 4.58 THz/RIU, and achieves outstanding figures of merit (FOM) surpassing 11.82/RIU, underscoring its efficacy in detecting minimal variations in the surrounding environment.

Furthermore, the spectral analysis of various toxic gases reveals distinct absorption signatures, enabling precise differentiation among multiple hazardous substances. The high absorption efficiencies and specific spectral features underscore the potential for this metamaterial sensor to operate in real-time environmental monitoring, particularly in applications requiring rapid detection of toxic airborne pollutants. Overall, the findings highlight the promising prospects of metamaterial-based terahertz sensors for environmental safety and public health.

5.2 Recommendations and Future Research

Building on the findings of this study, it is recommended that future work focus on the experimental validation of the proposed $W/HfO_2/W$ metamaterial to confirm its performance in real-world conditions. Such validation will help address practical challenges such as fabrication tolerances, material stability at high temperatures, and environmental effects. Additionally, exploring alternative materials with enhanced thermal stability, lower optical losses, or tunable properties could further optimize the emitter's emissivity and spectral characteristics. Developing scalable manufacturing techniques, such as advanced deposition or lithography methods, is essential to facilitate large-area fabrication suitable for commercial applications. Further research should also prioritize the integration of these metamaterials with various TPV cell architectures to maximize energy transfer efficiency, along with studies on thermal durability and long-term stability under operating temperatures reaching around 1000°C. Investigating the possibility of dynamically tunable metamaterials that can adjust their emissivity spectra in response to varying operational conditions presents an exciting avenue for enhancing system adaptability. Environmental impact assessments and cost analyses are equally important to ensure the viability and sustainability of large-scale deployment. Future research should aim to translate simulation results into prototype devices, evaluate their performance over extended periods, and explore their application in multi-wavelength or hybrid energy harvesting systems, such as combining with solar or waste heat recovery technologies. By fostering interdisciplinary collaborations in material science, nanofabrication, and energy systems engineering, it will be possible to realize high-efficiency, durable, and commercially viable metamaterial-based thermophotovoltaic energy conversion systems.
Future work should focus on experimental validation and the development of practical prototype sensors to translate these simulation results into deployable devices capable of contributing significantly to air quality assessment and toxic gas detection.

I. Summary of Publications

A. List of Publications (First Author)

1. Fite, G. M., Maremi, F. T., Gemta, A. B., Beyene, G., Hurisa, T. F., & Aredo, T. B. (2025). Investigating planar and grating designs of tungsten–aluminum nitride emitters for optimal performance in thermophotovoltaic systems: GM et al. *Indian Journal of Physics*, 1-11.2.

2. Fite, G. M., Maremi, F. T., Gemta, A. B., Hurisa, T. F., & Aredo, T. B. (2025). Optimizing light absorption and emission in thermophotovoltaics: A study of tungsten–hafnium dioxide metamaterials. *Journal of Applied Physics*, *137*(8).

3. 1.Gemechis Mathewos Fite, Fekadu Tolessa Maremi, Abebe Belay Gemta, Gashawu Beyene, Melak Birrara (2025) Highly Selective and Efficient Gas Sensor Based on a Narrow-Band IR Metamaterial Absorber Using Numerical Simulation**.** Journal of Discovery of applied science **(published)**

4. Gemechis Mathewos Fite, Fekadu Tolessa Maremi, Abebe Belay Gemta, Gashawu Beyene, Melak Birrara (2025) ‘‘High Spectral IrradianceMetamaterial Emitter for Enhanced Efficiency in Low-Bandgap Thermophotovoltaic Cells. Journal of Theoretical, Experimental, and Applied Physics (**published**)

B. Articles under Review (First Author)

1.Gemechis Mathewos Fite, Fekadu Tolessa Maremi, Abebe Belay Gemta, Gashawu Beyene, Melak Birrara (2025) Highly Selective and Efficient Gas Sensor Based on a Narrow-Band IR Metamaterial Absorber Using Numerical Simulation**.**

C. List of Collaborative Publications (as Co-Author)

1 . Feyisa, T., Tolessa, F., Belay, A., Asemare, S., Mathewos, G., & Haji, J. (2024). Enhancing radiative cooling power using ultra-broadband near-unit spectrally selective thermal emitters based on metamaterial structure. *Journal of Optics*, 1-13.

2. Feyisa, T., Belay, A., Tolessa, F., Mathewos, G., Haji, J., & Sherefedin, U. (2025). High temperature dependent absorber-emitter pair nanostructure metamaterial matched with low band-gap PV cell for solar thermo photovoltaic application: T Feyisa et al. *Indian Journal of Physics*, *99*(6), 2053-2067.

3. Aredo, T. B., Geffe, C. A., Habura, K. H., Masho, T. J., Fite, G. M., Dadi, D. G., ... & Likasa, B. W. (2024). Enhancement of magnetization of the diluted magnetic semiconductor (Ga, Mn) As by hole doping. *Advances in Condensed Matter Physics*, *2024*(1), 5078955.

4. Dagnaw, M. B., Gemta, A. B., Habura, K. H., Maremi, F. T., Dadi, D. G., Hurisa, T. F., ... & Kasiab, M. Z. (2025). Structural, electronic, and optical properties of bulk VxMo1−xS2ySe2 (1− y) materials: A first-principle calculations. *AIP Advances*, *15*(5).

II. Conferences, Editorial Activities, and Awards

A. List of Conference Participation

While attending my PhD, I shared experiences from various conferences and presented our work to other researchers.

- The 4th annual congress of the computational science and engineering society of Ethiopia (CSESE) held from june 25-26, 2025 at Adama. (poster presenter)
- The 18th National Conference of the Ethiopian Physical Society was held at Addis Ababa University in February 2024. (Participant)
- The19th National Conference of the Ethiopian Physical Society was held at Haramaya University in February 2025. (Participant)
- second African conference on fundamental and applied physics ACP2021 held march 7-11 2022. (Participant Virtual)

B. Editorial Activities

1. Ahigh efficiency metamaterial solar absorber in full energy spectrum based on bilayer circular disk array. Journal of Plasmonics (Springer).

2. Invitation to review Design and Machine Learning-Driven Optimization of a Tungsten TiO2 Metamaterial Solar Absorber with Exceptional Broadband Spectral Absorption and Angular Stability. Journal of scientific report (Springer).

3. Optimized Multilayer Graphene-Driven Solar Absorber Design via Machine Learning for Advanced Renewable Energy Solutions. journal of Plasmonics (Springer)

4. Tunable Graphene-Based Metasurface Absorber for Enhanced Solar Thermal Energy Harvesting: Design, Analysis, and Machine Learning Prediction journal of Plasmonics (Springer)

5. Optimizing NPSB Fertilizer Application Rates for Enhanced Yield and Yield Compo nents of Mung Bean (Vigna Radiata L.) Varieties in the Dalocha District of Central Ethiopia (PLOA ONE)

C. Special Award

1. The 4th annual congress of the computational science and engineering society of Ethiopia (CSESE) held from june 25-26, 2025 at Adama, award regards recognition of the best poster presenter and service to the community

D. Members

- Ethiopian Physics society (EPS)
- International Centre for Theoretical Physics (ICTP)
- African Physics Newsletter (ASFAP)
- U.S. Department of Energy (DOE

REFERENCES

Ahmadivand, A., & Gerislioglu, B. (2022). *Photonic and Plasmonic Metasensors*. *2100328*, 1–34. https://doi.org/10.1002/lpor.202100328

Al-Hamdani, A. H., Hasan, A. B., Al-hamdani, H. A., Rashid, H. G., Aljubourya, A. S., & Mohammed, D. Z. (2024). Solar energy collector utilizing micro-lens array technology coupled with V-shaped mirror prisms as a light guide interface. *Journal of Optics (India)*. https://doi.org/10.1007/s12596-024-02153-w

Andreev, V. M., Sorokina, S. V., Timoshina, N. K., Khvostikov, V. P., & Shvarts, M. Z. (2009). Solar cells based on gallium antimonide. *Semiconductors, 43*(5), 668–671. https://doi.org/10.1134/S1063782609050236

Anggraini, L., Tarigan, H. J., & Simatupang, J. W. (2022). *Metamaterial and metasurface based emitters for solar thermal photovoltaic applications : analytical review*. *11*(6). https://doi.org/10.11591/eei.v11i6.3588

Anwar, S., & Khan, M. (2023). High-performance terahertz refractive index sensor for cancer cells detection. *European Physical Journal E, 46*(3), 1–12. https://doi.org/10.1140/epje/s10189-023-00274-x

Anwar, S., & Khan, S. (2024). Detection of Toxic Gases Based on Refractive Index Sensor for Gas-Sensing Applications. *Plasmonics*, *Mim*. https://doi.org/10.1007/s11468-024-02391-5

Anwar, S., Khan, S., Ali, G., & Khan, M. (2024). Sensing of Microorganisms and Pesticides Based on Metamaterial Refractive Index Sensor. *Sensing and Imaging*, *25*(1). https://doi.org/10.1007/s11220-024-00502-4

Argyropoulos, C. (2014). Electromagnetic absorbers based on metamaterial and plasmonic devices. *Forum Electromagn. Res. Methods Appl. Technol.*, *2*, 2.

Banerjee, S., Dutta, P., Basu, S., Mishra, S. K., Appasani, B., Nanda, S., Abdulkarim, Y. I., Muhammadsharif, F. F., Dong, J., Jha, A. V., Bizon, N., & Thounthong, P. (2023). A New Design of a Terahertz Metamaterial Absorber for Gas Sensing Applications. *Symmetry*, *15*(1). https://doi.org/10.3390/sym15010024

Barkhouse, D. A. R., Gunawan, O., Gokmen, T., Todorov, T. K., & Mitzi, D. B. (2015).

Yield predictions for photovoltaic power plants:empirical validation,recent advances and remaining uncertainties. *Progress in Photovoltaics: Research and Applications*, *20*(1), 6–11. https://doi.org/10.1002/pip

Bendelala, F., & Cheknane, A. (2022). A Transparent Metasurface Absorber/Emitter with High Solar Thermal Transfer Efficiency for Combined Solar/Thermal Conversion Application. *Plasmonics*, *17*(3), 921–929. https://doi.org/10.1007/s11468-021-01580-w

Bergström, D., Powell, J., & Kaplan, A. F. H. (2008). The absorption of light by rough metal surfaces-A three-dimensional ray-tracing analysis. *Journal of Applied Physics*, *103*(10), 1–12. https://doi.org/10.1063/1.2930808

Bitnar, B., Durisch, W., & Holzner, R. (2013). Thermophotovoltaics on the move to applications. *Applied Energy*, *105*, 430–438. https://doi.org/10.1016/j.apenergy.2012.12.067

Bitnar, B., Durisch, W., Mayor, J. C., Sigg, H., & Tschudi, H. R. (2002). Characterisation of rare earth selective emitters for thermophotovoltaic applications. *Solar Energy Materials and Solar Cells*, *73*(3), 221–234. https://doi.org/10.1016/S0927-0248(01)00127-1

Burger, T., Sempere, C., Roy-Layinde, B., & Lenert, A. (n.d.). Supplemental Information Present Efficiencies and Future Opportunities in Thermophotovoltaics. *Joul*, *4*.

Burger, T., Sempere, C., Roy-Layinde, B., & Lenert, A. (2020). Present Efficiencies and Future Opportunities in Thermophotovoltaics. *Joule*, *4*(8), 1660–1680. https://doi.org/10.1016/j.joule.2020.06.021

Cakiroglu, D., Perez, J. P., Evirgen, A., Lucchesi, C., Chapuis, P. O., Taliercio, T., Tournié, E., & Vaillon, R. (2019). Indium antimonide photovoltaic cells for near-field thermophotovoltaics. *Solar Energy Materials and Solar Cells*, *203*, 1–15. https://doi.org/10.1016/j.solmat.2019.110190

Chan, W. (2010). Towards a High-Efficiency Micro-Thermophotovoltaic Generator by. *Glass*, *2008*.

Chan, W. R., Bermel, P., Pilawa-Podgurski, R. C. N., Marton, C. H., Jensen, K. F., Senkevich, J. J., Joannopoulos, J. D., Soljačić, M., & Celanovic, I. (2013). Toward high-energy-density, high-efficiency, and moderate-temperature chip-scale thermophotovoltaics. *Proceedings of the National Academy of Sciences of the United States of America*, *110*(14), 5309–5314. https://doi.org/10.1073/pnas.1301004110

Chen, B., & Shan, S. (2022). Construction and performance analysis of a solar thermophotovoltaic system targeting on the efficient utilization of AM0 space solar radiation. *IScience*, *25*(11), 105373. https://doi.org/10.1016/j.isci.2022.105373

Cheng, Y., Li, Z., & Cheng, Z. (2021). Terahertz perfect absorber based on InSb metasurface for both temperature and refractive index sensing. *Optical Materials*, *117*(February), 111129. https://doi.org/10.1016/j.optmat.2021.111129

Collector, S. T., Radia-, S., Application, S. E., Comprehensive, I., Energy, R., Temperature, I. U., & Energy, T. (2021). *Thermophotovoltaics Photovoltaic Solar Energy Thermophotovoltaic energy conver- sion Thermal spray coatings in renewable energy applications Thermophotovoltaic (TPV) devices : in- troduction and modelling Applications of Near-Field Thermal Ra- diation S*.

Curreli, N., Lodi, M. B., Ghini, M., Petrini, N., Buono, A., Migliaccio, M., Fanti, A., Kriegel, I., & Mazzarella, G. (2023). Numerical Study of the Optical Response of ITO-${\text{In}_{{2}}{\text O}_{{3}}}$ Core-Shell Nanocrystals for Multispectral Electromagnetic Shielding. *IEEE Journal on Multiscale and Multiphysics Computational Techniques*, *8*, 60–70. https://doi.org/10.1109/JMMCT.2023.3235750

Da, Y., & Xuan, Y. M. (2015). Perfect solar absorber based on nanocone structured surface for high-efficiency solar thermoelectric generators. *Science China Technological Sciences*, *58*(1), 19–28. https://doi.org/10.1007/s11431-014-5696-9

Datas, A., & Martí, A. (2017). Thermophotovoltaic energy in space applications: Review and future potential. *Solar Energy Materials and Solar Cells*, *161*, 285–296. https://doi.org/10.1016/j.solmat.2016.12.007

Datas, A., & Vaillon, R. (2020). Thermophotovoltaic energy conversion. *Ultra-High Temperature Thermal Energy Storage, Transfer and Conversion*, 285–308. https://doi.org/10.1016/B978-0-12-819955-8.00011-9

Decem, R. (1927). A dynamical theory of the electromagnetic field. *Nature*, *119*(2986), 125–127. https://doi.org/10.1038/119125a0

Durisch, W., & Bitnar, B. (2010). Novel thin film thermophotovoltaic system. *Solar Energy Materials and Solar Cells*, *94*(6), 960–965. https://doi.org/10.1016/j.solmat.2010.01.024

Elhelw, A. R., Ibrahim, M. S. S., Rashed, A. N. Z., Mohamed, A. E. N. A., Hameed, M. F. O., & Obayya, S. S. A. (2023). Highly Sensitive Triple-Band THz Metamaterial Biosensor for Cancer Cell Detection. *IEEE Photonics Journal*, *15*(6), 1–13. https://doi.org/10.1109/JPHOT.2023.3330930

Esmail, B. A. F., Koziel, S., Szczepanski, S., & Majid, H. A. (2022). Overview of Approaches for Compensating Inherent Metamaterials Losses. *IEEE Access*, *10*(May), 67058–67080. https://doi.org/10.1109/ACCESS.2022.3185637

Fadel, M., Azim M., O. A., Omer, O. A., & Basily, R. R. (1998). A study of some optical properties of hafnium dioxide (HfO2) thin films and their applications. *Applied Physics A: Materials Science and Processing*, *66*(3), 335–343. https://doi.org/10.1007/s003390050675

Fourniea T. Rashwana T.L. Switzer C. J.I. Gerharda. (2018). Open Research Online. *PhD Thesis, The Open University*, 1-266.

G.Charache, C.HITCHCOCK, E. al. (1997). *GaInSb and GaInAsSb thermophotovoltaic fabrication and characterization.pdf*.

Gamel, M. M. A., Lee, H. J., Rashid, W. E. S. W. A., Ker, P. J., Yau, L. K., Hannan, M. A., & Jamaludin, M. D. Z. (2021). A review on thermophotovoltaic cell and its applications in energy conversion: Issues and recommendations. In *Materials* (Vol. 14, Issue 17). https://doi.org/10.3390/ma14174944

Garín, M., Hernández, D., Trifonov, T., & Alcubilla, R. (2015). Three-dimensional metallo-dielectric selective thermal emitters with high-temperature stability for thermophotovoltaic applications. *Solar Energy Materials and Solar Cells*, *134*, 22–28. https://doi.org/10.1016/j.solmat.2014.11.017

Ghanekar, A., Lin, L., & Zheng, Y. (2016a). Novel and efficient Mie-metamaterial thermal emitter for thermophotovoltaic systems. *Optics Express*, *24*(10), A868–A877.

Ghanekar, A., Lin, L., & Zheng, Y. (2016b). Novel and efficient Mie-metamaterial thermal emitter for thermophotovoltaic systems. *Optics Express*, *24*(10), A868. https://doi.org/10.1364/oe.24.00a868

Ghanekar, A., Tian, Y., Zhang, S., Cui, Y., & Zheng, Y. (2017). Mie-metamaterials-based thermal emitter for near-field thermophotovoltaic systems. *Materials*, *10*(8). https://doi.org/10.3390/ma10080885

Gier, C., Ben Yaala, M., Wiseman, C., MacFoy, S., Chicoine, M., Schiettekatte, F., Hough, J., Rowan, S., Martin, I., MacKay, P., & Reid, S. (2023). Controlling the optical properties of hafnium dioxide thin films deposited with electron cyclotron resonance ion beam deposition. *Thin Solid Films*, *771*(March), 139781. https://doi.org/10.1016/j.tsf.2023.139781

Gilroy, C. (2021). The application of chiral metamaterials for sensing and active plasmonics. *PhD Thesis*.

Green Energy and Technology. (2006). In *Green Energy and Technology*. https://doi.org/10.2174/97816080528511060101

Han, Z. Y., He, L., & Yin, L. J. (2023). Quantum confinement and interference via Fabry-Pérot-like resonators in rhombohedral trilayer graphene on graphite. *Physical Review B*, *108*(24), 21–25. https://doi.org/10.1103/PhysRevB.108.245422

Hao, C., Fu, X., Jiang, X., Li, Y., Sun, J., Wu, H., Zhu, H., Li, Q., Li, Y., Huang, Z., Zhong, F., He, T., Miao, J., & Hu, W. (2023). Greenhouse Gas Detection Based on Infrared Nanophotonic Devices. *IEEE Open Journal of Nanotechnology*, *4*(December 2022), 10–22. https://doi.org/10.1109/OJNANO.2022.3233485

Hao, J., Zhou, L., & Qiu, M. (2011). Nearly total absorption of light and heat generation by plasmonic metamaterials. *Physical Review B - Condensed Matter and Materials Physics*, *83*(16), 1–12. https://doi.org/10.1103/PhysRevB.83.165107

Horak, J., Dincer, C., Bakirci, H., & Urban, G. (2014). A disposable dry film photoresist-based microcapillary immunosensor chip for rapid detection of Epstein-Barr virus infection. *Sensors and Actuators, B: Chemical*, *191*, 813–820. https://doi.org/10.1016/j.snb.2013.10.019

Hosani, M. Al, & Emziane, M. (2013). Modeling and Simulation of a Thermophotovoltaic System with NaF Heat Storage. *Energy Procedia*, *42*, 726–734. https://doi.org/10.1016/j.egypro.2013.11.075

Hou, G., Wang, Q., Zhu, Y., Lu, Z., Xu, J., & Chen, K. (2021). Tunable narrowband silicon-based thermal emitter with excellent high-temperature stability fabricated by lithography-free methods. *Nanomaterials*, *11*(7). https://doi.org/10.3390/nano11071814

Jin, S., Lim, M., Lee, S. S., & Lee, B. J. (2016). *Hyperbolic metamaterial-based near-field thermophotovoltaic system for hundreds of nanometer vacuum gap Abstract : 24*(6), 635–649. https://doi.org/10.1364/OE.24.00A635

Jung, I. A., Peng, Z., & Rahmat-Samii, Y. (2024). Recent Advances in Reconfigurable Electromagnetic Surfaces: Engineering Design, Full-Wave Analysis, and Large-Scale Optimization. *Electromagnetic Science*, *2*(3). https://doi.org/10.23919/emsci.2024.0020

Kality, A., City, S. U. B., Model, P., & For, E. (2025). *GRADE 12 PHYSICS MODEL EXAMINATIONS For more join us on Telegram @ samuelfromethiopia*. 1–11.

Kaur, K. P., Upadhyaya, T., Pandya, K., & Patel, U. (2023). Ultrathin High Q-Factor Perfect Metamaterial Absorber for Sensing Applications. *2nd International Conference on Wireless, Antenna and Microwave Symposium, WAMS 2023*, 1–5. https://doi.org/10.1109/WAMS57261.2023.10242878

Kudyshev, Z. A., Kildishev, A. V., Shalaev, V. M., & Boltasseva, A. (2019). High-efficiency emitter for thermophotovoltaics: Topology optimization. *2019 International Applied Computational Electromagnetics Society Symposium in Miami, ACES-Miami 2019*, *i*, 9–10.

Kumari, A., Yadav, A., Singh, O. P., & Sharan, P. (2024). A Review Of Surface Plasmon Resonance (SPR) Technology In Biosensing: Innovations, Applications And Future Trends. *Journal of Optics (India)*. https://doi.org/10.1007/s12596-024-02265-3

Kuznicki, Z. T., & Meyrueis, P. (2010). *PV Metamaterial Based on Nanostructured Si Zbigniew T. Kuznicki, Patrick Meyrueis Photonic Systems Laboratory, Pôle API Parc d'Innovation, Boulevard Sébastien Brant, BP 10413, 67400 Illkirch, France*. *1210*.

Landy, N. I., Sajuyigbe, S., Mock, J. J., Smith, D. R., & Padilla, W. J. (2008). Perfect metamaterial absorber. *Physical Review Letters*, *100*(20). https://doi.org/10.1103/PhysRevLett.100.207402

Lee, J., Cheon, S., Hong, S., & Nam, Y. (2017). International Journal of Heat and Mass Transfer A radioisotope thermophotovoltaic converter with nanophotonic emitters and filters. *International Journal of Heat and Mass Transfer*, *108*, 1115–1125. https://doi.org/10.1016/j.ijheatmasstransfer.2016.12.049

Lei, X., Li, Y., Huo, S., Sun, Z., Yu, H., Fang, L., Xu, S., Li, B., Wang, M., & Li, E. (2022). Design and Analysis of a Novel Compact Metamaterial Absorber Based on Double-Layer ITO Resistive Film for Improving Signal Integrity. *IEEE Access*, *10*, 24067–24079. https://doi.org/10.1109/ACCESS.2022.3155234

Li, W., Guler, U., Kinsey, N., Naik, G. V., Boltasseva, A., Guan, J., Shalaev, V. M., & Kildishev, A. V. (2014). Refractory plasmonics with titanium nitride: Broadband. *Advanced Materials*, *26*(47), 7959–7965. https://doi.org/10.1002/adma.201401874

Li, Y. (2009). Hybrid intelligent approach for modeling and optimization of semiconductor devices and nanostructures. *Computational Materials Science*, *45*(1), 41–51. https://doi.org/10.1016/j.commatsci.2008.04.030

Lin, S. Y., Fleming, J., Chow, E., Bur, J., Choi, K., & Goldberg, A. (2000). Enhancement and suppression of thermal emission by a three-dimensional photonic crystal. *Physical Review B - Condensed Matter and Materials Physics*, *62*(4), R2243–R2246. https://doi.org/10.1103/PhysRevB.62.R2243

Lin, S. Y., Moreno, J., & Fleming, J. G. (2003). Three-dimensional photonic-crystal emitter for thermal photovoltaic power generation. *Applied Physics Letters*, *83*(2), 380–382. https://doi.org/10.1063/1.1592614

Liu, Z., Zhang, Z., Xie, P., & Miao, Z. (2023). *Design of Selective TPV Thermal Emitters Based on Bayesian Optimization Nesting Simulated Annealing*.

Mahmud, S., Karim, M., Islam, S. S., Shuvo, M. K., Akter, T., Almutairi, A. F., & Islam, M. T. (2021). A Multi-Band Near Perfect Polarization and Angular Insensitive Metamaterial Absorber With a Simple Octagonal Resonator for Visible Wavelength. *IEEE Access*, *9*, 117746–117760. https://doi.org/10.1109/ACCESS.2021.3106588

Maqsood, I. (2011). *Design and Optimization of a Solar Thermophotovoltaic System By*.

Martínez, F. L., Toledano-Luque, M., Gandía, J. J., Cárabe, J., Bohne, W., Röhrich, J., Strub, E., & Mártil, I. (2007). Optical properties and structure of HfO2 thin films grown by high pressure reactive sputtering. *Journal of Physics D: Applied Physics*, *40*(17), 5256–5265. https://doi.org/10.1088/0022-3727/40/17/037

Mihai, L., Mihalcea, R., Tomescu, R., Paun, C., & Cristea, D. (2022). Selective Mid-IR Metamaterial-Based Gas Sensor System: Proof of Concept and Performances Tests. *Nanomaterials*, *12*(6), 1–14. https://doi.org/10.3390/nano12061009

Millikan, R. A. (1916). A Direct Photoelectric Determination of Planck's "<math><mi>h</mi></math>". *Physical Review*, *7*(3), 355–388. http://link.aps.org/doi/10.1103/PhysRev.7.355

Nam, Y., Yeng, Y. X., Lenert, A., Bermel, P., Celanovic, I., Soljačić, M., & Wang, E. N. (2014). Solar thermophotovoltaic energy conversion systems with two-dimensional tantalum photonic crystal absorbers and emitters. *Solar Energy Materials and Solar Cells*, *122*, 287–296. https://doi.org/10.1016/j.solmat.2013.12.012

Ni, Q., Ye, H., Shu, Y., & Lin, Q. (2016). A theoretical discussion on the internal quantum efficiencies of the epitaxial single crystal GaSb thin film cells with different p-n junctions. *Solar Energy Materials and Solar Cells*, *149*, 88–96. https://doi.org/10.1016/j.solmat.2015.12.039

Nicol, E. J., & Carbotte, J. P. (2005). Properties of the superconducting state in a two-band model. *Physical Review B - Condensed Matter and Materials Physics*, *71*(5), 1–18. https://doi.org/10.1103/PhysRevB.71.054501

Nitas, M., Kafesaki, M., & Arslanagic, S. (2024). Investigation of the Electromagnetic Behavior of Complementary Split-Ring Resonators: Toward a Novel CSRR Design. *IEEE Transactions on Microwave Theory and Techniques*, 1–10. https://doi.org/10.1109/TMTT.2024.3481330

Oh, M., Carlson, E., & Vandervelde, T. E. (2020). Design of an All-Semiconductor Selective Metamaterial Emitter in the Mid-IR Regime with Larger Feature Sizes for Thermophotovoltaic Energy Conversion Applications. *Journal of Electronic Materials*, *49*(6), 3504–3511. https://doi.org/10.1007/s11664-020-07972-8

Omair, Z., Scranton, G., Pazos-Outón, L. M., Xiao, T. P., Steiner, M. A., Ganapati, V., Peterson, P. F., Holzrichter, J., Atwater, H., & Yablonovitch, E. (2019). Ultraefficient thermophotovoltaic power conversion by band-edge spectral filtering. *Proceedings of the National Academy of Sciences of the United States of America*, *116*(31), 15356–15361. https://doi.org/10.1073/pnas.1903001116

Pappalardo, F., Romero Lairado, F., Louis de Canonville, C., Martin, C., Giacometti, G., Serin, G., Salomon, E., Angot, T., Gallais, L., Bisson, R., & Minissale, M. (2022). Optical Properties of Tungsten: A Parametric Study to Characterize the Role of Roughness, Surface Composition and Temperature. *Optics*, *3*(3), 216–224. https://doi.org/10.3390/opt3030021

Patel, S. K., Surve, J., Katkar, V., Parmar, J., Al-Zahrani, F. A., Ahmed, K., & Bui, F. M. (2022). Encoding and Tuning of THz Metasurface-Based Refractive Index Sensor with Behavior Prediction Using XGBoost Regressor. *IEEE Access*, *10*, 24797–24814. https://doi.org/10.1109/ACCESS.2022.3154386

Pfiester, N. A., & Vandervelde, T. E. (2017a). Selective emitters for thermophotovoltaic applications. *Physica Status Solidi (A) Applications and Materials Science*, *214*(1), 1–24. https://doi.org/10.1002/pssa.201600410

Pfiester, N. A., & Vandervelde, T. E. (2017b). Selective emitters for thermPfiester, N. A., & Vandervelde, T. E. (2017). Selective emitters for thermophotovoltaic applications. In Physica Status Solidi (A) Applications and Materials Science (Vol. 214, Issue 1). Wiley-VCH Verlag. https://doi.org/10.100. In *Physica Status Solidi (A) Applications and Materials Science* (Vol. 214, Issue 1). Wiley-VCH Verlag. https://doi.org/10.1002/pssa.201600410

Potyrailo, R. A., Hobbs, S. E., & Hieftje, G. M. (1998). Optical waveguide sensors in analytical chemistry: Today's instrumentation, applications and trends for future development. *Fresenius' Journal of Analytical Chemistry*, *362*(4), 349–373. https://doi.org/10.1007/s002160051086

Progress In Electromagnetics Research M, Vol. 8, 27–37, 2009. (2009). *8*, 27–37.

Qin, M., Zhang, L., & Wu, H. (2022). Dielectric Loss Mechanism in Electromagnetic Wave Absorbing Materials. *Advanced Science*, *9*(10), 1–24. https://doi.org/10.1002/advs.202105553

Racka-Szmidt, K., Stonio, B., Żelazko, J., Filipiak, M., & Sochacki, M. (2022). A review: Inductively coupled plasma reactive ion etching of silicon carbide. *Materials*, *15*(1). https://doi.org/10.3390/ma15010123

Raghu, S., Qi, X. L., Liu, C. X., Scalapino, D. J., & Zhang, S. C. (2008). Minimal two-band model of the superconducting iron oxypnictides. *Physical Review B - Condensed Matter and Materials Physics*, *77*(22), 1–4. https://doi.org/10.1103/PhysRevB.77.220503

Rahimi, Z., Parandin, F., Roshani, S., & Roshani, S. (2024). Design of 2D photonic crystal biosensor to detect cancer cells. *Journal of Optics (India)*, *0123456789*. https://doi.org/10.1007/s12596-024-02252-8

Ren, Y., Chen, J. K., & Zhang, Y. (2011). Optical properties and thermal response of copper films induced by ultrashort-pulsed lasers. *Journal of Applied Physics*, *110*(11). https://doi.org/10.1063/1.3662897

Rinnerbauer, V., Lenert, A., Bierman, D. M., Yeng, Y. X., Chan, W. R., Geil, R. D., Senkevich, J. J., Joannopoulos, J. D., & Wang, E. N. (2014). *Metallic Photonic Crystal Absorber-Emitter for Effi cient Spectral Control in High-Temperature Solar Thermophotovoltaics*. 1–10. https://doi.org/10.1002/aenm.201400334

Rinnerbauer, V., Lenert, A., Bierman, D. M., Yeng, Y. X., Chan, W. R., Geil, R. D., Senkevich, J. J., Joannopoulos, J. D., Wang, E. N., Soljačič, M., & Celanovic, I. (2014a). Metallic photonic crystal absorber-emitter for efficient spectral control in high-temperature solar thermophotovoltaics. *Advanced Energy Materials*, *4*(12). https://doi.org/10.1002/aenm.201400334

Rinnerbauer, V., Lenert, A., Bierman, D. M., Yeng, Y. X., Chan, W. R., Geil, R. D., Senkevich, J. J., Joannopoulos, J. D., Wang, E. N., Soljačič, M., & Celanovic, I. (2014b). Metallic photonic crystal absorber-emitter for efficient spectral control in high-temperature solar thermophotovoltaics. *Advanced Energy Materials*, *4*(12), 1–

10. https://doi.org/10.1002/aenm.201400334

Ross Macdonald, J. (1974). Simplified impedance/frequency-response results for intrinsically conducting solids and liquids. *The Journal of Chemical Physics*, *61*(10), 3977–3996. https://doi.org/10.1063/1.1681691

Saidov, M. S., Saidov, A. S., & Usmonov, S. N. (2008). Impurity thermophotovoltaic effect of the grain boundaries of technical-grade silicon. *Applied Solar Energy (English Translation of Geliotekhnika)*, *44*(1), 11–12. https://doi.org/10.3103/S0003701X08010040

Saloom, B. M., & Al-Dergazly, A. A. (2024). Numerical simulation of optimization the NCF dimension based on spectral response in optic filter. *Journal of Optics (India), 0123456789*. https://doi.org/10.1007/s12596-024-02209-x

Sang, S., Wang, Y., Feng, Q., Wei, Y., Ji, J., & Zhang, W. (2016). Progress of new label-free techniques for biosensors: A review. *Critical Reviews in Biotechnology, 36*(3), 465–481. https://doi.org/10.3109/07388551.2014.991270

Schossmann, A., & Bergmann, A. (2024). Millimeter-Wave Metamaterial-Based Strain Sensor Concept. *IEEE Sensors Journal*, *24*(10), 15900–15908. https://doi.org/10.1109/JSEN.2024.3382758

Science, A. (2015). *Control of Optical Properties of Surfaces for Improved Solar Thermophotovoltaic Systems by*.

Shruti, Pahadsingh, S., Appasani, B., Srinivasulu, A., Bizon, N., & Thounthong, P. (2023). A Reconfigurable Terahertz Metamaterial Absorber for Gas Sensing Applications. *Crystals*, *13*(2), 1–15. https://doi.org/10.3390/cryst13020158

Sreenivasulu, V. B., & Narendar, V. (2022). Design and Temperature Assessment of Junctionless Nanosheet FET for Nanoscale Applications. *Silicon*, *14*(8), 3823–3834. https://doi.org/10.1007/s12633-021-01145-w

Tabassum, S., Nayemuzzaman, S. K., Kala, M., Kumar Mishra, A., & Mishra, S. K. (2022). Metasurfaces for Sensing Applications: Gas, Bio and Chemical. *Sensors, 22*(18). https://doi.org/10.3390/s22186896

Tamiru, S., Tolessa, F., Alemu, B., Tiruneh, S., & Belay, A. (2023). *Research Article*

Numerical Study of High Spectral Efficiency and High-Temperature Energy Harvesting Metamaterial Emitter to Improve Thermophotovoltaic Performance. *September*.

Tao, L., Chen, Z., Li, Z., Wang, J., Xu, X., & Xu, J. Bin. (2021). Enhancing light-matter interaction in 2D materials by optical micro/nano architectures for high-performance optoelectronic devices. *InfoMat*, *3*(1), 36–60. https://doi.org/10.1002/inf2.12148

Valipour, A., Kargozarfard, M. H., Rakhshi, M., Yaghootian, A., & Sedighi, H. M. (2022). Metamaterials and their applications: An overview. *Proceedings of the Institution of Mechanical Engineers, Part L: Journal of Materials: Design and Applications*, *236*(11), 2171–2210. https://doi.org/10.1177/1464420721995858

Verma, S., Buznitsky, K., & Henry, A. (2025). Thermophotovoltaic performance metrics and techno-economics: Efficiency vs. power density. *Applied Energy*, *384*. https://doi.org/10.1016/j.apenergy.2025.125479

Veselago, V. G. (1968). The Electrodynamic of Substances with Simultaneous Negative Values of e and μ. *Soviet Physics Uspekhi*, *10*(4), 509–514.

Vora, A., Gwamuri, J., Pala, N., Kulkarni, A., Pearce, J. M., & Güney, D. O. (2014). Exchanging ohmic losses in metamaterial absorbers with useful optical absorption for photovoltaics. *Scientific Reports*, *4*, 1–13. https://doi.org/10.1038/srep04901

Wang, H., Chang, J. Y., Yang, Y., & Wang, L. (2016). Performance analysis of solar thermophotovoltaic conversion enhanced by selective metamaterial absorbers and emitters. *International Journal of Heat and Mass Transfer*, *98*, 788–798. https://doi.org/10.1016/j.ijheatmasstransfer.2016.03.074

Wang, H., Chen, Q., Wen, L., Song, S., Hu, X., & Xu, G. (2015). Titanium-nitride-based integrated plasmonic absorber/emitter for solar thermophotovoltaic application. *Photonics Research*, *3*(6), 329. https://doi.org/10.1364/prj.3.000329

Wang, H., Prasad Sivan, V., Mitchell, A., Rosengarten, G., Phelan, P., & Wang, L. (2015). Highly efficient selective metamaterial absorber for high-temperature solar thermal energy harvesting. *Solar Energy Materials and Solar Cells*, *137*, 235–242. https://doi.org/10.1016/j.solmat.2015.02.019

Wang, H., & Wang, L. (2013). *Perfect selective metamaterial solar absorbers*. *21*(November), 13311–13319. https://doi.org/10.1364/OE.21.0A1078

Wang, H., Wang, L., Phelan, P., Dai, L., & Rykaczewski, K. (2016). *Nano-Engineering Metamaterials and Metafilms for High-Efficiency Solar Energy Harvesting and Conversion*. *May*, 128.

Wang, Y., Wang, B., & Wang, R. (2023). Current Status of Detection Technologies for Indoor Hazardous Air Pollutants and Particulate Matter. *Aerosol and Air Quality Research*, *23*(12), 1–20. https://doi.org/10.4209/aaqr.230193

Wang, Z., Kortge, D., He, Z., Song, J., Zhu, J., Lee, C., Wang, H., & Bermel, P. (2022). Selective emitter materials and designs for high-temperature thermophotovoltaic applications. *Solar Energy Materials and Solar Cells, 238*. https://doi.org/10.1016/j.solmat.2021.111554

Wang, Z., Lin, S., Ge, Y., Chen, Z., Zhao, J., Chen, J., Zhou, Z., & Bird, T. S. (2024). Unlock the Potentials of Large-Element-Spacing Arrays: A Meta-Lens Solution for Grating-Lobe Suppression and Gain Enhancement. *Electromagnetic Science*, *2*(4). https://doi.org/10.23919/emsci.2024.0030

Woolf, D., Hensley, J., Cederberg, J. G., Bethke, D. T., Grine, A. D., & Shaner, E. A. (2014). Heterogeneous metasurface for high temperature selective emission. *Applied Physics Letters*, *105*(8). https://doi.org/10.1063/1.4893742

Wu, C., Iii, B. N., John, J., Milder, A., Zollars, B., Savoy, S., & Shvets, G. (n.d.). *Metamaterial-based integrated plasmonic absorber / emitter for solar thermo-photovoltaic systems*. *024005*. https://doi.org/10.1088/2040-8978/14/2/024005

Wynn, M. T., Van Der Aalst, W., Verbeek, E., & Di Stefano, B. (2024). The IEEE XES Standard for Process Mining: Experiences, Adoption, and Revision [Society Briefs]. *IEEE Computational Intelligence Magazine, 19*(1), 20–23. https://doi.org/10.1109/MCI.2023.3333141

Yangjian, Z., Chuhuan, F., Qi, L., Xin, S., & Hongbin, Y. (2019). Dynamic Reflection Phase Modulation in Terahertz Metamaterial. *IEEE Photonics Journal, 11*(4). https://doi.org/10.1109/JPHOT.2019.2926499

Yi Xiang Yeng. (2014). *Three-dimensional photonic crystals for high temperature applications*. *2008*.

Zhang, Z., Liu, M., Ibrahim, M. M., Wu, H., Wu, Y., Li, Y., & Mersal, G. A. M. (2022). Flexible polystyrene / graphene composites with epsilon - near - zero properties. *Advanced Composites and Hybrid Materials*, 1054–1066. https://doi.org/10.1007/s42114-022-00486-3

Zhong, Y., Du, L., Liu, Q., Zhu, L., Zou, Y., & Zhang, B. (2021). All-Silicon Terahertz Metasurface with Sharp Fano Resonance and Its Sensing Applications. *IEEE Photonics Journal*, *13*(2). https://doi.org/10.1109/JPHOT.2021.3065096

Zhou, Z., Zhang, B., Jiang, C., & Wu, H. (2022). Design and theoretical study of a metamaterial absorber-emitter pair matched with a low-bandgap PV cell for an STPV system. *Optical and Quantum Electronics*, *54*(12), 1–20. https://doi.org/10.1007/s11082-022-04173-x

Zhu, J., Wang, X., Wu, Y., Su, Y., Jia, T., Yang, H., Zhang, L., Qi, Y., & Wen, X. (2020). Plasmonic Refractive Index Sensors Based on One- and Two-Dimensional Gold Grating on a Gold Film. *Photonic Sensors*, *10*(4), 375–386. https://doi.org/10.1007/s13320-020-0598-x